ANNALS OF CARNEGIE MUSEUM

VOL. 90, NUMBER 1, PP. 1–36 30 JUNE 2024

BASICRANIAL ANATOMY OF *LEPTICTIS HAYDENI* LEIDY, 1868 (MAMMALIA, EUTHERIA, LEPTICTIDAE)

JOHN R. WIBLE
Curator, Section of Mammals, Carnegie Museum of Natural History
5800 Baum Boulevard, Pittsburgh, Pennsylvania 15206
wiblej@carnegiemnh.org

ORNELLA C. BERTRAND
[Research Associate, Section of Mammals, Carnegie Museum of Natural History]
Institut Català de Paleontologia Miquel Crusafont, Universitat Autònoma de
Barcelona, Edifici ICTA-ICP, Cerdanyola del Vallès, Barcelona, Spain
ornella.bertrand@icp.cat

ABSTRACT

Leptictis haydeni Leidy, 1868, from the early Oligocene of South Dakota is the type species of the genus and is known only from the well-preserved holotype cranium. The anatomy of its basicranium is described and illustrated based on CT scan data and the primary neurovascular structures are reconstructed. Comparisons are made with a cranium of *Leptictis dakotensis* (Leidy, 1868) also based on CT scan data. Numerous differences between the two are identified, including the shape of the hypophyseal fossa, the size and orientation of the posterior clinoid process, the depth of the sulcus for the capsuloparietal emissary vein, the size of the petrosal contribution to the middle cranial fossa and to the epitympanic recess, the position of the exit of the auditory tube from the middle ear, the size of the entotympanic, the presence of a styliform process on the entotympanic, and the shape of the ectopterygoid process of the alisphenoid, which added to the few prior reported dental differences justify retaining separate species. The ramus inferior of the stapedial artery, identified by prior authors as present in *L. dakotensis*, is shown to be absent in both species. Additional comparisons are made with the early Eocene palaeoryctid *Eoryctes melanus* Thewissen and Gingerich, 1989, also based on CT scans. These three taxa share details of the tympanic processes and epitympanic wings of the bones of the middle ear, the pattern of the dural sinuses and the large size of the sigmoid sinus, the well-developed exposure of the parietal on the occiput, and the unusual course of the nerve of the pterygoid canal, suggestive of a possible close phylogenetic relationship.

KEY WORDS: dural sinuses; endocranium; neurovascular reconstruction; petrosal; ramus inferior of stapedial artery

INTRODUCTION

Leptictids are extinct insectivorous mammals that have long played a central role in discussions of early placental evolution (e.g., Gregory 1910; Szalay 1977; Novacek 1986; Gunnell et al. 2007; Hooker 2013), and have been posited as close relatives of extant insectivorous groups, including lipotyphlans (Novacek 1986) and macroscelideans (Rose 1999; Asher et al. 2003). Recent phylogenetic trees (Velazco et al. 2022) identify the earliest leptictid as Late Cretaceous *Gypsonictops* Simpson, 1927, in a clade with *Prodiacodon* Matthew, 1929, *Palaeictops* Matthew, 1899, and *Leptictis* Leidy, 1868, which are primarily Paleocene, Eocene, and Oligocene in age, respectively. In addition to these and several other North American genera (e.g., *Blacktops* Meehan and Martin, 2010, *Megalepticis* Meehan and Martin, 2012, and *Stenoleptictis* Korth, 2022), leptictids are reported from the Oligocene of Asia (Kellner and McKenna 1996; Tong and Wang 2006) and the Paleogene of Europe (McKenna and Bell 1997), but the latter have been placed in the Pseudorhynchocyonidae (Hooker 2013). It remains unclear if leptictids are placental mammals (e.g., O'Leary et al. 2013) or stem eutherians outside of Placentalia (Wible et al. 2007, 2009; Velazco et al. 2022).

In 1868, Leidy named two new insectivore taxa found together in White River, South Dakota, each based on partial crania, *Leptictis haydeni* and *Ictops dakotensis*, with the former much more complete than the latter. By the early 1900's, a number of other species of *Ictops* were named (e.g., Matthew 1899, 1903; Douglass 1901, 1905) but not of *Leptictis*. In 1967, Van Valen synonymized *I. dakotensis* with *L. haydeni*, finding the differences between them trivial. Novacek (1976) agreed that the differences did not warrant separation at the generic level, but recognized them as valid species of *Leptictis*, which had priority over *Ictops*. However, as *L. haydeni* was known by only one specimen, he proposed the type of *I. dakotensis* as the type of *Leptictis*. Not all authors agreed with this. In their review of leptictids, Gunnell et al. (2007) identified *L. haydeni* as the type species (see also Meehan and Martin 2010). Between the review by Gunnell et al. (2007) and the recent paper by Korth (2022), there are nine recognized species of *Leptictis*.

From the standpoint of anatomy, the most completely known leptictid is the Oligocene *L. dakotensis*. Its skull has been described in detail most notably by Butler (1956) and Novacek (1986), its brain endocast by Novacek (1982, 1986), and its postcranium by Cavigelli (1997) and Rose (1999, 2006). Ruf et al. (2016) reported on the inner ear of *Leptictis* sp. from the Brule Formation Fitterer Ranch locality of North Dakota, which has yielded *L. dakotensis* and two indeterminate leptictid jaws (Korth et al. 2023). The basicranium and its reconstructed vasculature of *L. dakotensis* are treated by Butler (1956) and Novacek (1980, 1986) but the two are not entirely in agreement. For

example, they differ in their reconstructed courses for the end branches of the stapedial artery, the superior and inferior rami. These authors did not study the same specimens, so the reported differences may be real and therefore represent polymorphisms. The type cranium of *L. haydeni* has been described and illustrated by Leidy (1869) and Scott and Jepsen (1938), but it has not been treated to the same level of detail as *L. dakotensis*.

The impetus for this study was to report observations on the type of *L. haydeni* based on CT scan data, with a focus on the basicranium and cranial vasculature. Fortunately, we gained access to the CT scans of another specimen, *Leptictis* sp., which we identify as *L. dakotensis*. The basicranial studies of *L. dakotensis* by Butler (1956) and Novacek (1980, 1986) predate the now common use of CT scan data. Therefore, access to this second specimen allowed us to address the incongruities between these two authors, to update terminological usages, and to make comparisons with *L. haydeni*. As *Leptictis* continues to play a major role in most contemporary phylogenetic analyses, our goal is to evaluate and update as much of the relevant anatomy of these structures as possible.

MATERIALS AND METHODS

The last major revision of *Leptictis* was by Novacek (1976). Following Novacek (1976), Gunnell et al. (2007) provisionally listed nine species of *Leptictis* (*L. haydeni* Leidy, 1868, *L. acutidens* (Douglass, 1901), *L. bullatus* (Matthew, 1899), *L. dakotensis* (Leidy, 1868), *L. douglassi* Novacek, 1976, *L. major* (Douglass, 1905), *L. montanus* (Douglass, 1905), *L. thomsoni* (Matthew, 1903), and *L. wilsoni* Novacek, 1976). Korth (2022) placed *L. thomsoni* in a new genus *Stenoleptictis* and recognized the validity of another species, *L. intermedius* (Douglass, 1905).

Butler (1956) reported on three *Leptictis* crania, two referred to *L. dakotensis* and a third to *Mesodectes cuniculus* (= *caniculus*), which Novacek (1976) referred to *L. dakotensis*. Photographs of five cranial specimens of *L. dakotensis* are figured in Novacek (1986). However, it is unknown what specimens provided the basis for the numerous reconstructions in Novacek (1986: figs. 1, 5-10, 13-15, 17-20, 22, 26-29). These are credited to Sam McDowell without reference to specific specimens. At the time of Butler's (1956) publication, McDowell was also preparing to publish on *Leptictis*. Butler (1956) published first, and McDowell (1958), in a subsequent paper, noted that Butler's results on *Leptictis* "are essentially the same as my own." McDowell (1958) did not use his reconstructions of *Leptictis* but gave them to Novacek.

The two specimens CT scanned for the current report are: (1) *Leptictis haydeni* ANSP 11402, Mauvaises Terre, White River, South Dakota (Fig. 1). Leidy (1868) named *L. haydeni*, illustrating and describing the cranium in the next year (1869: plate XXIV, figs. 25-27). He did not identify a type, but ANSP 11402, as the only known specimen, is considered the type (Novacek 1976). Scott and Jepsen (1938: plate IV, figs. 1, 1a-c) included drawings of the type in various views. Lillegraven (1969: fig. 28) illustrated upper and lower postcanine dentitions for AMNH 74963 as *L. haydeni*, but these do not have the offset between the penultimate and ultimate premolars noted by Scott and Jepsen (1938; see below). We note that a search for *L. haydeni* on iDigBio.org (February 1, 2024) revealed eight additional specimens between four North American institutions. We have not investigated these specimens, which have not yet been formally added to the hypodigm for the species that still only includes the holotype ANSP 11402.

(2) *Leptictis* sp. SDSM 62369, Brule Formation, Reva Gap, Slim Buttes, Harding County, South Dakota (Fig. 2). Of the two species known from the Brule of South Dakota, *L. dakotensis* and *L. bullatus*, SDSM 62369 resembles the former in dimensions, the arrangement of the temporal crests, and the presence of a reduced metacone on the M3, absent in *L. bullatus* (Matthew 1899). We provisionally refer SDSM 62369 to *L. dakotensis*. This specimen was incorrectly referred to as AMNH (American Museum of Natural History) 62369 in Gould (1995).

Scott and Jepsen (1938:21) distinguished *L. haydeni* from other *Leptictis* (= *Ictops* Leidy, 1868) regarding the structure and position of the upper penultimate premolar (Fig. 3). In *L. haydeni* (Fig. 3A), this tooth has "a simple, compressed cone, without accessory cusps of any sort" compared to the usual complex penultimate premolar (Fig. 3B) with "a large, crescentic internal cusp and a small postero-external one." Additionally, in the former this tooth is offset lingually from the ultimate premolar and molars (Fig. 3A) in contrast to a more gradual taper across the premolar-molar series (Fig. 3B). Only the left upper penultimate premolar is preserved in *L. haydeni* and it is heavily worn (Fig. 3A). Nevertheless, contra Scott and Jepsen (1938), the outline of the tooth is not that of a simple, compressed cone as it is much wider distally than mesially. The main cusp, the paracone, is in the mesial half and has a narrow mesial cingulum. A worn crest slopes discobuccally from the paracone and appears to have had a reduced metacone. Lingual to this crest and at a similar height is a prominent bulge in the position of a small protoconal lobe, which may have sported a protocone. What genuinely distinguishes the upper penultimate premolar of *L. haydeni* is that it has two subequal roots, mesial and distal; this tooth in other *Leptictis* typically has three roots. In *L. dakotensis* SDSM 62369, the largest root is situated under the protocone, the smallest under the metacone, and the third under the paracone. There are small parastylar and metastylar lobes, and a cingulum on the distal half of the protoconal lobe. The protocone is less than half the height of the paracone but of only slightly smaller girth. The metacone is intermediate in height but of smaller girth.

Both specimens were scanned at the Microscopy and Imagery Facility (MIF) at the American Museum of Natural History. *Leptictis haydeni* ANSP 11402 was scanned with the following parameters: voltage of 190 kV, current

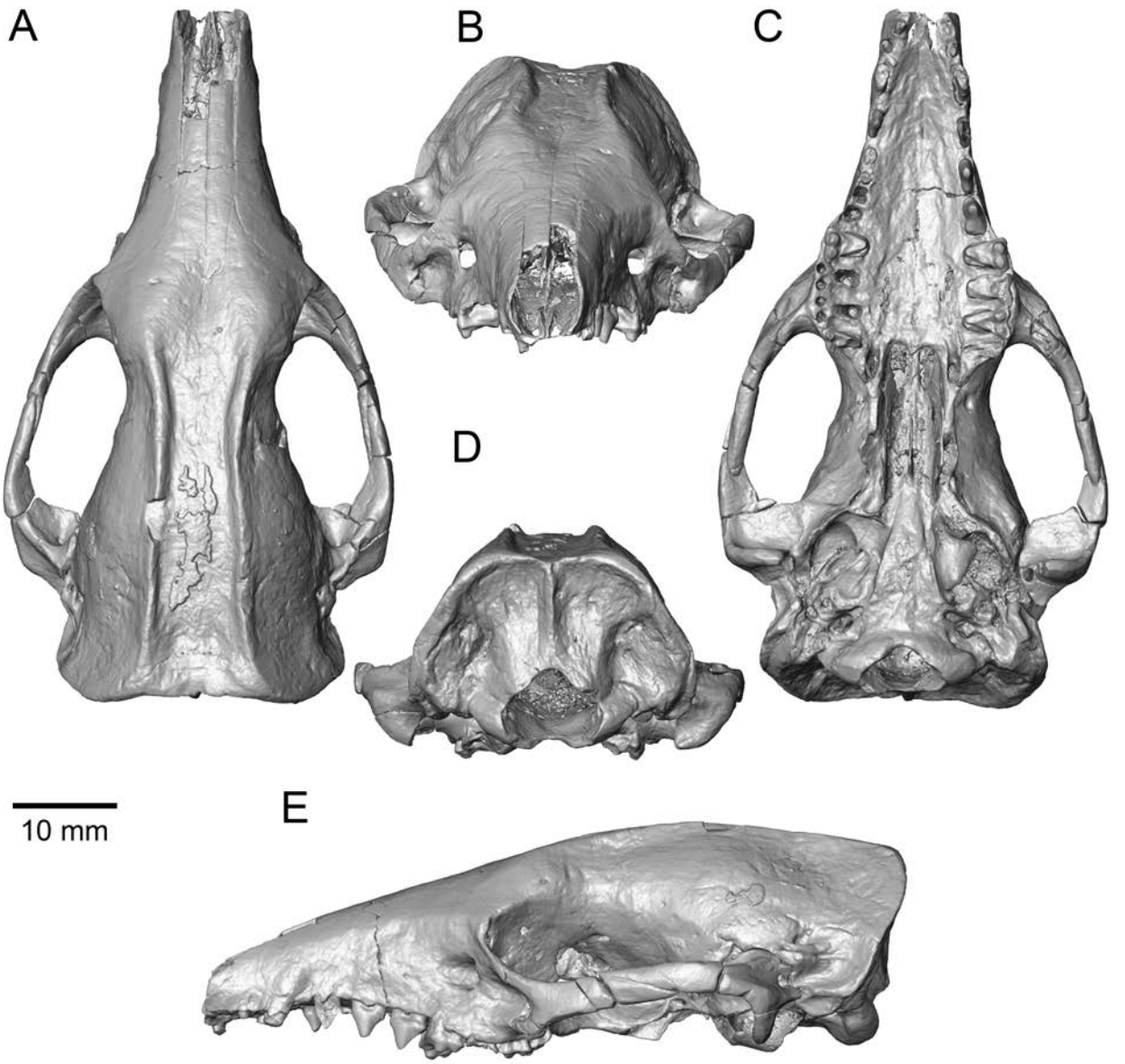

Fig. 1.— *Leptictis haydeni* ANSP 11402, cranium isosurface from CT scans in **A,** dorsal, **B,** anterior, **C,** ventral, **D,** posterior, and **E,** left lateral views.

of 180 μA, and a voxel size of 0.04348457 mm; *L. dakotensis* SDSM 62369 was scanned at a voltage of 170 kV, current of 190 μA, and voxel size of 0.03438626 mm.

Terminology for the basicranium and its neurovascular structures follows prior works of the first author (e.g., Wible 2003, 2008; Wible and Spaulding 2013). Where appropriate, terms are used from the Nomina Anatomica Veterinaria (2017). Numbering of premolars follows O'Leary et al. (2013), where the primitive eutherian formula included five upper and lower premolars; *Leptictis* has only four, with the lost one the middle one of the primitive five.

Institutional Abbreviations:

AMNH American Museum of Natural History, New York, New York
ANSP Academy of Natural Sciences of Philadelphia, Philadelphia, Pennsylvania
CM Carnegie Museum of Natural History, Pittsburgh, Pennsylvania
F:AM Frick Collections, American Museum of Natural History, New York, New York
KUVP Vertebrate Paleontology, University of Kansas,

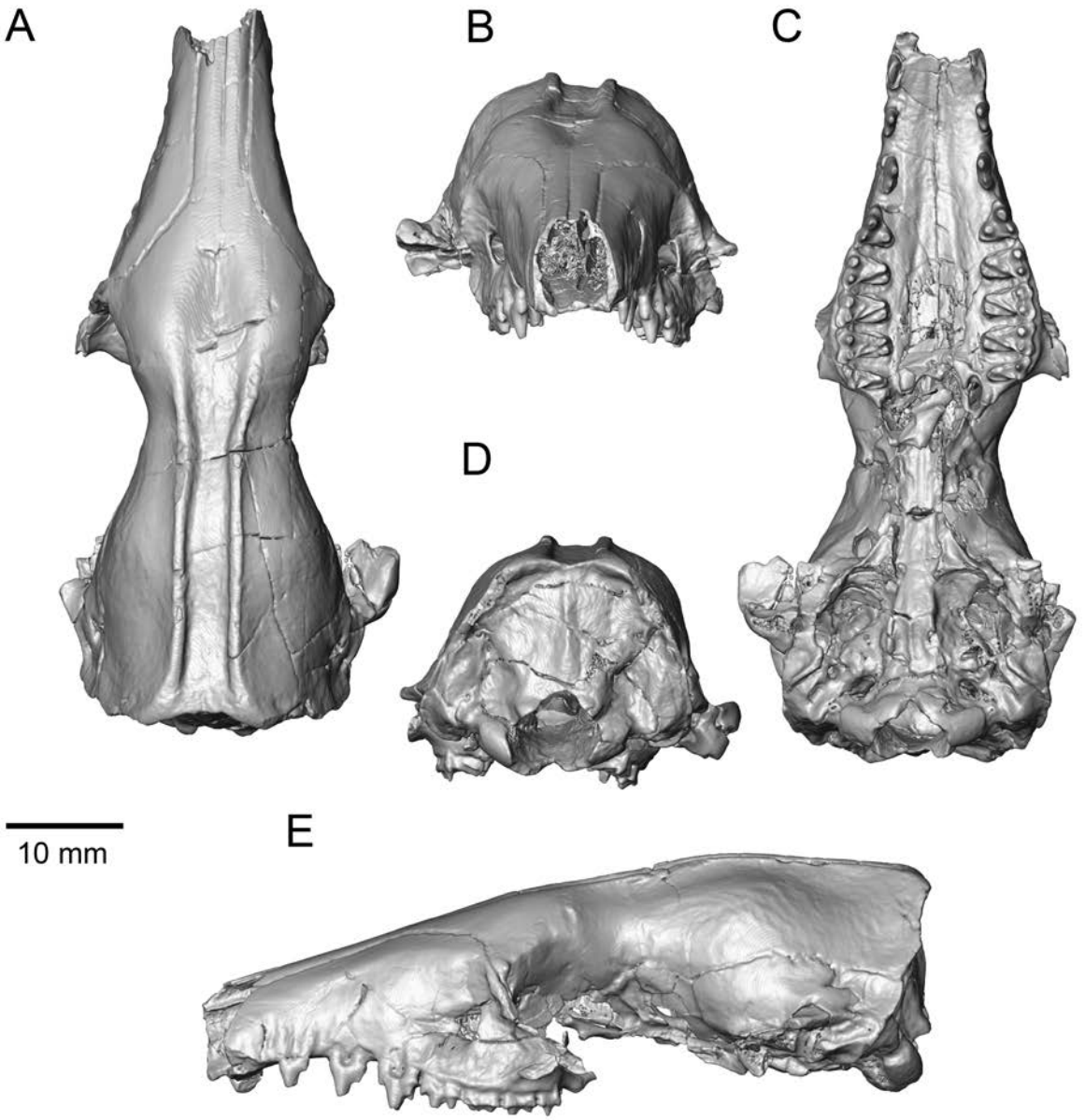

Fig. 2.—*Leptictis dakotensis* SDSM 62369, cranium isosurface from CT scans in **A,** dorsal, **B,** anterior, **C,** ventral, **D,** posterior, and **E,** left lateral views.

Lawrence, Kansas
MCZ Museum of Comparative Zoology, Harvard University, Cambridge, Massachusetts
SDSM South Dakota School of Mines, Rapid City, South Dakota
UM Museum of Paleontology, University of Michigan, Ann Arbor, Michigan
USNM United States National Museum, Smithsonian Institution, Washington, D.C.

DESCRIPTIONS

Leptictis haydeni ANSP 11402

Leidy (1869) provided general descriptions of ANSP 11402. As some terminology he employed is out of fashion, we have included synonyms in the Appendix along with alternative terms and interpretations used by several other authors describing leptictids. ANSP 11402 (Fig. 1) appears little changed since it was figured by Leidy (1869)

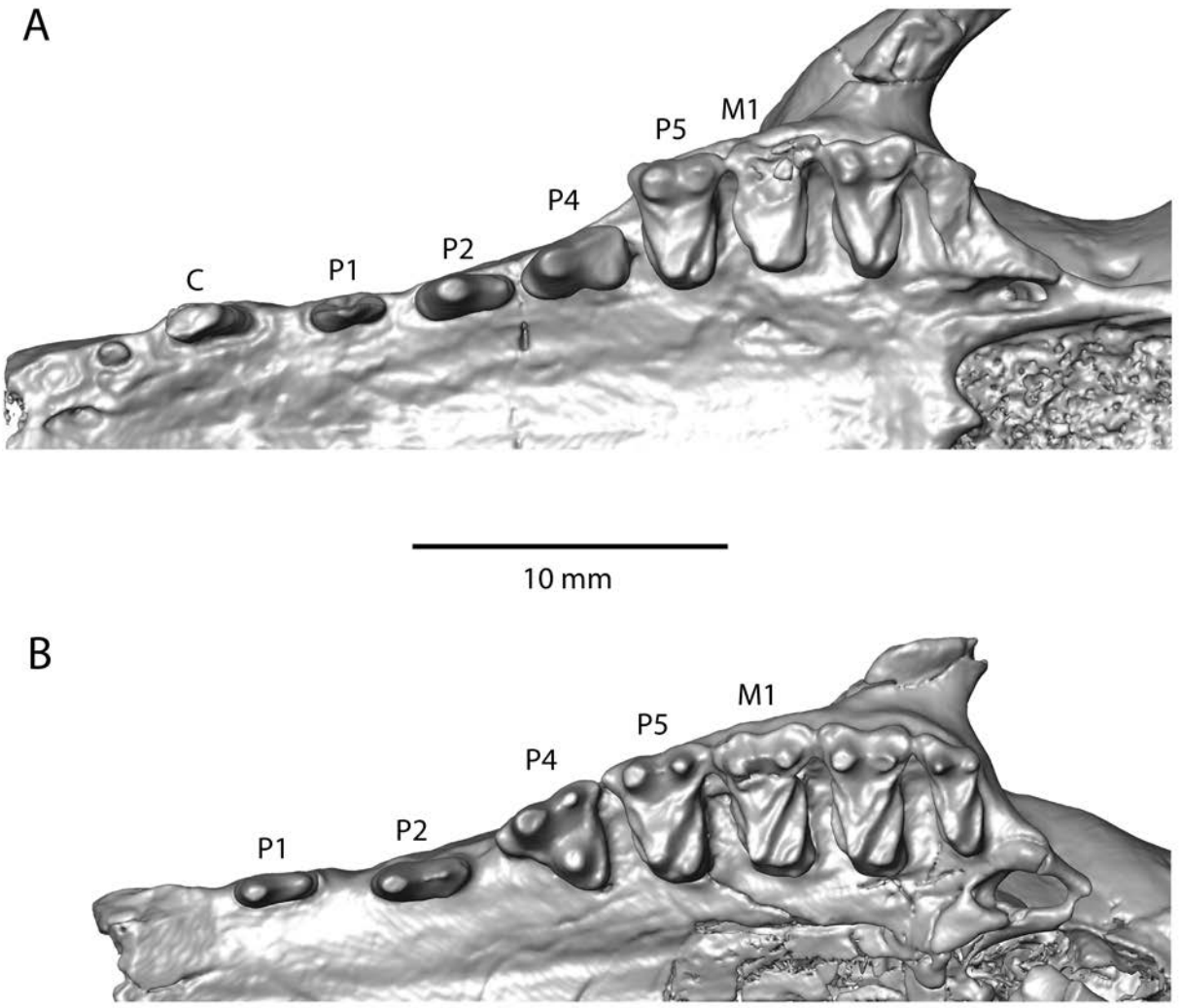

Fig. 3.—Left upper dentition isosurface from CT scans in occlusal view. **A,** *Leptictis haydeni* ANSP 11402, **B,** *Leptictis dakotensis* SDSM 62369. Abbreviations: **C,** upper canine; **M1,** first upper molar; **P1,** first upper premolar; **P2,** second upper premolar; **P4,** fourth upper premolar; **P5,** fifth upper premolar.

and Scott and Jepsen (1938). The most substantive alteration concerns the right basicranium, now visible (Fig. 1C), but concealed by matrix in the drawing by Scott and Jepsen (1938: pl. IV, fig. 1b). The cranium appears little distorted with the principal missing bone at the anteriormost rostrum and within parts of the nasal cavity and both orbits. As is evident in posterior view (Fig. 1D), the interior of the cranium contains numerous small particles similar in density to the fossil, which complicates illustration; this is not the case with *L. dakotensis* SDSM 62369 (Fig. 2D). We segmented the basi- and alisphenoid and the right petrosal of ANSP 11402 in Avizo, and describe and illustrate their endocranial surfaces. The remaining endocranial surfaces of ANSP 11402 are discussed in the comparative section.

The central mesocranium houses the nasopharynx posterior to the choanae (internal nasal aperture) within the ventrally open basipharyngeal canal. The major elements of the mesocranial roof are the midline parts of the sphenoid complex, the presphenoid anteriorly and the basisphenoid posteriorly ("ps" and "bs" in Fig. 4A), which are separated by a narrow gap. The presphenoid has a low midline keel that broadens slightly posteriorly; the basisphenoid is flat. Ventral to the presphenoid and basisphenoid is another midline element, a parasphenoid (Wible et

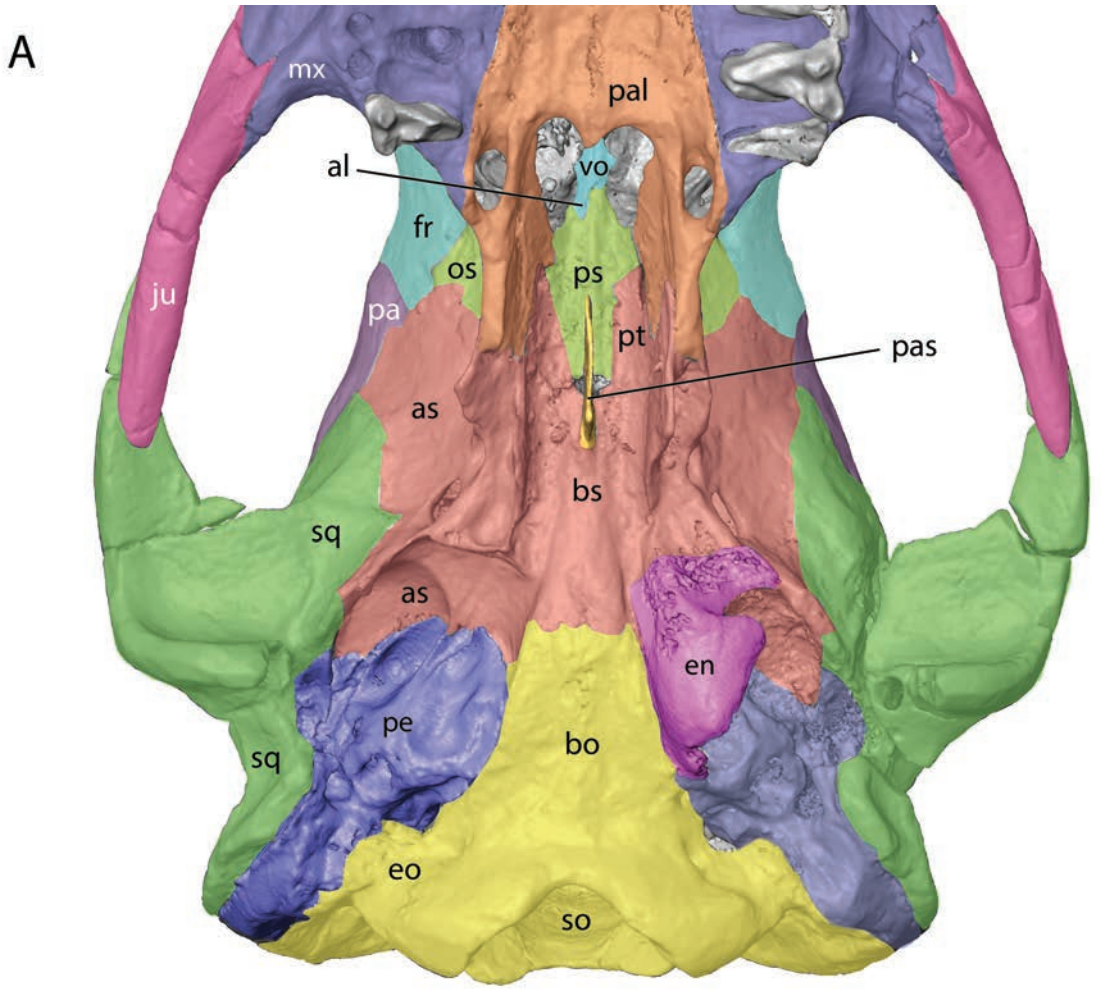

Fig. 4.—*Leptictis haydeni* ANSP 11402, meso- and basicranium isosurface from CT scans in ventral view. **A,** bones colored following preserved sutural pattern; **B,** segmentation of entotympanic, parasphenoid, and petrosal. Asterisk in B is groove for nerve of pterygoid canal; arrow in B shows course of auditory tube; question mark in B indicates a sulcus of unknown function in the basisphenoid suggested to accommodate the auditory tube in *L. dakotensis* (Novacek 1986). Abbreviations: **al,** ala of vomer; **as,** alisphenoid; **asc,** alisphenoid canal; **at,** auditory tube; **bo,** basioccipital; **bs,** basisphenoid; **cf,** carotid foramen; **ecp,** ectopterygoid process; **egp,** entoglenoid process of squamosal; **en,** entotympanic; **enf,** entoglenoid facet (on alisphenoid); **enp,** entopterygoid process; **eo,** exoccipital; **er,** epitympanic recess; **fm,** foramen magnum; **fo,** foramen ovale; **fr,** frontal; **gf,** glenoid fossa; **Gf,** Glaserian fissure; **gica,** groove for internal carotid artery; **ham,** pteryoid hamulus; **hf,** hypoglossal foramen; **hs,** hypotympanic sinus (on alisphenoid); **ips,** inferior petrosal sinus foramen; **jf,** jugular foramen; **ju,** jugal; **M3,** upper third molar; **me,** mastoid exposure of petrosal; **mpf,** minor palatine foramen; **mx,** maxilla; **oc,** occipital condyle; **os,** orbitosphenoid; **otc,** orbitotemporal canal (anterior opening); **pa,** parietal; **pal,** palatine; **pas,** parasphenoid; **pcp,** paracondylar process of exoccipital; **pe,** petrosal; **pgf,** postglenoid foramen; **pgp,** postglenoid process; **pns,** posterior nasal spine; **pr** promontorium of petrosal; **ps,** presphenoid; **pt,** pterygoid; **ptc,** posttympanic crest; **ptf,** pterygoid fossa; **ptp,** posttympanic process of squamosal; **so,** supraoccipital; **sq,** squamosal; **tpas,** tympanic process of alisphenoid; **vo,** vomer; **zpmx,** zygomatic process of maxilla.

al. 2018; "pas" in Fig. 4A), that divides the rear of the basipharyngeal canal into left and right sides. As preserved, this thin bone only contacts the basisphenoid, being separated from the presphenoid by a narrow gap. The ventral margin of the parasphenoid appears to be natural; it is tallest posteriorly and tapers anteriorly. It is unclear if there is bone missing from the parasphenoid, which, for example, may have filled in the gap between it and the presphenoid. The anterior end of the presphenoid is underlain by the posterior end of the vomer ("vo" in Fig. 4A). The vomer is asymmetric here and is certainly broken to an unknown degree. The vomer has a short ala (wing) on the right side ("al" in Fig. 4A) that is incomplete on the left.

The lateral walls of the basipharyngeal canal are formed by the sub-parallel entopterygoid processes ("enp" in Fig. 4B). The anterior half of the lateral wall is formed by the

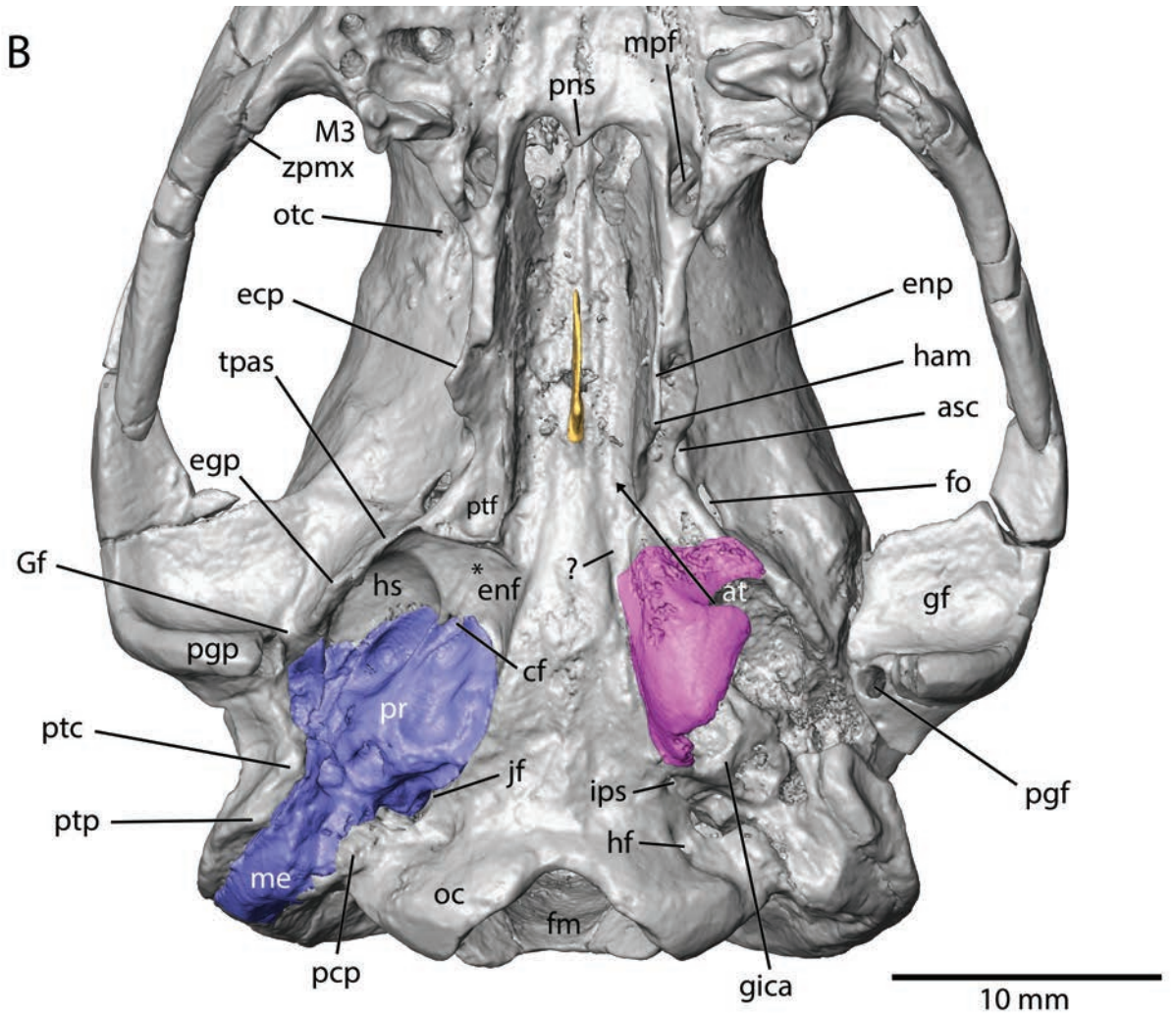

perpendicular process of the palatine ("pal" in Fig. 4A) and the posterior half by the pterygoid bone ("pt" in Fig. 4A), which sits medial to the palatine. While the palatine is confined to the lateral wall, the pterygoid extends medially into the roof underlying the pre- and basisphenoid; however, the pterygoids do not come close to meeting on the midline. The posteroventral aspect of the better-preserved left pterygoid appears unbroken; it is slightly thickened and ends in a 120 degree angle that represents the pterygoid hamulus ("ham" in Fig. 4B). The posterior base of the pterygoid is fused seamlessly to the basi- and alisphenoid ("as" in Fig. 4A). Lateral to the pterygoid hamulus is the laterally flaring ectopterygoid process of the alisphenoid ("ecp" in Fig. 4B), which also ends posteriorly at a 120 degree angle. There is a distinct muscular fossa between the ento- and ectopterygoid processes, the pterygoid fossa for the medial (internal) pterygoid muscle (Turnbull 1970; "ptf" in Fig. 4B).

Posterior to the ectopterygoid process is a low crest ("tpas" in Fig. 4B) that forms the lateral margin of the pterygoid fossa. This crest divides into a medial section that forms the posterior margin of the pteryoid fossa and a lateral section that curves posterolaterally. Based on the left side, both sections are in contact with the entotympanic ("en" in Fig. 4A) and represent the tympanic process of the alisphenoid. The lateral section is continuous with a more robust crest on the squamosal ("sq" in Fig. 4A), the entoglenoid process of the squamosal ("egp" in Fig. 4B).

Lateral to the ectopteryoid process and alisphenoid tympanic process are three large openings in the alisphenoid (Fig. 5). The posterior one, the foramen ovale ("fo" in Fig. 5), is the largest; the anterior two are the anterior and posterior openings of the short alisphenoid canal ("asc" in Fig. 5). A small foramen in the posteromedial aspect of the posterior opening is a transverse canal foramen ("tcf" in Fig. 5) that communicates across the midline of the basisphenoid. Anterodorsal to the right alisphenoid canal are five orbital foramina arrayed in an arc (four on the left side). From posteroventral to posterodorsal these are the large sphenorbital fissure ("sof" in Fig. 5) between the

ali- and orbitosphenoid ("os" in Fig. 5), the large optic foramen ("of" in Fig. 5) within the orbitosphenoid, two ethmoidal foramina connected by a groove (a ventral foramen in the orbitosphenoid and a dorsal one ["vef" and "def" in Fig. 5] between that bone and the frontal ["fr" in Fig. 5]), and the anterior opening of the orbitotemporal canal ("otc" in Fig. 5) between the frontal and orbitosphenoid. The left side differs in having only a single ethmoidal foramen between the frontal and orbitosphenoid and two tiny nutrient foramina in positions described as suboptic foramina by Butler (1956) and Novacek (1986). The anterior nutrient foramen lies below the optic foramen in the orbitosphenoid; the posterior one is in the alisphenoid in the medial wall of the sphenorbital fissure. Both orbits are damaged anterior to the optic foramen. Visible on both sides (but not shown in the figures) are the anteroventral contour of the sphenopalatine foramen between the palatine and frontal, the maxillary foramen entirely within the maxilla, and the lacrimal foramen entirely within the lacrimal in the orbit. Above the orbital rim is a small frontal diploic vein foramen in the frontal ("fdv" in Fig. 5); it opens into a diploic space that does not cross the midline and has a small endocranial opening in the roof of the rostral cranial fossa.

Turning to the basicranium, both sides are generally well preserved with only slight damage (Fig. 4). There are cracks in the squamosals and a missing section of bone from the left squamosal and petrosal. No ear ossicles or the ectotympanic bone are preserved, and the large entotympanic element is only found on the left side. The absence of this element on the right is helpful in that it displays facets on other bones that contacted the entotympanic.

The midline elements are the basisphenoid and basioccipital ("bo" in Fig. 4A) with the suture between them at the level of the anterior extent of the petrosal. Whereas the basisphenoid is flat anteriorly above the parasphenoid, posteriorly it has a raised convex center that broadens posteriorly with lateral wings extending to the entopterygoid processes. Posterior to the entopterygoid processes, the basisphenoid's lateral margin is abrupt with lateral wings at a more dorsal plane that continue as the epitympanic wings of the alisphenoids (see below). The central shape on the basisphenoid continues onto the basioccipital, where the surface is generally flat, although there is a weak raised midline eminence immediately anterior to the foramen magnum ("fm" in Fig. 4B). The ventral surface of the basioccipital is significantly raised compared to the petrosals, which is not evident in ventral view (Fig. 4) but is striking in the oblique ventrolateral view on the right side where the entotympanic is missing (Fig. 5). The lateral edge of the basioccipital's ventral surface is a sharp, arced crest that on its dorsolateral aspect slopes abruptly into the ear region to contact the petrosal and the alisphenoid. Based on the left side, this sloped surface provides a broad facet that abutted the entotympanic (below we will encounter adjacent facets for the entotympanic on the alisphenoid and petrosal). The crest and entotympanic facet surface on the basioccipital represent a tympanic process of the basioccipital ("tpbo" in Fig. 5). The crest and facet continue a short distance anteriorly onto the basisphenoid forming a tympanic process of that bone ("tpbs" in Fig. 5). Posterior to the basioccipital tympanic process is an entrance into a small canal between the basioccipital and petrosal for the inferior petrosal sinus visible on the left side but hidden from view on the right ("ips" in Fig. 4B).

The paired lateral elements of the basicranium are the alisphenoids, squamosals, petrosals, exoccipitals ("eo" in Fig. 4A), and entotympanics. As is typical in adult mammals, the alisphenoids are not differentiated suturally from the basisphenoid (and the pterygoids) and the exoccipitals are not differentiated from the basioccipital. We identify these elements following the practice used by the first author in prior publications (e.g., Wible 2008; Wible and Spaulding 2013). At the posterior contact between the petrosal and squamosal, there is some fusion between the two bones.

Posterior to its tympanic process, the alisphenoid has a broad surface that slopes dorsally and posteriorly to contact the petrosal (Fig. 4) and represents an epitympanic wing (sensu MacPhee 1981). The medial and lateral ends of the epitympanic wing are downturned, the former contacting the basioccipital tympanic process (Fig. 5) and the latter the squamosal entoglenoid process (Fig. 4B). This construction forms a large concavity at the front of the ear region. Within this concavity are two distinct surfaces (Fig. 4B). The slightly smaller and more dorsally positioned lateral surface is a smooth concavity that housed part of the middle ear cavity, a hypotympanic sinus (sensu Archer 1976; "hs" in Figs. 4B, 5). The medial surface is bisected by an anteromedially directed groove for the nerve of the pterygoid canal ("*" in Figs. 4B, 5). This groove leads to a foramen within the anteriormost part of the medial surface that is hidden in ventral view by the medial section of the alisphenoid tympanic process. A canal runs forward from the foramen and ultimately opens in the endocranial floor of the sphenorbital fissure. En route, this canal joins and then leaves the transverse canal that crosses the basisphenoid midline. Based on the left side, the entotympanic covers this medial surface of the alisphenoid ("enf" in Fig. 4B) except for a small area at its posterolateral end where the groove originates. This encloses most of the groove for the nerve of the pterygoid canal in a complete canal. Immediately posterior to the origin of the groove is the well-developed carotid foramen ("cf" in Fig. 4B) in the suture between the alisphenoid and petrosal.

Dorsolateral to the entoglenoid process of the squamosal is the mediolaterally broad glenoid fossa ("gf" in Figs. 4B, 5), whose surface is generally flat. The glenoid is bordered posteriorly by a robust postglenoid process ("pgp" in Figs. 4B, 5), which is the tallest process on the basicranium (Fig. 6A). The articular surface of the glenoid extends onto the anterior face of the postglenoid process (Fig. 4B). Posteromedial to the postglenoid process is the large postglenoid foramen ("pgf" in Fig. 4B), medial to which is a gap between the postglenoid and entoglenoid processes,

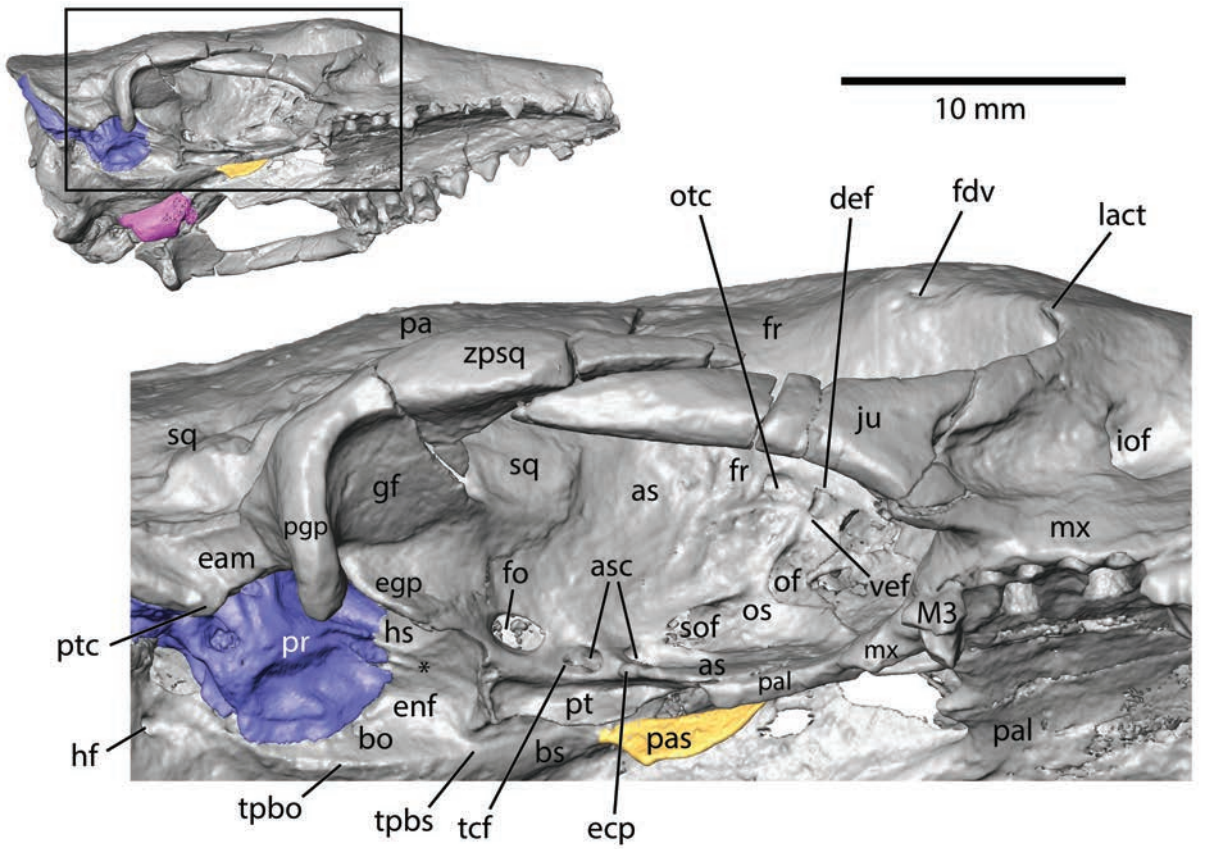

Fig. 5.—*Leptictis haydeni* ANSP 11402, right orbit isosurface from CT scans in oblique in ventrolateral view. Asterisk is in groove for nerve of pterygoid canal. Petrosal in blue; parasphenoid in gold. Abbreviations: **as,** alisphenoid; **asc,** alisphenoid canal; **bo,** basioccipital; **bs,** basisphenoid; **def,** dorsal ethmoidal foramen; **eam,** external acoustic meatus; **ecp,** ectopterygoid process; **egp,** entoglenoid process of squamosal; **enf,** entoglenoid facet (on alisphenoid and basioccipital); **enp,** entopterygoid process; **fdv,** frontal diploic vein foramen; **fo,** foramen ovale; **fr,** frontal; **gf,** glenoid fossa; **hf,** hypoglossal foramen; **hs,** hypotympanic sinus; **iof,** infraorbital foramen; **ju,** jugal; **lact,** lacrimal tubercle; **M3,** upper third molar; **mx,** maxilla; **of,** optic foramen; **os,** orbitosphenoid; **otc,** orbitotemporal canal (anterior opening); **pa,** parietal; **pal,** palatine; **pas,** parasphenoid; **pgp,** postglenoid process; **pr,** promontorium of petrosal; **pt,** pterygoid; **ptc,** posttympanic crest; **sof,** sphenorbital fissure; **sq,** squamosal; **tcf,** transverse canal foramen; **tpbo,** tympanic process of basioccipital; **tpbs,** tympanic process of basisphenoid; **vef,** ventral ethmoidal foramen; **zpsq,** zygomatic process of squamosal.

the Glaserian fissure ("Gf" in Fig. 4B). Behind the postglenoid process is a shallowly concave surface on the squamosal that slopes dorsolaterally and forms the roof of the external acoustic meatus ("eam" in Fig. 5). Behind that is a mediolaterally compressed eminence on the squamosal that contacts a similar shaped eminence on the petrosal. Both eminences run obliquely, posterolaterally to anteromedially. The posterior end of the squamosal eminence is the posttympanic process and the anterior end is the posttympanic crest (sensu Wible et al. 2004; "ptp" and "ptc" in Fig. 4B); the parallel structures on the petrosal are the paroccipital process and tympanohyal (see below).

On the braincase wall, a well-developed suprameatal crest (sensu Wible 2008; "smc" in Fig. 7A) extends posteriorly from the dorsal margin of the zygomatic process ("zpsq" in Fig. 7A), bisecting the lateral squamosal surface. The dorsal half of the squamosal has three foramina for rami temporales ("frt" in Fig. 7A), with the middle one the largest. The ventral half has one large suprameatal foramen ("smf" in Fig. 7A) comparable in size to the postglenoid foramen. The suprameatal foramen sits in the anterior aspect of a distinct suprameatal fossa (sensu Novacek 1986; "smfs" in Fig. 7A) and is directed posterolaterally. These four foramina on the lateral surface of the squamosal communicate with each other and with the postglenoid foramen internally. Please note that the term suprameatal fossa is also used for a non-homologous depression in the squamosal roof of the external acoustic meatus in some carnivorans (e.g., Tedford 1976; Schmidt-Kittler 1981) possibly for the pars flaccida of the tympanic membrane (Hunt 1987).

The exoccipital is posterolateral to and continuous with the basioccipital (Fig. 4A). The two bones in extant juvenile placentals are distinguished by an oblique suture that

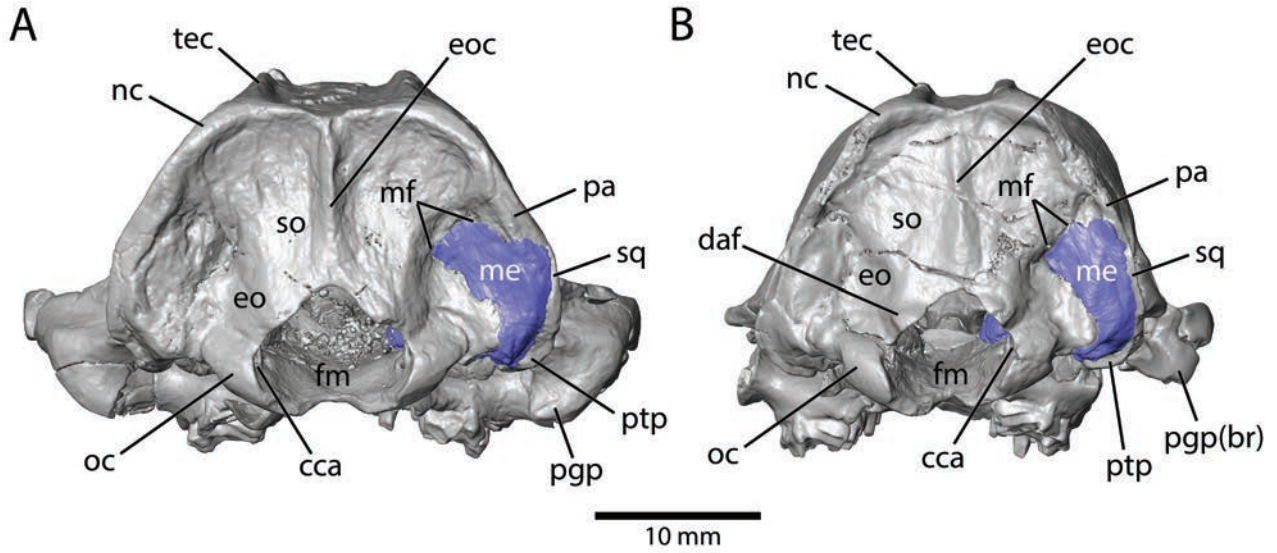

Fig. 6.—Crania isosurfaces from CT scans in posterior view. **A,** *Leptictis haydeni* ANSP 11402; **B,** *Leptictis dakotensis* SDSM 62369. Petrosal in blue. Abbreviations: **cca,** condyloid canal; **daf,** dorsal atlantal facet; **eo,** exoccipital; **eoc,** external occipital crest; **fm,** foramen magnum; **me,** mastoid exposure of petrosal; **mf,** mastoid foramen; **nc,** nuchal crest; **oc,** occipital condyle; **pa,** parietal; **pgp,** postglenoid process; **pgp(br),** postglenoid process (broken); **ptp,** posttympanic process; **so,** supraoccipital; **sq,** squamosal; **tec,** temporal crest.

runs anterolaterally from the anterior rim of the foramen magnum toward the jugular foramen such that the hypoglossal foramen is entirely in the exoccipital and that the basioccipital separates the occipital condyles from each other along the anterior rim (Wible and Spaulding 2013). The left exoccipital of ANSP 11402 has a single hypoglossal foramen ("hf" in Figs. 4B, 5) on the ventral and dorsal surfaces, whereas the right has two dorsal foramina leading to a single ventral one. The jugular foramen ("jf" in Fig. 4B) is the largest in the cranium after the foramen magnum. At the posterolateral corner of the exoccipital is a low rounded eminence, the paracondylar process ("pcp" in Fig. 4B).

The preserved left entotympanic can be treated in two parts: a thick anterior part and a laminar, bowl-shaped posterior part (Fig. 4). The former anterior part occupied facets on the tympanic process of the basioccipital and the tympanic process and epitympanic wing of the alisphenoid, where it enclosed the nerve of the pterygoid canal (see above). The latter posterior part occupied facets on the tympanic process of the basioccipital and rostral tympanic process (Fig. 8) and epitympanic wing of the petrosal (see below). The bone of the anterior part does not appear to be fully ossified and, therefore, may contain some cartilage. The bowl of the posterior part encloses the anteromedial area of the middle ear cavity and has a deep notch in its anterolateral aspect that marked the passageway of the auditory tube ("at" and arrow in Fig. 4B) connecting the middle ear to the nasopharynx. Most of the lateral border of the bowl appears unbroken, and therefore, the entotympanic did not fully cover the pars cochlearis in ventral view (Fig. 4A). However, there is breakage on the posterior margin of the bowl that reveals that part of the entotympanic is missing, and facets on the petrosal suggest that the entotympanic extended farther posterolaterally, possibly reaching the entrance of the internal carotid artery into the middle ear ("gica" in Figs. 4B, 9A; see below). Rostral to the anteromedial corner of the entotympanic is a narrow sulcus on the basisphenoid ("?" in Fig. 4B) that dead ends posteriorly at the entotympanic and does not communicate with the middle ear. Novacek (1986: fig. 20) identified a similar sulcus in *L. dakotensis* as for the Eustachian canal [=auditory tube], which would require a conduit into the middle ear. *Leptictis haydeni* clearly lacks such a conduit and elsewhere has an appropriately positioned notch in the entotympanic for the auditory tube. If correctly identified by Novacek (1986), the course of the auditory tube is quite different between *L. dakotensis* and *L. haydeni*.

The main elements in posterior view are the supraoccipital ("so" in Fig. 6A) and the paired exoccipitals and mastoid exposures of the petrosals ("me" in Fig. 6A). There is also a triangular exposure of parietal ("pa" in Fig. 6A) between the supraoccipital and mastoid exposure. Two mastoid foramina are present on the dorsal border of the mastoid exposure ("mf" in Fig. 6A): a medial one between the petrosal and supraoccipital and a lateral one at the juncture of those two bones with the parietal. On the left side is a remnant of the suture between the exoccipital and supraoccipital. It shows that the supraoccipital contributed to the dorsal rim of the foramen magnum. The supraoccipital also extends onto the top of the braincase (Fig. 7A). On the occiput midline, the supraoccipital has a sharp

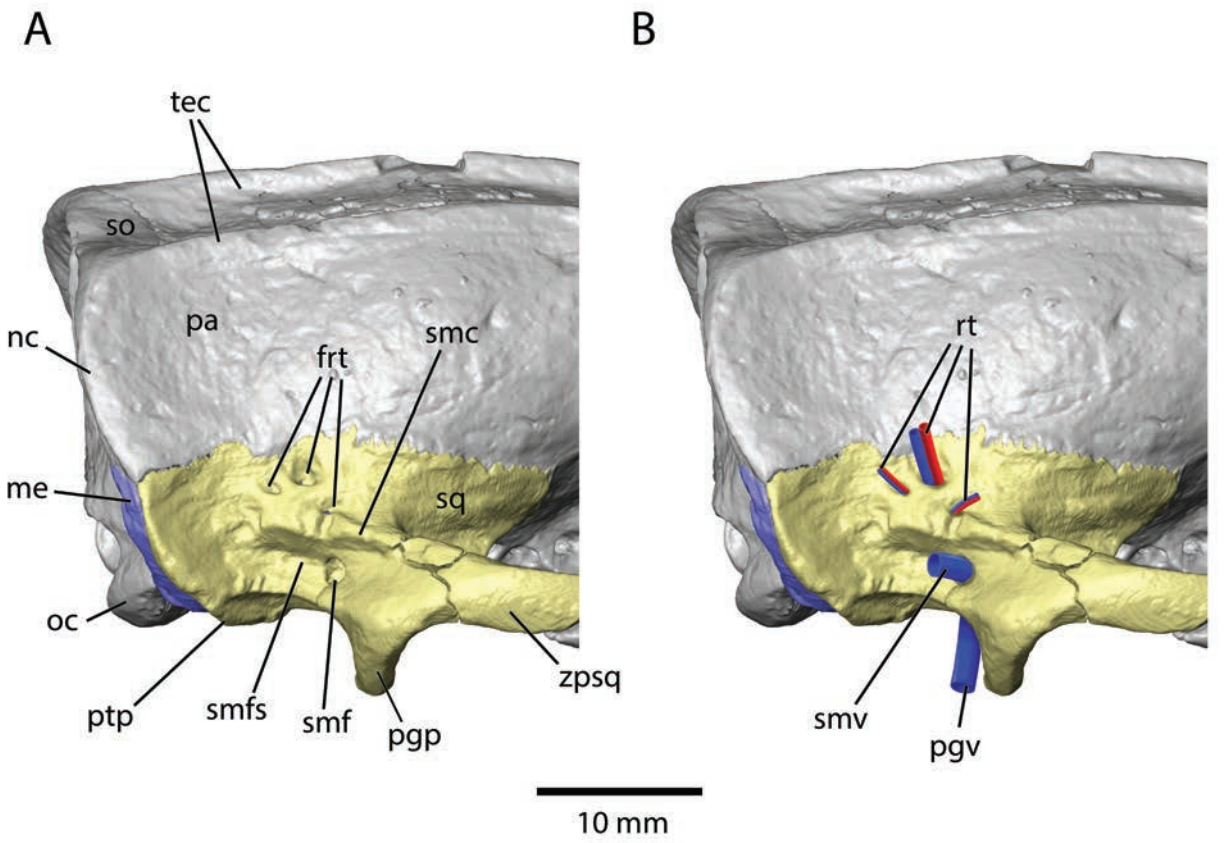

Fig. 7.—**A,** *Leptictis haydeni* ANSP 11402, right posterior braincase isosurface from CT scans in oblique lateral view. (mastoid exposure of petrosal in blue; squamosal in yellow); **B,** with major vessels (arteries in red, veins in blue) reconstructed on squamosal. Abbreviations: **frt,** foramen for ramus temporalis; **me,** mastoid exposure of petrosal; **nc,** nuchal crest; **oc,** occipital condyle; **pa,** parietal; **pgp,** postglenoid process; **pgv,** postglenoid vein; **ptp,** posttympanic process; **rt,** ramus temporalis; **smc,** suprameatal crest; **smf,** suprameatal foramen; **smfs,** suprameatal fossa; **smv,** suprameatal vein; **so,** supraoccipital; **sq,** squamosal; **tec,** temporal crest; **zpsq,** zygomatic process of squamosal.

external occipital crest ("eoc" in Fig. 6A) that is continuous dorsally with the prominent nuchal crest ("nc" in Fig. 6A). From dorsomedial to ventrolateral, the nuchal crest is formed by the supraoccipital, parietal, and squamosal, ending at the posttympanic process. The occipital condyle on the exoccipital ("oc" in Fig. 6A) is roughly as tall as wide. Medial to the condyle, within the foramen magnum is the posterior opening of the condyloid canal ("cca" in Fig. 6A).

Both petrosals show some damage but most features can be reconstructed between the two sides. We illustrate the more complete right petrosal, although it too has some broken surfaces. The petrosal is considered in two parts, the anteroventromedial pars cochlearis (housing the cochlear duct and saccule) and the posterodorsolateral pars canalicularis (housing the utricle and semicircular canals).

In ventral view, in situ in the cranium (Fig. 4A), the lateral border of the petrosal contacts the squamosal, the anterior border primarily the alisphenoid, the anteromedial border the basioccipital, and the posteromedial border the exoccipital. The broad gap between the basioccipital and exoccipital contacts is the jugular foramen ("jf" in Fig. 4B). The narrow posterior border of the petrosal is exposed on the occiput as the mastoid exposure (Fig. 6).

In ventral view of the isolated petrosal, the rounded eminence at the back of the pars cochlearis is the promontorium ("pr" in Fig. 9A). Opening into the rear of the promontorium is the large aperture of the cochlear fossula or round window ("acf" in Fig. 9A), which is damaged on both sides. Opening into the posterolateral surface of the promontorium is the fenestra vestibuli or oval window ("fv" in Fig. 9A), which is well preserved bilaterally and recessed in a shallow vestibular fossula. The stapedial ratio (length to width; Segall 1970) is 1.9 on the right and 2.0 on the left. The bar of bone separating the round and oval windows is the crista interfenestralis ("*" in Fig. 9A); its breadth is subequal to the length of the oval window.

Crossing the promontorium are subtle vascular grooves for the internal carotid artery and its primary branch, the stapedial artery ("gica" and "gsa" in Fig. 9A). The internal carotid groove starts posteriorly on the promontorium ventromedial to the aperture of the cochlear fossula and

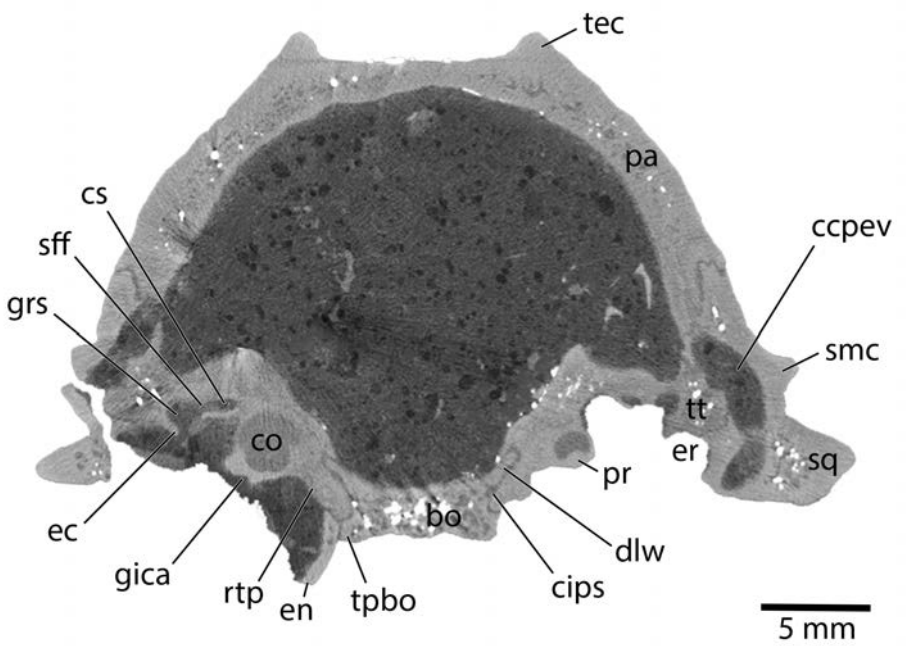

Fig. 8.—*Leptictis haydeni* ANSP 11402, coronal CT section 403 through basicranium at secondary facial foramen. Some white mineral deposits were removed from the endocranial cavity to reduce glare. Abbreviations: **bo,** basioccipital; **cips,** canal for inferior petrosal sinus; **ccpev,** canal for capsuloparietal emissary vein; **co,** cochlear duct; **cs,** cavum supracochleare; **dlw,** dorsolateral wing of basioccipital; **ec,** epitympanic crest; **en,** entotympanic; **er,** epitympanic recess; **gica,** groove for internal carotid artery; **grs,** groove for ramus superior; **pa,** parietal; **pr,** promontorium of petrosal; **rtp,** rostral tympanic process of petrosal; **sff,** secondary facial foramen; **smc,** suprameatal crest; **sq,** squamosal; **tec,** temporal crest; **tpbo,** tympanic process of basioccipital; **tt,** tegmen tympani.

curves anteriorly. It gives off laterally a narrower groove for the stapedial artery directed at the fenestra vestibuli. The internal carotid groove continues forward and then angles anteromedially into a deep sulcus that ends at the carotid foramen between the petrosal and alisphenoid ("cf" in Fig. 4B). The internal carotid and stapedial arteries are reconstructed into these grooves in Figure 10A ("ica" and "sa"); as typical for mammals (Evans and Christensen 1979), the internal carotid artery is accompanied by the sympathetic internal carotid nerve ("icn" in Fig. 10A). The sharp lateral wall of the internal carotid groove is continuous with a crest on the alisphenoid epitympanic wing that forms the medial wall of the hypotympanic sinus and represents an anterior septum (sensu MacPhee 1981; "ase" in Fig. 9A). The anterior septum and deep carotid sulcus are anterior to the promontorium on a laminar shelf, the epitympanic wing ("ew" in Fig. 9A), and divide the wing into medial and lateral parts. The lateral part has an oval-shaped concavity, much longer than wide, that housed the tensor tympani muscle ("ttf" in Fig. 9A). The medial part is continuous with a ventromedially directed digitiform shelf, the rostral tympanic process ("rtp" in Figs. 8, 9A), which abuts the tympanic process of the basioccipital. The ventromedial surface of the rostral tympanic process has a narrow facet (dashed lines in Fig. 9A) that based on the left side contacted the entotympanic (Fig. 8).

In ventral view (Fig. 9A), the pars canalicularis is lateral and posterolateral to the pars cochlearis. The tallest structure on the pars canalicularis is the mediolaterally compressed paroccipital process ("pp" in Fig. 9A) at the posterolateral corner, which abutted the posttympanic process and crest of the squamosal (Fig. 4). At the anterior end of the paroccipital process is the medially directed tympanohyal ("th" in Fig. 9A). The tympanohyal is short, rounded, and sits opposite the crista interfenestralis. Arising from the anterior face of the paroccipital process is a narrow crest, the crista parotica ("cp" in Fig. 9A), which is broken on the right side. On the left side, the crista parotica continues forward as the epitympanic crest to a prominent anteroventrally directed process, the tegmen tympani, and forms the medial wall of the epitympanic recess ("tt" and "er" in Figs. 8, 9A), the space over the mallear-incudal articulation. The epitympanic recess is oval, longer than wide, with its medial half on the petrosal and lateral half on the squamosal (Figs. 4B, 8). In the rear of the epitympanic recess is a distinct depression, the fossa incudis, for the short process of the incus on the anterior face of the paroccipital process, lateral to the crista parotica (not visible in the figures). In the isolated petrosal, the tegmen tympani ends as a broad, rounded process ("tt" in Figs. 9A, 11A), but in the intact cranium, much of this is covered laterally by the squamosal and the tegmen tapers to a point (Fig. 4).

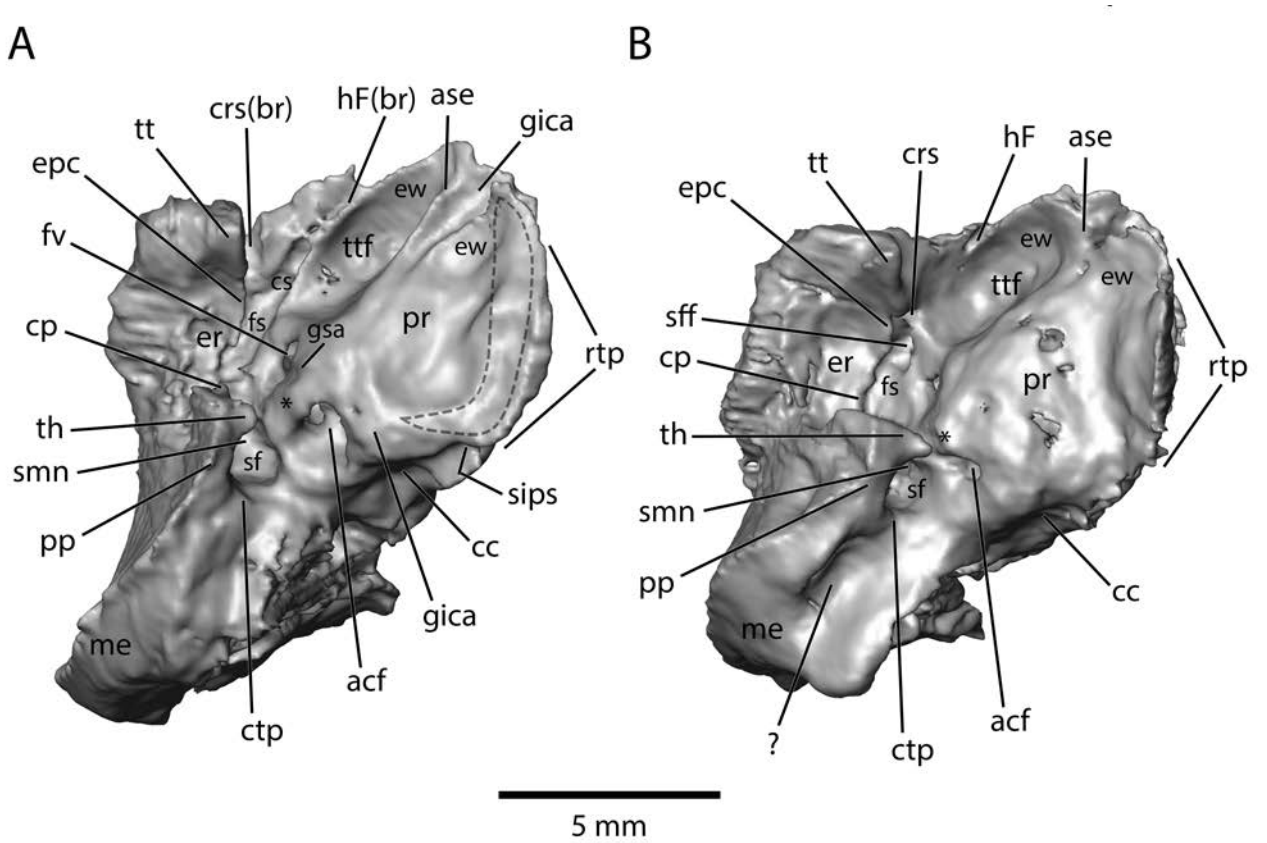

Fig. 9.—Right petrosal isosurfaces from CT scans in ventral view (anterior to top of page). **A,** *Leptictis haydeni* ANSP 11402; **B,** *Leptictis dakotensis* SDSM 62369. Asterisk is on crista interfenestralis; question mark in B indicates a sulcus of uncertain function suggested to accommodate the digastric muscle (Novacek 1986). Based on the left side of ANSP 11402, missing bone enclosed the canal for the ramus superior and floored the cavum supracochleare to form a secondary facial foramen. Abbreviations: **acf,** aperture of cochlear fossula; **ase,** anterior septum; **cc,** cochlear canaliculus; **cp,** crista parotica; **crs,** canal for ramus superior; **crs(br),** canal for ramus superior (broken); **cs,** cavum supracochleare; **ctp,** caudal tympanic process; **epc,** epitympanic crest; **er,** epitympanic recess; **ew,** epitympanic wing; **fs,** facial sulcus; **fv,** fenestra vestibuli; **gica,** groove for internal carotid artery; **gsa,** groove for stapedial artery; **hF,** hiatus Fallopii; **hF(br),** hiatus Fallopii (broken); **me,** mastoid exposure; **pp,** paroccipital process; **pr,** promontorium; **rtp,** rostral tympanic process; **sf,** stapedius fossa; **sff,** secondary facial foramen; **sips,** sulcus for inferior petrosal sinus; **smn,** stylomastoid notch; **th,** tympanohyal; **tt,** tegmen tympani; **ttf,** tensor tympani fossa.

In ventral view of the cranium, the anterior face of the tegmen tympani abuts the squamosal (Fig. 4A), but this is a thin veneer dorsal to which is a broader contact with the alisphenoid ("sas" in Fig. 11A). The medial margin of the tegmen tympani is continuous with the crest on the alisphenoid and squamosal forming the lateral wall of the hypotympanic sinus ("hs" in Fig. 4B).

Between the crista parotica and oval window is a longitudinal gutter serving for the passageway of the facial nerve and stapedial artery, the facial sulcus ("fs" in Fig. 9A). On the right side, the facial sulcus bifurcates anteriorly into two sulci, one directed anteromedially for the facial nerve ("cs" in Fig. 9A) and the other slightly anterolaterally for the stapedial artery ("crs" in Fig. 9A). Both sulci continue forward to the anterior end of the petrosal; the medial one has some bits of bone that enclose short canals. The left side of ANSP 11402 preserves more bone here, and at least some of the bone missing on the right side is the result of breakage (Fig. 8). The two sulci on the right side are canals on the left side (and on SDSM 62369 in Fig. 9B), and there are openings at the anterior and posterior ends of both canals. Posteriorly, these are the secondary facial foramen medially ("sff" in Fig. 8) and the foramen for the ramus superior of the stapedial artery laterally. Anteriorly, the medial canal opens on the basicranium between the petrosal and alisphenoid at the hiatus Fallopii ("hF(br)" in Fig. 9A) for the greater petrosal nerve; the lateral canal for the ramus superior opens endocranially in the middle cranial fossa ("crs" in Fig. 11A). Missing bone on the right petrosal reveals the cavum supracochleare for the geniculate ganglion of the facial nerve, which is floored on the left ("cs" in Figs. 8, 9A); in the dorsomedial aspect of the right cavum supracochleare is the primary facial foramen leading to the internal acoustic meatus (not visible in the

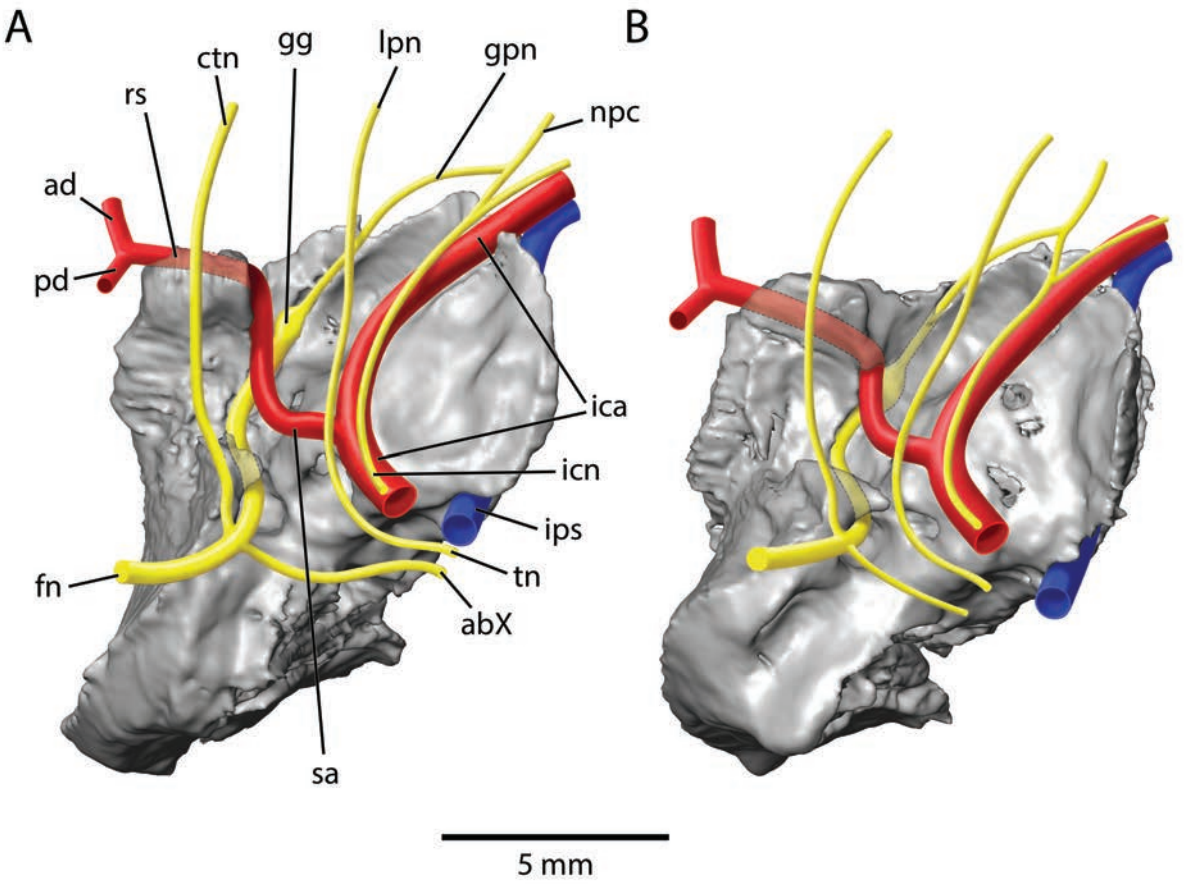

Fig. 10.—Right petrosal isosurfaces from CT scans in ventral view with major neurovascular structures reconstructed (arteries in red; veins in blue; nerves in yellow). **A,** *Leptictis haydeni* ANSP 11402; **B,** *Leptictis dakotensis* SDSM 62369. The neurovascular structures in A and B are essentially identical and are labeled only in A. The geniculate ganglion and greater petrosal nerve in A are exposed due to damage; they are enclosed in bone on the left petrosal of ANSP 11402 as on both sides of SDSM 62369. Abbreviations: **abX,** auricular branch of vagus nerve; **ad,** anterior division of ramus superior; **ctn,** chorda tympani nerve; **fn,** facial nerve; **gg,** geniculate ganglion; **gpn,** greater petrosal nerve; **ica,** internal carotid artery; **icn,** internal carotid nerve; **ips,** inferior petrosal sinus; **lpn,** lesser petrosal nerve; **npc,** nerve of pterygoid canal; **pd,** posterior division of ramus superior; **rs,** ramus superior of stapedial artery; **sa,** stapedial artery; **tn,** tympanic nerve.

figures). We reconstruct the facial nerve, ramus superior, and their branches in Figure 10A ("fn" and "rs").

Recessed in the interval between the tympanohyal and crista interfenestralis is the well-developed fossa for the stapedius muscle ("sf" in Fig. 9A). It is oval with its long axis anterolateral to posteromedial. There is no visible continuation of the facial sulcus lateral to the stapedius fossa, but the facial nerve must have taken that route to reach its exit from the middle ear (Fig. 10A) at the stylomastoid notch ("smn" in Fig. 9A) behind the tympanohyal. There is little in the way of crests on the rear of the pars canalicularis. Running medially from the base of the paroccipital process is a subtle crest, the lateral section (lateral to the stapedius fossa) of the caudal tympanic process of the petrosal (sensu MacPhee 1981; "ctp" in Fig. 9A). The medial and lateral sections (medial to the stapedius fossa) of the caudal tympanic process are absent.

In dorsal view, two large openings dominate the endocranial surface: the internal acoustic meatus on the pars cochlearis ("fai" and "fas" in Fig. 12A) and the subarcuate fossa on the pars canalicularis ("saf" in Fig. 12A). The internal acoustic meatus is shallow with a low transverse crest ("tc" in Fig. 12A) delimiting the foramen acusticum inferius from the foramen acusticum superius. Ventral to the medial edge of the pars cochlearis is a ventromedially directed shelf that represents the dorsal surface of the rostral tympanic process. Where the rostral tympanic process meets the pars cochlearis is a deep sulcus best seen in medial view (Fig. 13A). This sulcus is not vascular but holds the lateral ends of the dorsolateral wings on the basisphenoid and basioccipital ("dlw" in Fig. 8). Anterior to the internal acoustic meatus is the relatively broad prefacial commissure at the edge of which is a distinct crista petrosa ("pfc" and "crp" in Fig. 12A). The crista petrosa extends

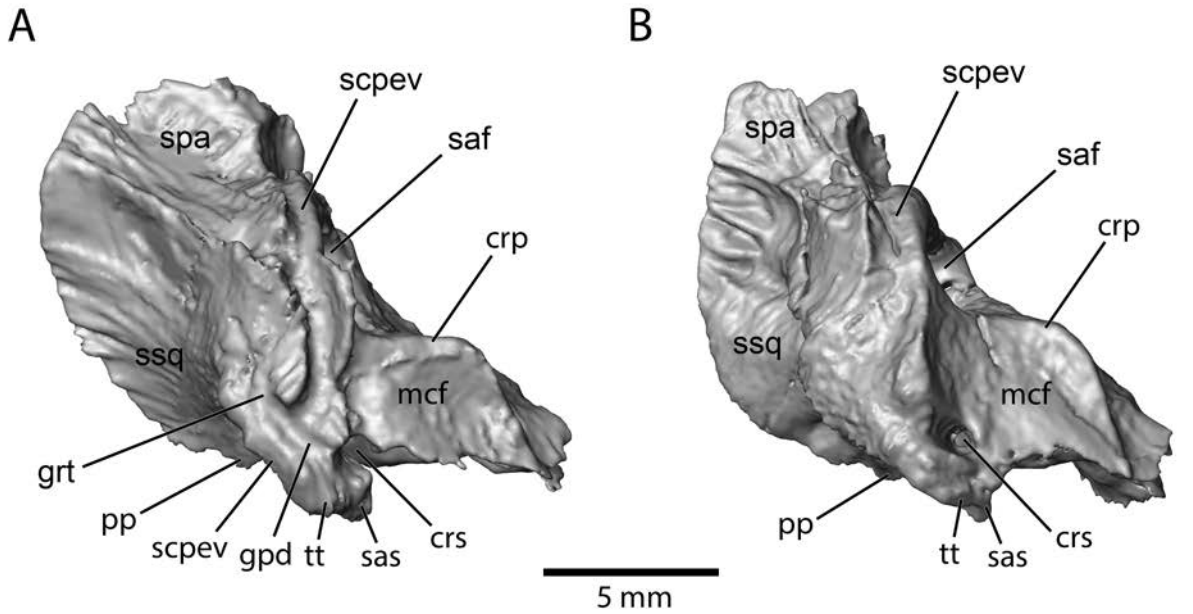

Fig. 11.—Right petrosal isosurfaces from CT scans in oblique anterolateral view (anterior to right of page). **A,** *Leptictis haydeni* ANSP 11402; **B,** *Leptictis dakotensis* SDSM 62369. Based on the left side of ANSP 11402, missing bone enclosed the canal for the ramus superior. Abbreviations: **crp,** crista petrosa; **crs,** canal for ramus superior; **gpd,** groove for posterior division of ramus superior; **grt,** groove for ramus temporalis; **mcf,** surface in middle cranial fossa; **pp,** paroccipital process; **saf,** subarcuate fossa; **sas,** surface for alisphenoid; **scpev,** sulcus for capsuloparietal emissary vein; **spa,** surface for parietal; **ssq,** surface for squamosal; **sss,** sulcus for sigmoid sinus; **tt,** tegmen tympani.

posteriorly onto the pars canalicularis and forms the anterior margin of the subarcuate fossa. Anterior to the crista is a very narrow surface of petrosal that contributes to the rear wall of the middle cranial fossa and abuts the alisphenoid ("mcf" in Figs. 11A, 12A).

The subarcuate fossa is round, deeper than wide, and much larger than the internal acoustic meatus (Fig. 12A). Its posterior half is rimmed by large venous sulci, for the sigmoid sinus posteromedially and for the capsuloparietal emissary vein posterolaterally ("sss" and "scpev" in 12A). In the sulcus for the sigmoid sinus is a vascular foramen that opens within the dorsal depth of the subarcuate fossa, which we term the dorsal subarcuate foramen ("dsf" in Fig. 12A). A second much larger ventromedial aperture opens into the medial depth of the subarcuate fossa from the sulcus for the sigmoid sinus, which we term the medial subarcuate fenestra ("msf" in Figs. 12A, 13A). Both of these openings into the subarcuate fossa are preserved bilaterally and are not the result of damage. The sulcus for the capsuloparietal emissary vein continues onto the lateral surface of the pars canalicularis (Fig. 11A) where its walls are higher, producing a deeper sulcus. On the lateral aspect of the tegmen tympani, the sulcus for the capsuloparietal emissary vein near its ventral terminus is interrupted by a groove perpendicular to it carrying the posterior division of the ramus superior ("gpd" in Fig. 11A). Posterior to the sulcus for the capsuloparietal emissary vein, the groove for the posterior division turns dorsally as the groove for the ramus temporalis ("grt" in Fig. 11A). This groove leads to the foramina for rami temporales in the squamosal reported above (Fig. 7A). The groove for the posterior division is continuous anteriorly with the canal for the ramus superior, which on the right side is damaged (Fig. 11A) but is enclosed in the petrosal on the left. The groove for the posterior division leads to the suprameatal and postglenoid foramina (Figs. 4B, 7A). Most of the lateral surface of the pars canalicularis is covered by the squamosal ("sqs" in Fig. 11A) but there is a triangular dorsolateral area that is covered by the parietal ("spa" in Fig. 11A).

The endocranial surface of the basisphenoid and alisphenoids is shown in Figure 14. The main structure on the basisphenoid is the hypophyseal fossa ("hyf" in Fig. 14), which is oval, wider than long. On either side of the fossa is the groove for the internal carotid artery ("gica" in Fig. 14), which fades out anteriorly. The raised posterior wall of the hypophyseal fossa is formed by the prominent dorsum sellae ("ds" in Fig. 14). The lateral end of the dorsum sellae on the left side sports a well-developed posterior clinoid process, which ends in a triangular flattened point that is not in the same plane as the dorsum sellae but is bent anteriorly ("pclp" in fig. 14). The right posterior clinoid process is missing as is some of the dorsum sellae, given that its preserved dorsal edge appears broken. Anterior to the hypophyseal fossa is the endocranial aperture of the pterygoid canal in the basisphenoid ("pc" in Fig. 14) and lateral to that is the foramen ovale in the alisphenoid ("fo" in Fig. 14). A broad sulcus for the trigeminal ganglion extends from the foramen ovale to the sphenorbital fissure ("trs" and "sof" in Fig. 14).

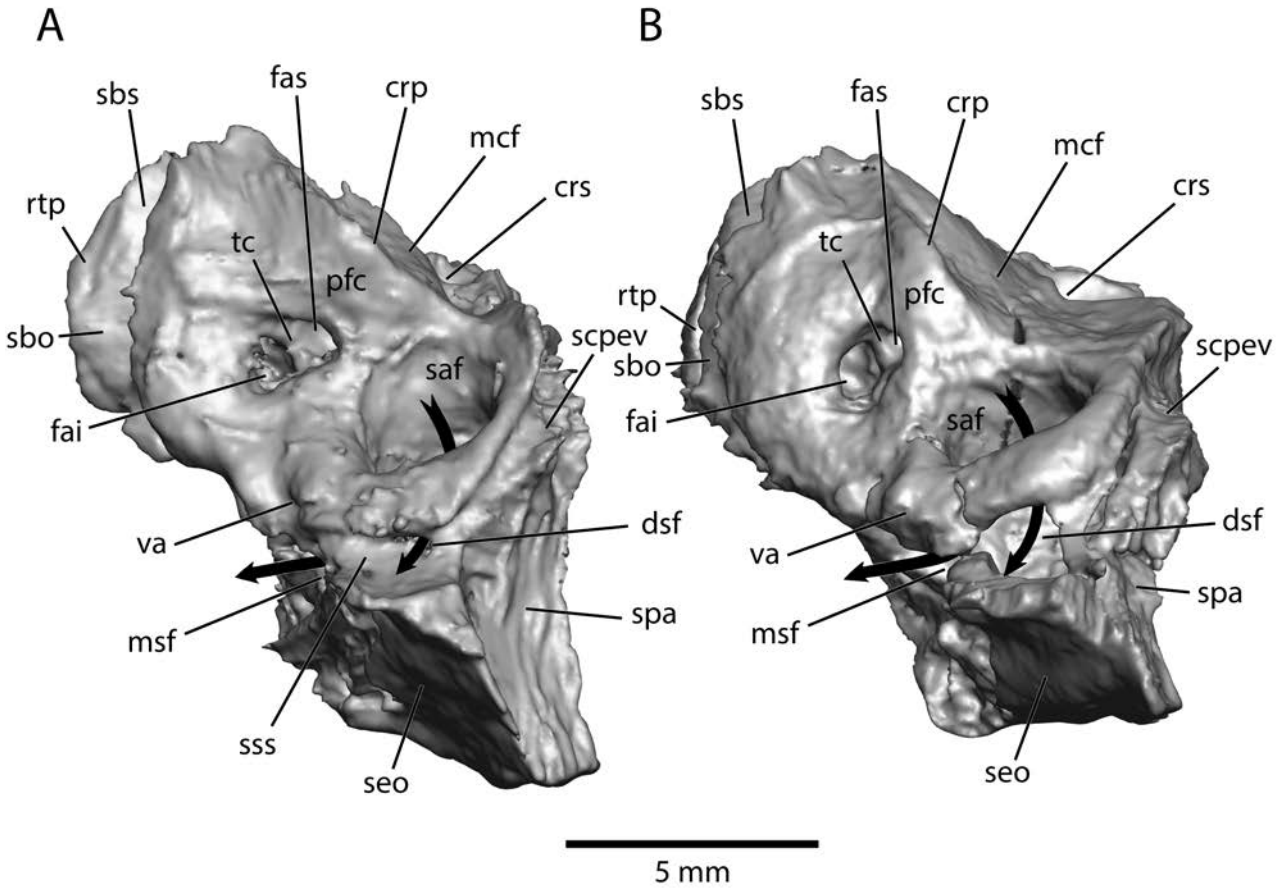

Fig. 12.—Right petrosal isosurfaces from CT scans in dorsal view (anterior to top of page). **A,** *Leptictis haydeni* ANSP 11402; **B,** *Leptictis dakotensis* SDSM 62369. Abbreviations: **crp,** crista petrosa; **crs,** canal for ramus superior; **dsf,** dorsal subarcuate foramen; **fai,** foramen acusticum inferius; **fas,** foramen acusticum superius; **mcf,** surface in middle cranial fossa; **msf,** medial subarcuate fenestra; **pfc,** prefacial commissure; **rtp,** rostral tympanic process; **saf,** subarcuate fossa; **sbs,** surface for dorsolateral wing of basisphenoid; **sbo,** surface for dorsolateral wing of basioccipital; **sbs,** surface for dorsolateral wing of basisphenoid; **scpev,** sulcus for capsuloparietal emissary vein; **seo,** surface for exoccipital; **spa,** surface for parietal; **ssq,** surface for squamosal; **sss,** sulcus for sigmoid sinus; **tc,** transverse crest; **va,** vestibular aqueduct.

Leptictis dakotensis SDSM 62369

This cranium is not as well preserved as *L. haydeni* ANSP 11402 (Fig. 2) regarding its three dimensionality and bone representation. The midline of the posterior palate is raised, and there is some left-right asymmetry. The basicranium (Fig. 15) has numerous cracks and broken structures; for example, little of the zygomas and ento- and ectopterygoid crests remain. As the external surfaces of *L. dakotensis* have been treated in detail by Butler (1956) and Novacek (1986), we focus on features of SDSM 62369 that differ from those reported previously. As some differences are terminological and not morphological, we remind the reader that the Appendix provides a list of synonyms that have been used in describing leptictids.

The orbital foramina resemble those described by Novacek (1986) for *L. dakotensis* with three exceptions. First, Novacek (1986: fig. 10) illustrated two supraorbital foramina (= frontal diploic vein foramina here) above the orbital rim in *L. dakotensis*, noting that this could be single or paired; SDSM 62369 has only one per side. Additionally, each side of SDSM 62369 has two small foramina in the vicinity of the optic foramen, one above and one below, with both opening into a large vascular space in the presphenoid. The one below is the suboptic foramen ("sbof," indicated on the fossil's right side in Fig. 15), and the one above, the supra-optic foramen (sensu Gregory 1910; "spof," indicated on the fossil's left side in Fig. 15). Butler (1956) reported a suboptic foramen for *L. dakotensis* that was in the medial wall of the sphenorbital fissure, but Novacek (1986) was not able to confirm this.

As in *L. haydeni* ANSP 11402, SDSM 62369 has a transverse canal foramen in the basisphenoid anterior to the foramen ovale (not visible in the figures). Further as in

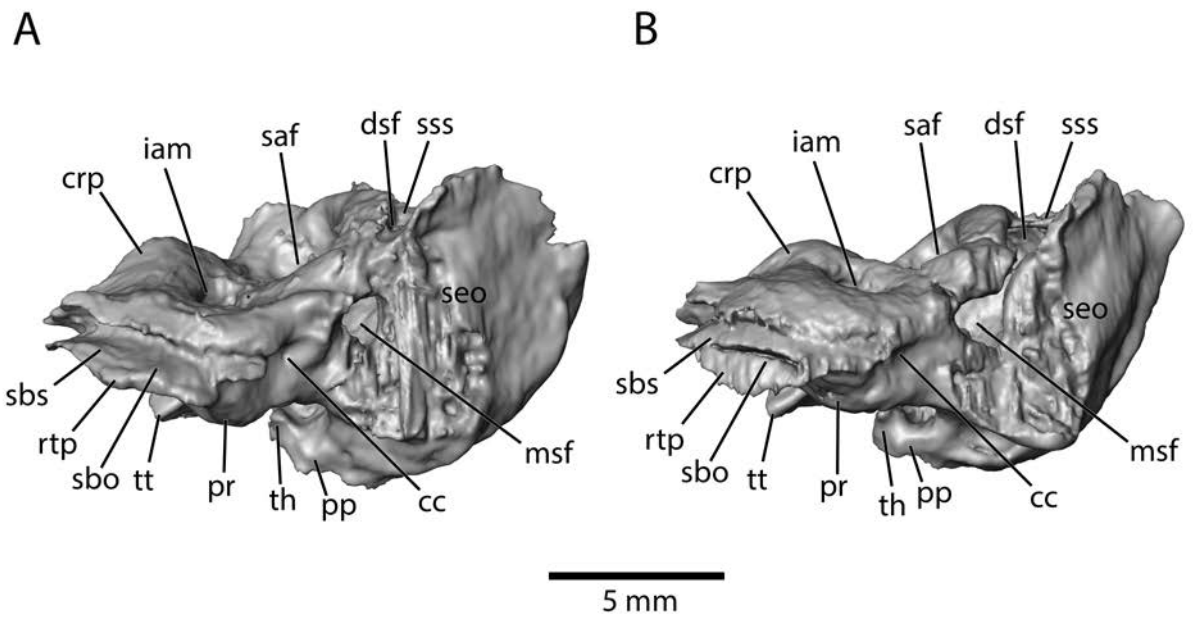

Fig. 13.—Right petrosal isosurfaces from CT scans in oblique medial view (anterior to left of page). **A,** *Leptictis haydeni* ANSP 11402; **B,** *Leptictis dakotensis* SDSM 62369. Abbreviations: **cc,** cochlear canaliculus; **crp,** crista petrosa; **dsf,** dorsal subarcuate foramen; **iam,** internal acoustic meatus; **msf,** medial subarcuate fenestra; **pp,** paroccipital process; **pr,** promontorium; **rtp,** rostral tympanic process; **saf,** subarcuate fossa; **sbo,** surface for dorsolateral wing of basioccipital; **sbs,** surface for dorsolateral wing of basisphenoid; **seo,** surface for exoccipital; **sss,** sulcus for sigmoid sinus; **th,** tympanohyal; **tt,** tegmen tympani.

L. haydeni, it communicates across the midline at a level posterior to the transverse canal foramen. Butler (1956) did not report this opening, while Novacek (1986: figs. 10, 20, 26) found this opening but termed it a foramen subovale and reconstructed the artery of the pterygoid canal in it rather than a vein (see below).

In the basispharyngeal canal, Novacek (1986:40) reported "a well-developed vertical keel" on the midline of the presphenoid in *L. dakotensis*. Stereophotographs of *L. dakotensis* MCZ 19678 (Novacek 1986: fig. 21) show the keel is also beneath the basisphenoid. SDSM 62369 does not have a midline keel, but there is a shallow depression on the anterior basisphenoid ("*" in Fig. 15) in the same place that *L. haydeni* ANSP 11402 has a facet for the parasphenoid.

The basioccipital has a transverse crack anterior to the foramen magnum and is displaced dorsally there (Fig. 15). Anterior to the transverse crack are crests on the midline and lateral margins (i.e., tympanic processes) of the ventral surface of the basioccipital ("tpbo" in Fig. 15), with the left lateral crest damaged. The midline crest and right tympanic process are much more prominent in SDSM 62369 than in *L. haydeni* ANSP 11402 (Fig. 4B) or in the *L. dakotensis* specimens illustrated by Novacek (1986: figs. 2A, 21, 23).

Regarding the foramina for temporal rami on the lateral braincase, there appear to be only two per side in SDSM 62369 (Fig. 2E), a larger anterodorsal one directed dorsally and a smaller posteroventral one directed posteriorly. Butler (1956: fig. 1) illustrated three for *L. dakotensis* and Novacek (1986: figs. 1, 17) showed four.

To date, the petrosal of *L. dakotensis* has not been illustrated isolated from the basicranium. Butler (1956: fig. 3) published drawings of the left petrosal in situ in ventral view, and Novacek (1986: figs. 15, 18–20, 22, 26) the right petrosal in situ in ventral, dorsal, and lateral views; Novacek (1986: figs. 21, 23) also provided stereophotographs of both ear regions of *L. dakotensis* MCZ 19678 in ventral view. We segmented the better-preserved right petrosal of SDSM 62369 in Avizo and illustrate it isolated from the basicranium in four views (Figs. 9B, 10B, 11B, 12B, 13B). Starting with the ventral view (Figs. 9B, 10B), most of the differences shown by SDSM 62369 concern the course of the facial nerve and branches of the stapedial artery, which neither Butler (1956) or Novacek (1986) fully illustrated or described. As in the left side of *L. haydeni* ANSP 11402, SDSM 62369 has a facial sulcus lateral to the fenestra vestibuli that leads forward to the secondary facial foramen ("fs" and "sff" in Fig. 9B), which in turn leads into an enclosed canal with two exits. The main exit is dorsomedially into the foramen acusticum superius of the internal acoustic meatus ("fas" in Fig. 12B) and the secondary one is at the hiatus Fallopii at the anteroventral edge of the petrosal ("hF" in Fig. 9B). We reconstruct the facial

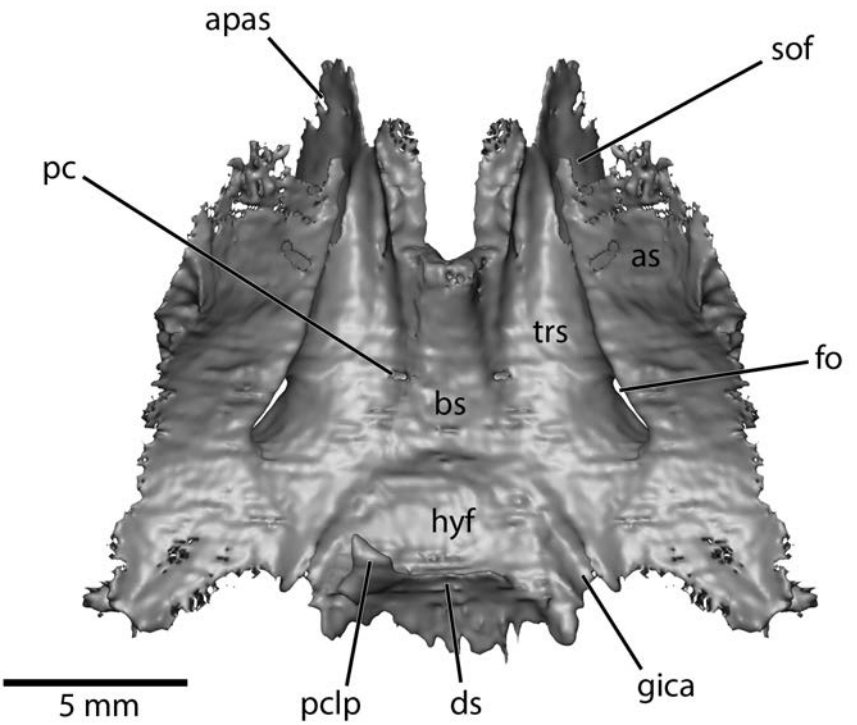

Fig. 14.—*Leptictis haydeni* ANSP 11402, basi- and alisphenoid isosurfaces from CT scans in dorsal view (anterior to top of page). The dorsum sellae is damaged and the right posterior clinoid process is completely missing. Abbreviations: **apas,** anterior process of alisphenoid; **as,** alisphenoid; **bs,** basisphenoid; **ds,** dorsum sellae; **fo,** foramen ovale; **gica,** groove for internal carotid artery; **hyf,** hypophyseal fossa; **pc,** pterygoid canal; **pclp,** posterior clinoid process; **sof,** sphenorbital fissure; **trs,** trigeminal sulcus.

nerve and branches in this canal in Figure 10B as we did in *L. haydeni* ANSP 11402 (Fig. 10A). Butler (1956: fig. 3) illustrated the posterior opening of this canal (our secondary facial foramen) and used dashed lines to show most of this enclosed canal but not the anterior exit at the hiatus Fallopii; he incorrectly reconstructed the ramus inferior of the stapedial artery within this structure, a route unknown for this artery and only known for the facial nerve. Novacek (1986:59) reported but did not illustrate the secondary facial foramen (his opening at the apex of the facial canal) and wrote that "the hiatus Fallopii is not clearly seen on the broken leading edge of isolated petrosals." We speculate that the *L. dakotensis* studied by Butler (1956) and Novacek (1986) have a hiatus Fallopii (and facial nerve course) as in SDSM 62369 that would be revealed via CT scanning.

Turning to the ramus superior of the stapedial artery, as in the left side of *L. haydeni* ANSP 11402, SDSM 62369 has a canal through the tegmen tympani, the posterior opening of which is just anterior to the secondary facial foramen ("crs" in Fig. 9B). Butler (1956: fig. 3) illustrated a comparable aperture, but Novacek (1986) did not indicate a foramen for the ramus superior in any figures. He wrote (1986:61) "The superior ramus of the stapedial… exits from the otic cavity in its usual position–a foramen behind the epitympanic recess." It is unclear to what foramen Novacek (1986) referred. The posterior opening into the ramus superior canal in SDSM 62369 is certainly not behind the epitympanic recess, but is near the anterior aspect of this space (Fig. 9B). We reconstruct the ramus superior on SDSM 62369 (Fig. 10B) resembling the condition in *L. haydeni* ANSP 11402 ("rs" in Fig. 10A).

Next, we address the ramus inferior of the stapedial artery in *L. dakotensis*. As in *L. haydeni* ANSP 11402, we did not find any bony indication of the presence of this artery in SDSM 62369. As noted above, Butler's (1956) reconstruction of a ramus inferior in *L. dakotensis* was mistaken in that he used structures related to the course of the facial nerve. Novacek (1986:55) wrote "The inferior ramus of the stapedial probably exited the tympanic cavity in a small foramen at the forward apex of facial canal [= secondary facial foramen], a point just anterior and lateral to the fenestra ovalis [= fenestra vestibuli]." It is unclear to what Novacek (1986) referred as such a small foramen was not labelled in any of his illustrations; the only opening in this position in SDSM 62369 is the secondary facial foramen (Fig. 9B). The presence of a ramus inferior canal in some *L. dakotensis* and absence in others seems unlikely, and without bony evidence, we interpret this artery as absent, a condition that is not unusual among extant placentals (Wible 1987).

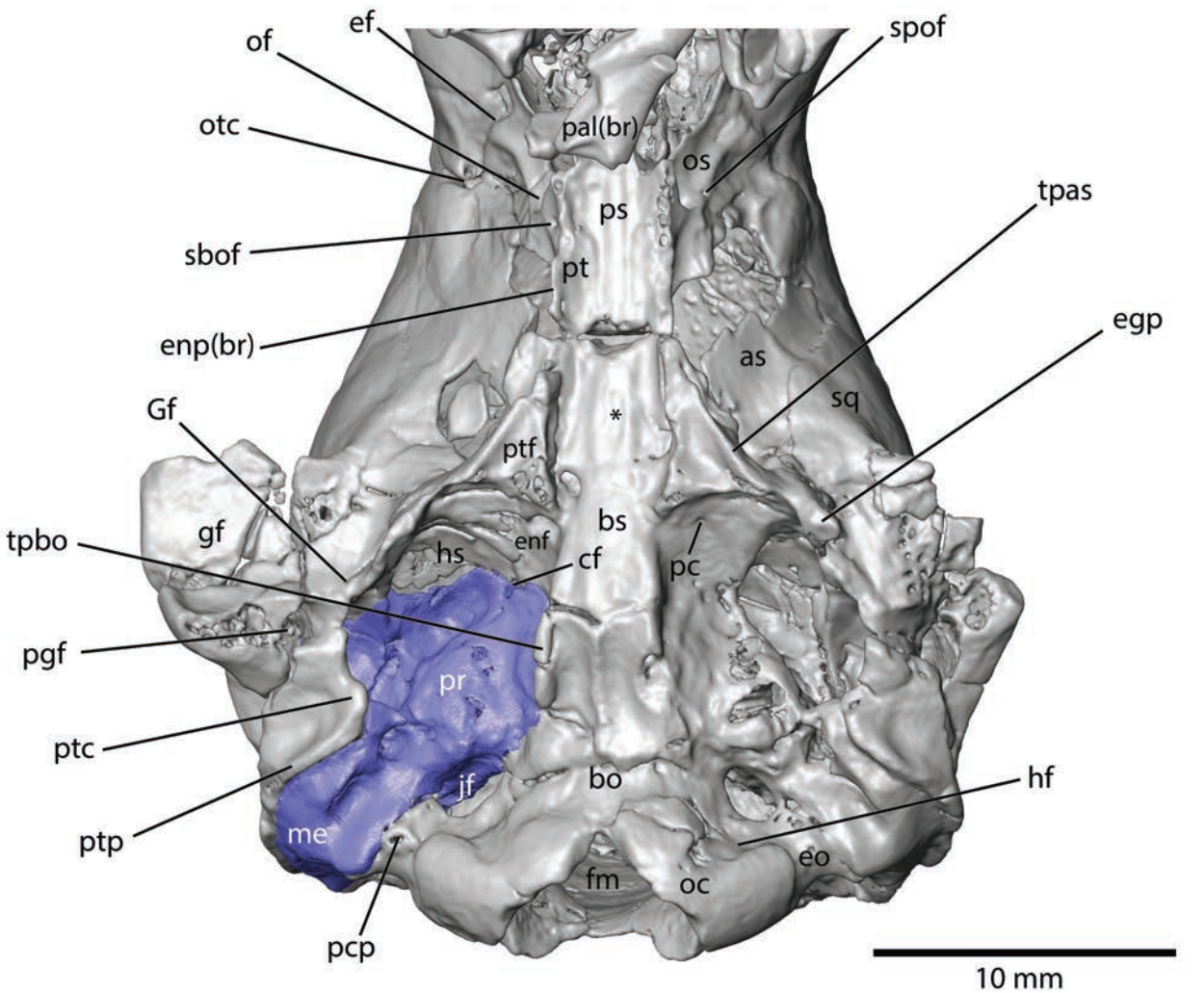

Fig. 15.—*Leptictis dakotensis* SDSM 62369, meso- and basicranium isosurface from CT scans in ventral view. Asterisk is in shallow depression on anterior basisphenoid. Abbreviations: **as,** alisphenoid; **bo,** basioccipital; **bs,** basisphenoid; **cf,** carotid foramen; **ef,** ethmoidal foramen; **egp,** entoglenoid process of squamosal; **enf,** entoglenoid facet (on alisphenoid); **enp(br),** entopterygoid process (broken); **eo,** exoccipital; **fm,** foramen magnum; **fr,** frontal; **gf,** glenoid fossa; **Gf,** Glaserian fissure; **hf,** hypoglossal foramen; **hs,** hypotympanic sinus (on alisphenoid); **jf,** jugular foramen; **me,** mastoid exposure of petrosal; **oc,** occipital condyle; **of,** optic foramen; **os,** orbitosphenoid; **otc,** orbitotemporal canal (anterior opening); **pal(br),** palatine (broken); **pc,** pterygoid canal; **pcp,** paracondylar process of exoccipital; **pgf,** postglenoid foramen; **pr** promontorium of petrosal; **ps,** presphenoid; **pt,** pterygoid; **ptc,** posttympanic crest; **ptf,** pterygoid fossa; **ptp,** posttympanic process of squamosal; **sbof,** suboptic foramen; **sq,** squamosal; **spof,** supraoptic foramen; **tpas,** tympanic process of alisphenoid; **tpbo,** tympanic process of basioccipital.

The ventral surface of the right pars cochlearis of SDSM 62369 is devoid of vascular grooves (Fig. 9B), whereas the left preserves a stapedial sulcus medial to the fenestra vestbuli. Both sides have an anterior septum directed at the carotid foramen in the petrosal-alisphenoid suture. Other *L. dakotensis* preserve distinct promontorial grooves for both the internal carotid and stapedial arteries along with the anterior septum (Butler 1956; McDowell 1958; Novacek 1986). We suggest the absence of vascular grooves in SDSM 62369 is the result of either overzealous preparation (note the small holes in the promontorial surfaces in Figures 2C and 9B) or perhaps postmortem environmental action (such as from water). This may also account for the absence of clear indication of a facet for the entotympanic on the rostral tympanic process where this bullar element is known to attach in other *L. dakotensis* (Novacek 1986). Posterior to the aperture of the cochlear fossula, SDSM 62369 lacks any raised lip of bone (Fig. 9B) that could represent part of the caudal tympanic process (sensu MacPhee 1981). In contrast, the stereophotographs of *L. dakotensis* MCZ 19678 in Novacek (1986: figs. 21, 23) show a raised lip here that could be a low medial section of the caudal tympanic process (sensu MacPhee 1981).

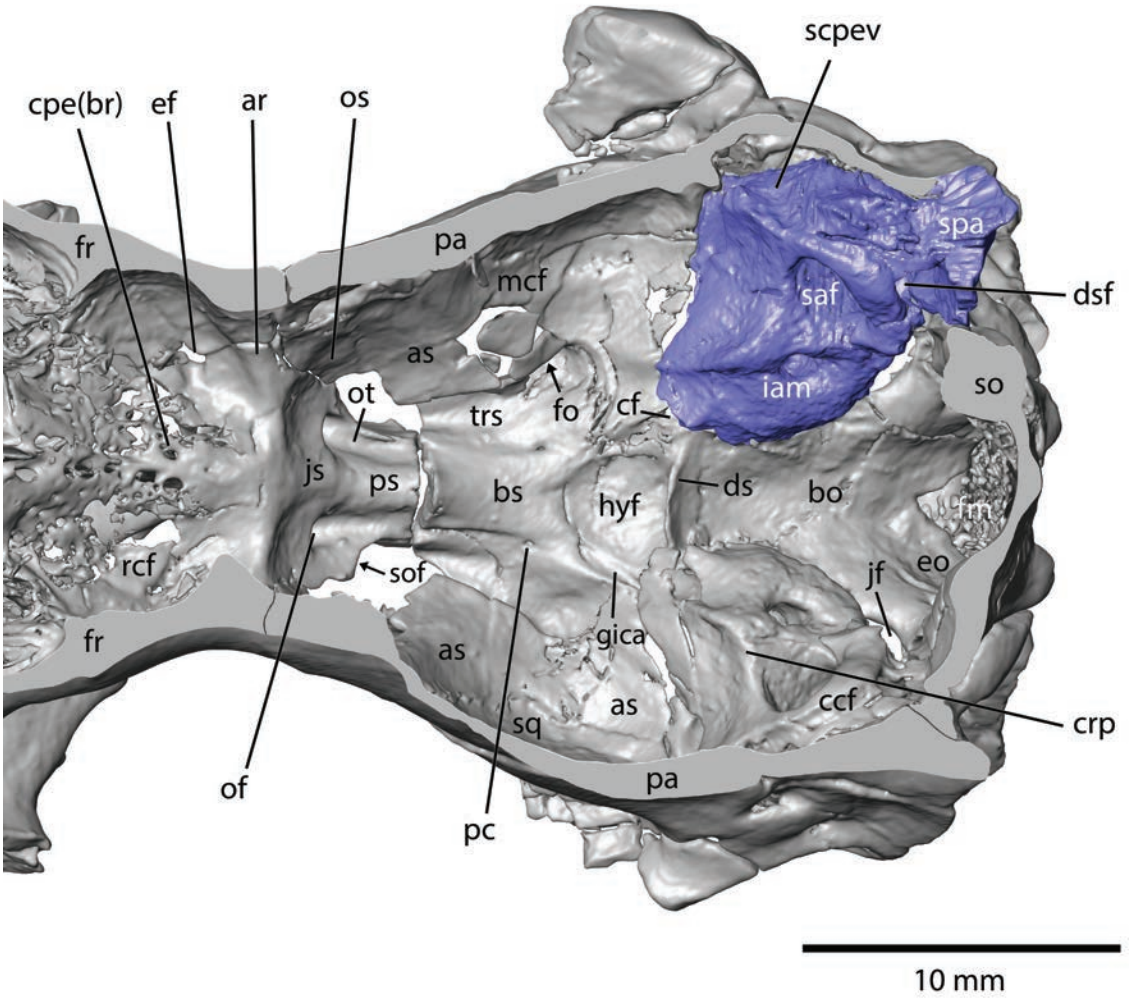

Fig. 16.—*Leptictis dakotensis* SDSM 62369, endocranium isosurface from CT scans in dorsal view. Cut surfaces indicated by uniform gray. Abbreviations: **ar,** annular ridge; **as,** alisphenoid; **bo,** basioccipital; **bs,** basisphenoid; **ccf,** caudal cranial fossa; **cf,** carotid foramen; **cpe(br),** cribriform plate (broken); **crp,** crista petrosa; **ds,** dorsum sellae; **dsf,** dorsal subarcuate fenestra; **ef,** ethmoidal foramen; **eo,** exoccipital; **fo,** foramen ovale; **fr,** frontal; **hyf,** hypophyseal fossa; **gica,** groove for internal carotid artery; **iam,** internal acoustic meatus; **jf,** jugular foramen; **js,** jugum sphenoidale; **mcf,** middle cranial fossa; **of,** optic foramen; **os,** orbitosphenoid; **ot,** optic tract; **pa** parietal; **pc,** pterygoid canal; **ps,** presphenoid; **rcf,** rostral cranial fossa; **saf,** subarcuate fossa; **scpev,** sulcus for capsuloparietal emissary vein; **so,** supraoccipital; **sof,** sphenorbital fissure; **spa,** surface for parietal; **sq,** squamosal; **trs,** trigeminal sulcus.

Novacek (1986:71) wrote in *L. dakotensis* "a large, ossified mastoid tubercle [=tympanohyal] that incorporates the tympanohyal, has a distinct, ventral depression and is well directed medially, nearly contacting the promontorium." SDSM 62369 has a tympanohyal that nearly touches the promontorium but there is only a very faint concavity on its posteroventral aspect ("th" in Fig. 9B). Novacek (1986:56) also observed that in *L. dakotensis* "the mastoid process [=paroccipital process of the petrosal] has a well-developed groove for the digastric muscle that runs diagonally for most of its ventral exposure." This groove is clearly shown in the stereophotographs of *L. dakotensis* MCZ 19678 (Novacek 1986: figs. 21, 23). This feature is present in SDSM 62369 ("?" in Fig. 9B), although it is more subtle than in MCZ 19678. It is doubtful that this structure is related to the digastric muscle, as that muscle attaches to the paracondylar process of the exoccipital, while neck muscles (e.g., sternomastoid) are attached to the paroccipital process of the petrosal (Evans and Christensen 1979; Antón et al. 2004). The well-developed sulcus in MCZ 19678 appears more like a neurovascular structure than a muscular attachment. A possible candidate is the occipital artery, which lies in the general vicinity (Evans and Christensen 1979).

The lateral view of the right petrosal of SDSM 62369 is dominated by the broad, shallow sulcus for the capsuloparietal emissary vein ("scpev" in Fig. 11B) that was enclosed

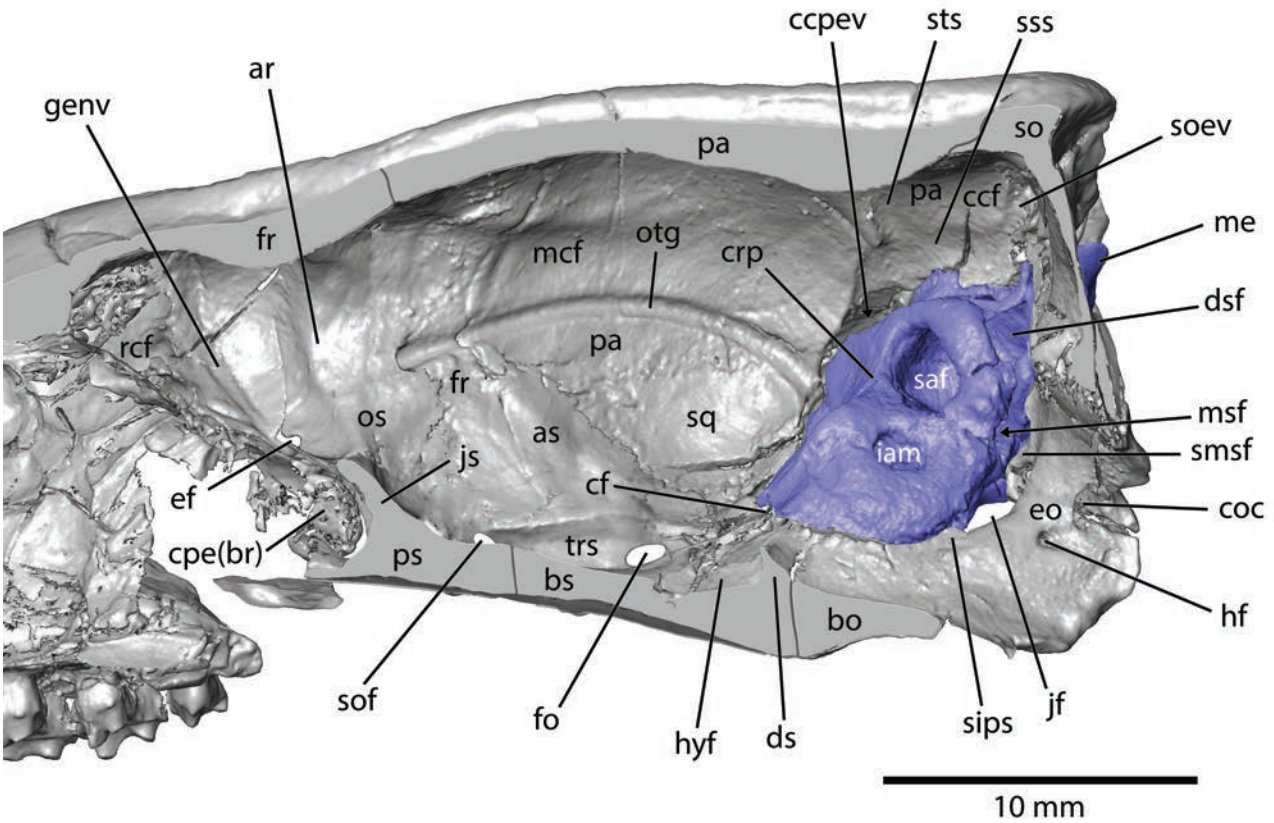

Fig. 17.—*Leptictis dakotensis* SDSM 62369, endocranium isosurface from CT scans in medial view. Cut surfaces indicated by uniform gray. Abbreviations: **ar,** annular ridge; **as,** alisphenoid; **bo,** basioccipital; **bs,** basisphenoid; **ccf,** caudal cranial fossa; **ccpev,** canal for capsuloparietal emissary vein; **cf,** carotid foramen; **coc,** condyloid canal; **cpe(br),** cribriform plate (broken); **crp,** crista petrosa; **ds,** dorsum sellae; **dsf,** dorsal subarcuate fenestra; **ef,** ethmoidal foramen; **eo,** exoccipital; **fo,** foramen ovale; **fr,** frontal; **genv,** groove for ethmoidal nerve and vessels; **hf,** hypoglossal foramen; **hyf,** hypophyseal fossa; **iam,** internal acoustic meatus; **jf,** jugular foramen; **js,** jugum sphenoidale; **mcf,** middle cranial fossa; **me,** mastoid exposure of petrosal; **msf,** medial subarcuate fenestra; **os,** orbitosphenoid; **otg,** orbitotemporal groove; **pa** parietal; **ps,** presphenoid; **rcf,** rostral cranial fossa; **saf,** subarcuate fossa; **sips,** sulcus for inferior petrosal sinus; **smsf,** sulcus on exoccipital leading to medial subarcuate fenestra; **so,** supraoccipital; **soev,** sulcus for occipital emissary vein; **sof,** sphenorbital fissure; **sq,** squamosal; **sss,** sulcus for sigmoid sinus; **sts,** sulcus for transverse sinus; **trs,** trigeminal sulcus.

in a canal laterally by the squamosal. Novacek (1986: fig. 18) illustrated the same broad sulcus on the petrosal for *L. dakotensis* but labeled it as the superior petrosal sinus; however, this vessel is endocranial and not between the petrosal and squamosal (Evans and Christensen 1979). Novacek (1986: fig. 18) also labeled the surface posterior to the capsuloparietal emissary vein as for a squamosal sinus. In SDSM 62369, this surface is tightly covered by the squamosal and there are no vascular spaces.

The dorsal and medial views of the right petrosal of SDSM 62369 (Figs. 12B, 13B) show the presence of large medial and dorsal openings into the subarcuate fossa, which we confirm are similarly arranged on the left side. The bone here on both sides is not pristinely preserved; there are cracks, and the edges of these openings are not entirely smooth, especially the dorsal opening. *Leptictis haydeni* ANSP 11402 has a large, more rounded medial subarcuate fenestra and a small dorsal subarcuate foramen ("msf" and "dsf" in Figs. 12A, 13A). Given the resemblances between ANSP 11402 and SDSM 62369 in this area, we interpret the medial and dorsal openings into the subarcuate fossa in both as real; however, the size of these in SDSM 62369 is likely exaggerated. We provisionally term the large dorsal opening in SDSM 62369 as the dorsal subarcuate fenestra.

On the occiput, SDSM 62369 has two mastoid foramina: a medial one between the petrosal and supraoccipital and a lateral one at the junction of those two bones with the parietal ("mf" in Fig. 6B). Novacek (1986: fig. 29) reported and illustrated a single large mastoid foramen in the position of the lateral one in SDSM 62369. Additionally, Novacek (1986: fig. 15) labeled but did not discuss further a paramastoid foramen that appears to be between the petrosal and squamosal in the position of a posttemporal foramen (e.g., Wible et al. 2004: fig. 40). This opening is not included in Novacek's (1986: fig. 29) view of the

occiput and does not occur in SDSM 62369.

Dorsal and medial views of the endocranial surfaces of SDSM 62369 are shown in Figures 16 and 17. Novacek (1986: figs. 15, 16) included some descriptions of the endocranium and published two dorsal views, one a drawing and the other stereophotographs of *L. dakotensis* AMNH 38919. As supplement to Novacek's descriptions, we make the following observations here. The endocranium is partitioned into three spaces: the rostral, middle, and caudal cranial fossae ("rcf", "mcf", and "ccf" in Figs. 16, 17), which housed the olfactory bulbs, cerebrum, and cerebellum, respectively. The floor of the rostral cranial fossa is formed primarily by the broken cribriform plate of the ethmoid ("cpe(br)" in Fig. 16) with a narrow area of presphenoid forming the posterior rim. The better-preserved left side of the cribriform plate has six well-developed foramina just off the midline with the dorsalmost one roughly three times the size of the others (not visible in the figures); it likely represents the cribroethmoidal foramen (sensu Moore 1981) for the ethmoidal nerve. Lateral to the midline on the left side are approximately 50 additional foramina of varying sizes, but at least a fourth of the left plate is missing. The midline is not raised to form a crista galli. In the ventrolateral aspect of the rostral cranial fossa away from the cribriform plate is the single ethmoidal foramen between the orbitosphenoid and frontal with a broad groove leading anterodorsally from it ("genv" in Fig. 17) for the ethmoidal nerve and vessels ("enav" in Fig. 18). In the midline roof of the rostral cranial fossa is a distinct sulcus on a low crest for the dorsal sagittal sinus (not visible in the figures). The rear of the rostral cranial fossa is marked by the low, rounded annular ridge ("ar" in Figs. 16, 17) that starts on the frontal on the dorsal midline and extends onto the orbitosphenoid.

The middle cranial fossa is bordered anteriorly by the annular ridge and posteriorly by the sulcus for the transverse sinus on the parietal ("sts" in Fig. 17), the crista petrosa, and the dorsum sellae on the basisphenoid ("ds" in Figs. 16, 17), which mark the position of the tentorium cerebelli. The midline floor of the fossa is formed by the presphenoid and basisphenoid. The anterior half of the presphenoid is sloped anterodorsally and forms the yoke or jugum sphenoidale ("js" in Figs. 16, 17). Posterior to the jugum, the central part of the presphenoid is rod-shaped and flanked laterally by deep, parasagittal sulci for the optic tracts ("ot" in Fig. 16) that lead to the left and right optic foramina. There is no clear indication of a sulcus for the optic chiasm on the presphenoid between the optic foramina. Posterolateral to the left optic foramen is the orbitosphenoid roof of the sphenorbital fissure, but parts of the orbitosphenoids are missing from both sides.

The central rod-shape on the presphenoid continues onto the basisphenoid, but quickly broadens into a more gently rounded structure that is interrupted posteriorly by the roughly circular hypophyseal fossa ("hyf" in Fig. 16). The posterior wall of the hypophyseal fossa is formed by the prominent dorsum sellae, posterior to which is the suture between the basisphenoid and basioccipital in the caudal cranial fossa (Figs. 16, 17). The dorsum sellae shows some minor asymmetry suggesting breakage and the left petrosal has been shifted dorsomedially. Anterolateral to the hypophyseal fossa are a pair of small foramina in the basisphenoid that transmitted the nerve of the pterygoid canal ("pc" in Fig. 16) to the sphenorbital fissure. Lateral to the hypophyseal fossa is a well-developed groove for the internal carotid artery and nerve that ends posteriorly at the endocranial aperture of the carotid foramen between the alisphenoid and petrosal ("gica" and "cf" in Fig. 16; "ican" in Fig. 18). The bulk of the middle cranial fossa floor lateral to basisphenoid is formed by the sizeable alisphenoid. It houses a deep, elongate trigeminal sulcus ("trs" in Figs. 16, 17) for the trigeminal ganglion that stretches from the sphenorbital fissure to the foramen ovale.

The basisphenoid depicted in Novacek's (1986: fig. 15) drawing differs in several features from SDSM 62369. At its anterior end it has a pair of rounded ridges that Novacek (1986: fig. 15) identified as the tuberculum sellae. These paired ridges are not present in SDSM 62369 or in the stereophotographs of *L. dakotensis* AMNH 38919 (Novacek 1986: fig. 16). Novacek (1986: fig. 15) reported and illustrated small foramina on either side of the tuberculum sellae that he suggested were for veins draining internal spaces of the basisphenoid and presphenoid; these foramina appear present in AMNH 38919 (Novacek 1986: fig. 16) but are absent in SDSM 62369. Lastly, he (1986: fig. 15) included distinct posterior clinoid processes on the lateral ends of the dorsum sellae, which appear to be based on *L. dakotensis* AMNH 3944 (Novacek 1986: fig. 24A). As noted above, the dorsum sellae in SDSM 62369 is damaged and the presence of posterior clinoid processes is unknown.

The main element of the lateral wall of the middle cranial fossa is the parietal, but there are also contributions from front to back from the orbitosphenoid, frontal, alisphenoid, squamosal, and petrosal (Fig. 17). Running nearly the length of the lateral wall is the prominent orbitotemporal groove ("otg" in Fig. 17), which accommodated the anterior division of the ramus superior (= ramus supraorbitalis of Wible 1987) and accompanying vein ("ad" in Fig. 18). The orbitotemporal groove is on the squamosal posteriorly, the frontal anteriorly, and the parietal in between (Fig. 17). The roof of the middle cranial fossa (not visible in the figures) is formed primarily by the parietal with a small contribution from the frontal anteriorly. The roof has a low midline crest for the dorsal sagittal sinus that bifurcates posteriorly for the paired transverse sinuses; in contrast to the rostral cranial fossa, there is no sulcus for the dorsal sagittal sinus in the middle cranial fossa.

The midline floor of the caudal cranial fossa of SDSM 62369 is formed by the gently concave basioccipital and a narrow strip of basisphenoid behind the dorsum sellae (Figs. 16, 17). The central portion of the basioccipital is depressed compared to its lateral margins and it slopes posteroventrally toward the foramen magnum. Although not visible in the figures, the lateral margins of the basisphenoid and

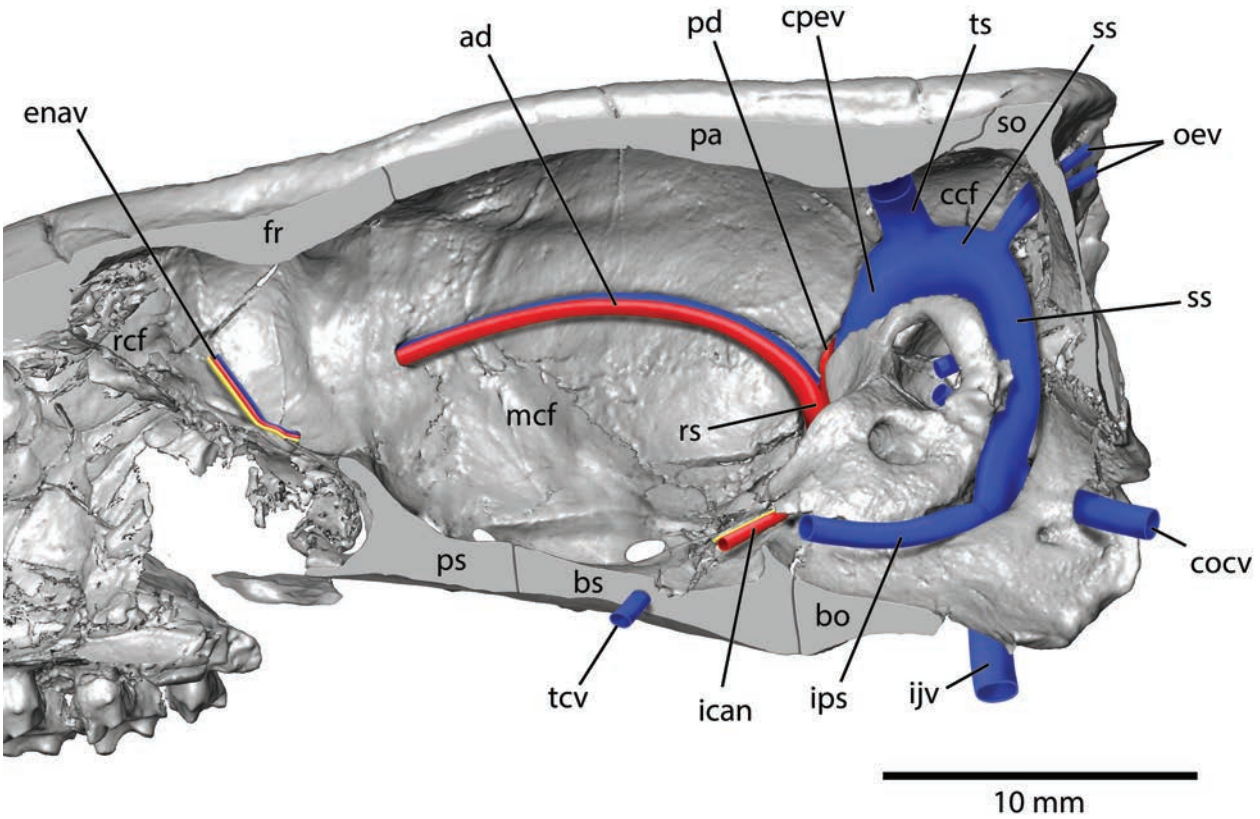

Fig. 18.—*Leptictis dakotensis* SDSM 62369, endocranium isosurface from CT scans in medial view with reconstruction of neurovascular structures (arteries in red, veins in blue, nerves in yellow). Cut surfaces indicated by uniform gray. Abbreviations: **ad,** anterior division of ramus superior and accompanying vein; **bo,** basioccipital; **bs,** basisphenoid; **ccf,** caudal cranial fossa; **cocv,** condyloid canal vein; **cpev,** capsuloparietal emissary vein; **enav,** ethmoidal nerve, artery, and vein; **fr,** frontal; **ican,** internal carotid artery and nerve; **ijv,** internal jugular vein; **ips,** inferior petrosal sinus; **mcf,** middle cranial fossa; **oev,** occipital emissary vein; **pa** parietal; **pd,** posterior division of ramus superior; **ps,** presphenoid; **rcf,** rostral cranial fossa; **rs,** ramus superior; **so,** supraoccipital; **ss,** sigmoid sinus; **tcv,** transverse canal vein; **ts,** transverse sinus.

basioccipital have dorsolateral wings that contact the dorsal surface of the rostral tympanic process (Figs. 12B, 13B) as described above for *L. haydeni* ANSP 11402 (Figs. 8, 12A, 13A). These wings are also visible in cross-sections of *L. dakotensis* AMNH 3944 in Novacek (1986: figs. 24B, 25A). The main element of the lateral wall of the caudal cranial fossa is the petrosal with some exoccipital posteroventrally and parietal dorsally (Fig. 17). The main element of the roof is the parietal with a narrow strip of supraoccipital posteriorly, while the posterior wall is formed by supraoccipital and exoccipital (neither the roof nor posterior wall are visible in the figures). Both the roof and posterior wall have depressions reflecting the surface of the cerebellum; the large central depression is for the vermis cerebelli and the paired lateral depressions for the cerebellar hemispheres. The endocast of *L. dakotensis* F:AM 96730 illustrated by Novacek (1982: fig. 1, 1986: fig. 30) has a fissura prima, which divides the vermis into rostral and caudal lobes (Evans and Christensen 1979), but this fissure appears to be absent in SDSM 62369.

The main structures left to describe in the caudal cranial fossa are related to the endocranial venous system. A broad sulcus on the parietal for the transverse sinus ("sts" in Fig. 17) runs posteroventrally from the dorsal midline toward the pars canalicularis of the petrosal. This sulcus ends at an even broader longitudinal sulcus that is primarily on the parietal but with a contribution from the pars canalicularis. The anterior end of this broad sulcus runs ventrally into a canal between the squamosal and petrosal for the capsuloparietal emissary vein ("ccpev" in Fig. 17) that leads to the postglenoid and suprameatal foramina. The rest of this broad sulcus runs posteriorly as the sulcus for the sigmoid sinus ("sss" in Fig. 17). The sulcus for the sigmoid sinus bends ventrally along the posterior rim of the subarcuate fossa and ultimately ends at the jugular foramen. En route, the sulcus for the sigmoid sinus gives origin to four distributary channels.

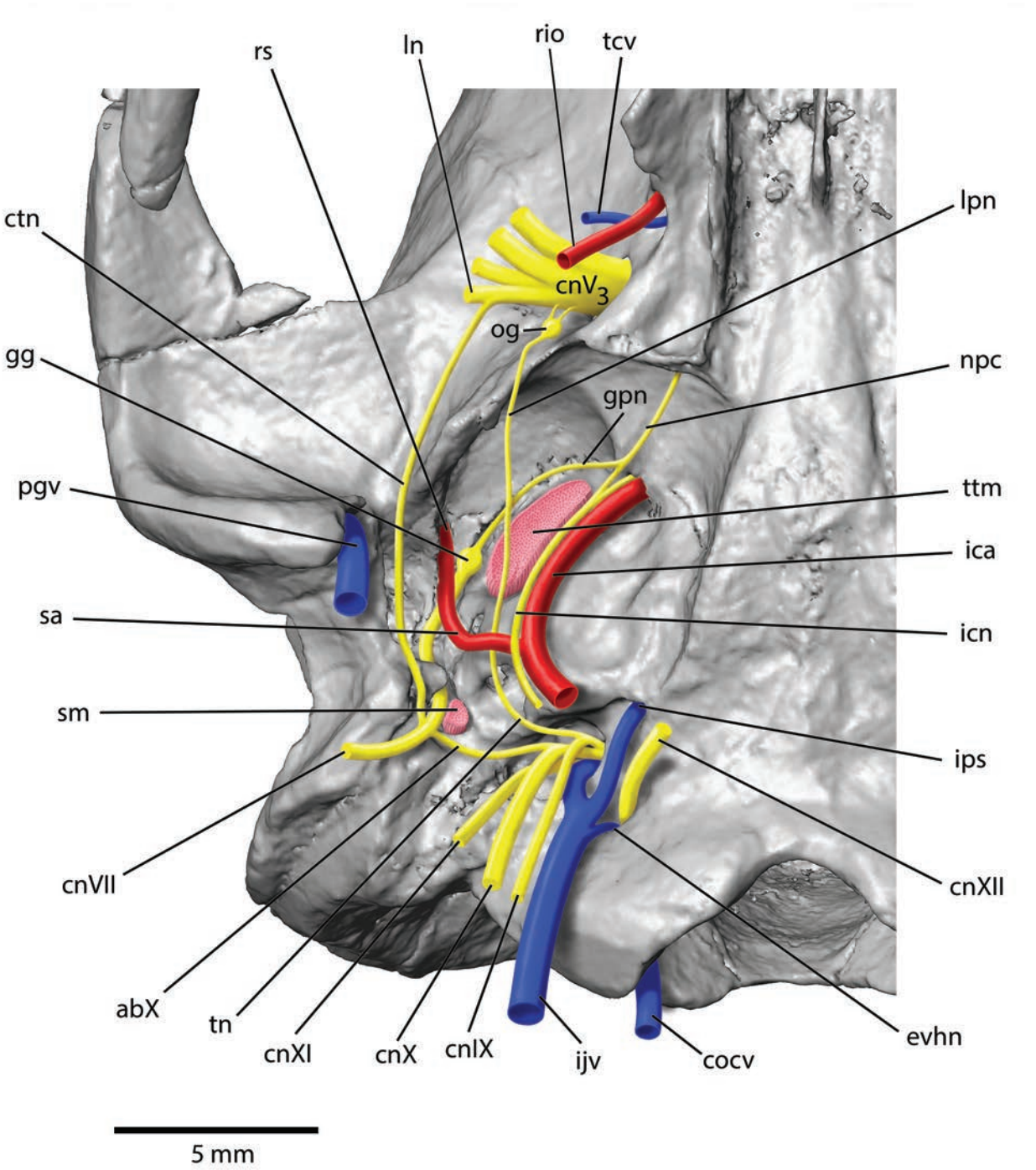

Fig. 19.—*Leptictis haydeni* ANSP 11402, left basicranium isosurface from CT scans in ventral view (see Fig. 4) with neurovascular (arteries in red; veins in blue; nerves in yellow) and middle-ear ossicular muscle reconstructions (in pink). The geniculate ganglion and greater petrosal nerve are exposed due to damage; they are enclosed in bone on the left petrosal of ANSP 11402 as on both sides of *Leptictis dakotensis* SDSM 62369. Abbreviations: **abX,** auricular branch of vagus; **cnIX,** ninth cranial nerve (glossopharyngeal nerve); **cnV3,** third division of fifth cranial nerve (mandibular branch of trigeminal nerve); **cnVII,** seventh cranial nerve (facial nerve); **cnX,** tenth cranial nerve (vagus nerve); **cnXI,** eleventh cranial nerve (accessory nerve); **cnXII,** twelfth cranial nerve (hypoglossal nerve); **cocv,** condyloid vein; **ctn,** chorda tympani nerve; **evhn,** emissary vein with hypoglossal nerve; **gg,** geniculate ganglion of facial nerve; **gpn,** greater petrosal nerve; **ica,** internal carotid artery; **icn,** internal carotid nerve; **ijv,** internal jugular vein; **ips,** inferior petrosal sinus; **ln,** lingual nerve; **lpn,** lesser petrosal nerve; **npc,** nerve of pterygoid canal; **og,** otic ganglion; **pgv,** postglenoid vein; **rio,** ramus infraorbitalis; **rs,** ramus superior; **sa,** stapedial artery; **sm,** stapedius muscle; **tcv,** transverse canal vein; **tn,** tympanic nerve; **ttm,** tensor tympani muscle.

The dorsalmost channel, the sulcus for the occipital emissary vein ("soev" in Fig. 17), runs posterodorsally towards the occiput, ending at the two mastoid foramina described above (Fig. 6B). The ventralmost channel, the condyloid canal ("coc" in Fig. 17), is entirely in the exoccipital and directs its contents toward the foramen magnum. In between are the dorsal and medial subarcuate fenestrae in the pars canalicularis ("dsf" and "msf" in Fig. 17), which connect the sulcus for the sigmoid sinus with the subarcuate fossa. A broad, short sulcus on the exoccipital ("smsf" in Fig. 17) perpendicular to the sulcus for the sigmoid sinus is directed to the medial subarcuate fenestra, providing further evidence that the opening is real and a vascular conduit.

Novacek (1986:59, fig. 25B) reported a shallow sulcus curving "on the intracranial surface of the petrosal roughly parallel to the lateral edge of the basioccipital" that he called the sulcus medialis and suggested it conveyed the inferior petrosal sinus. SDSM 62369 has a similar shallow sulcus that is best indicated just anterior to the jugular foramen shared between the basioccipital and petrosal ("sips" in Fig. 17).

Neurovascular Reconstruction

In addition to its association with the inner, middle, and outer ears, the mammalian basicranium is crossed by major nerves, arteries, and veins. Some neurovascular elements leave bony impressions and, therefore, can be reconstructed in fossils. In the foregoing, the descriptions of both *L. haydeni* ANSP 11402 and *L. dakotensis* SDSM 62369 included references to some soft-tissue reconstructions with the goal of aiding the reader in understanding the complex anatomy (Figs. 7, 10, 18). Here, we treat these systems in a holistic manner to provide a more comprehensive overview. Unless noted, the following reconstructions apply to both ANSP 11402 and SDSM 62369. We have two more figures that include reconstructions. The first (Fig. 19) shows a ventral view of the main basicranial neurovascular structures in *L. haydeni* ANSP 11402, which is largely in accord with Novacek's (1986: fig. 26) reconstruction of *L. dakotensis* in the same view; the few differences will be noted below. The second (Fig. 20) is an oblique anteromedial view of the isolated right petrosal of *L. dakotensis* SDSM 62369 with the main vascular components. The bases for these reconstructions are primarily the first author's works on vasculature in extant mammals (e.g., Wible 1984, 1987).

Arteries.— The cranial arterial pattern began in the neck with the bifurcation of the internal and external carotid arteries. The internal carotid artery, as usual accompanied by the internal carotid nerve (Wible 1984), a branch of the superior cervical ganglion of the sympathetic trunk, approached the middle ear. As reconstructed by Novacek (1986: fig. 20), the artery and nerve in *L. dakotensis* entered the middle ear through a gap between the petrosal, entotympanic, and ectotympanic. Our specimens preserve no ectotympanics, so we cannot comment on that. Only *L. haydeni* ANSP 11402 preserves any entotympanic, and because it is broken posteriorly, we do not know if it reached as far as the carotid entrance (Fig. 4B). Consequently, the true nature of the carotid's entrance into the middle ear in our specimens is unknown.

Within the middle ear, the internal carotid artery and nerve curved anteromedially near the rim of the round window, then across the promontorium, and onto the anterior septum before reaching the carotid foramen between the petrosal and alisphenoid (Figs. 10, 19). Well-developed grooves mark this passage in *L. haydeni* ANSP 11402 (Fig. 9A), but are lacking in *L. dakotensis* SDSM 62369 (Fig. 9B); nevertheless, we reconstruct the artery and nerve in the latter based on the presence of grooves in other specimens of *L. dakotensis* (Butler 1956; McDowell 1958; Novacek 1986). The internal carotid artery and nerve emerge endocranially and run anteromedially in a groove lateral to the hypophyseal fossa (Fig. 18). With the vertebral artery, the internal carotid artery supplies the cerebral circulation and likely sends an ophthalmic artery with the optic nerve out the optic foramen. An alternative route for the ophthalmic artery that occurs in some extant mammals (Bugge 1974; Wible 1984) is off the external carotid artery.

On the promontorium, anterior to the round window, the internal carotid artery supplies the stapedial artery, which runs laterally in a groove and then across the oval window (Figs. 10, 19). Medial to the oval window, the stapedial artery supplies a small ramus posterior to the stapedius muscle in some mammals (Wible 1987), but we did not include that in our reconstructions as the *Leptictis* specimens studied here show no evidence for this vessel. Lateral to the oval window, the stapedial artery turned forward in the facial sulcus with the facial nerve (Figs. 10, 19). The facial nerve and stapedial artery diverged at the secondary facial foramen where the nerve turned medially; the artery continued forward and entered a canal in the petrosal as the ramus superior (Figs. 10, 19). The ramus superior turned laterally in a groove on the petrosal and divided into its anterior and posterior divisions (Figs. 10, 20).

The anterior division of the ramus superior ran forward in the orbitotemporal groove on the squamosal, parietal, and frontal with accompanying vein (Figs. 17, 18) to reach the orbit via the anterior opening of the orbitotemporal canal between the frontal and orbitosphenoid ("otc" in Fig. 5). Within the cranial cavity, the anterior division likely provided blood to the meninges; however, as there are no vascular grooves connected to the orbitotemporal groove (Fig. 17), we have not included meningeal branches in our reconstruction. Within the orbit, the anterior division as the ramus supraorbitalis (Wible 1987) sent branches with the ophthalmic division of the trigeminal nerve (V_1) including an ethmoidal artery in the ethmoidal foramen ("enav" in Fig. 18) that ran in a groove in the rostral cranial fossa (Fig. 17). The posterior division of the ramus superior ran medial to the capsuloparietal emissary vein and supplied two rami temporales with accompanying veins ("rt" and "vrt" in Fig.

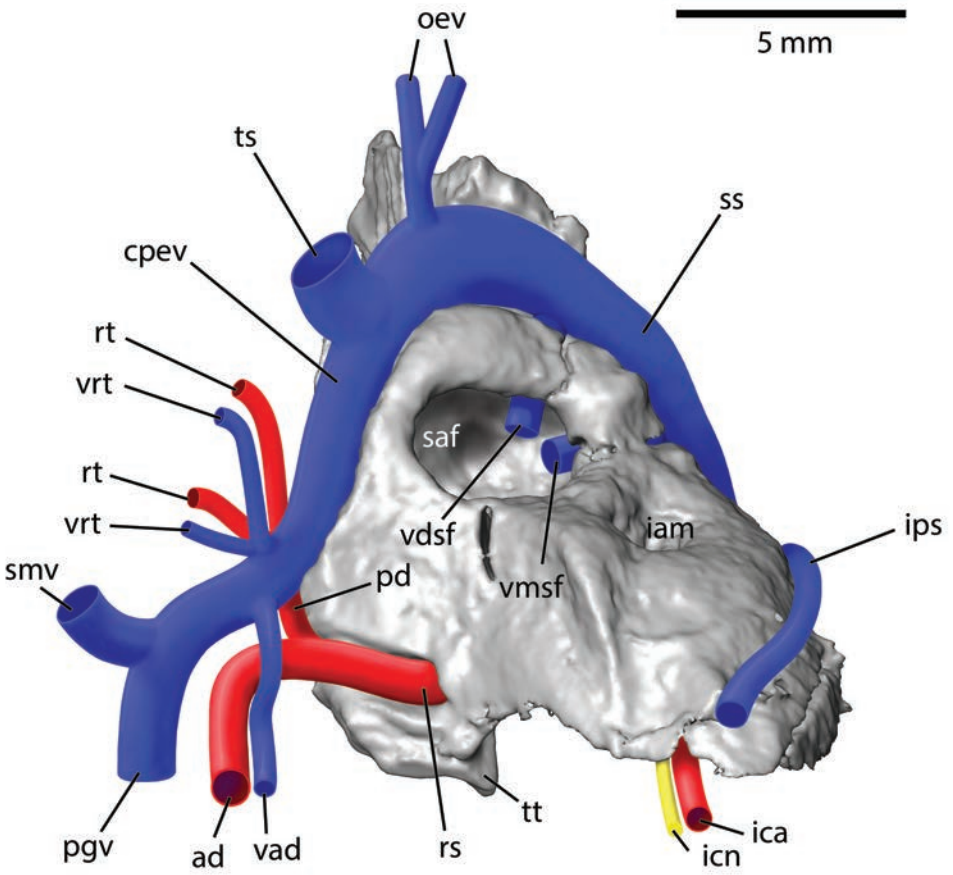

Fig. 20.—*Leptictis dakotensis* SDSM 62369, left petrosal isosurface from CT scans in oblique anteromedial view (dorsal to top of page) with reconstruction of major vascular structures (arteries in red; veins in blue; nerves in yellow). Abbreviations: **ad,** anterior division of ramus superior; **cpev,** capsuloparietal emissary vein; **iam,** internal acoustic meatus; **ica,** internal carotid artery; **icn,** internal carotid nerve; **ips,** inferior petrosal sinus; **oev,** occipital emissary vein; **pd,** posterior division of ramus superior; **pgv,** postglenoid vein; **rs,** ramus superior of stapedial artery; **rt,** ramus temporalis; **saf,** subarcuate fossa; **smv,** suprameatal vein; **ss,** sigmoid sinus; **ts,** transverse sinus; **tt,** tegmen tympani; **vad,** vein accompanying anterior division; **vdsf,** vein in dorsal subarcuate fenestra; **vmsf,** vein in medial subarcuate fenestra; **vrt,** vein accompanying ramus temporalis.

20) that exited foramina in the squamosal bone (Fig. 7) to reach the temporalis muscle. The posterior division and rami temporales left imprints on the petrosal of *L. haydeni* ANSP 11402 (Fig. 11A), but not *L. dakotensis* SDSM 62369 (Fig. 11B).

Novacek (1986: fig. 26) reconstructed two arteries in *L. dakotensis* that we do not include in our reconstructions: the ramus inferior of the stapedial artery and the artery of the pterygoid canal. Regarding the ramus inferior, as noted above, this vessel was also reconstructed by Butler (1956), but he placed it in what we identify as the facial canal. Novacek (1986:55) wrote that the ramus inferior likely passed through a small foramen near the "forward apex of the facial canal," but did not illustrate this aperture. We were unable to find such a foramen in either *L. haydeni* ANSP 11402 or *L. dakotensis* SDSM 62369, nor did we find any groove that might have transmitted the ramus inferior in the vicinity of the canal for the ramus superior (see, for example, *Echinosorex gymnurus* in Cartmill and MacPhee 1980: fig. 2). A route for the ramus inferior that occurs in some extant mammals is with the chorda tympani nerve via the Glaserian fissure (Klaauw 1931), which is the gap between the postglenoid and entoglenoid processes in both *Leptictis* specimens studied here ("Gf" in Fig. 4B). However, there are no grooves in the vicinity of the Glaserian fissure indicating a ramus inferior in *L. haydeni* ANSP 11402 or *L. dakotensis* SDSM 62369. Without evidence of its presence, we do not include the ramus inferior in our reconstruction as there are alternative routes in extant mammals through the external carotid system for blood to

reach the tissues in the ramus inferior's area of distribution (Bugge 1974; Wible 1984, 1987).

Regarding the artery of the pterygoid canal, Novacek (1986: fig. 26) reconstructed it arising from the internal carotid artery just posterior to the carotid foramen in *L. dakotensis*. It traveled forward below the alisphenoid with the nerve of the pterygoid canal (= vidian nerve) and then disappeared into the pterygoid canal. Although it was drawn smaller in girth than the internal carotid artery in Novacek's figure, the artery of the pterygoid canal was depicted as a very substantial vessel. We did not include an artery of the pterygoid canal in our vascular reconstruction of *L. haydeni* and *L. dakotensis*, only a nerve of the pterygoid canal in the groove on the alisphenoid ("npc" in Fig. 19). Such an artery branching from the carotid has been reported for a few extant mammals (e.g., *Echinosorex gymnurus* in Cartmill and MacPhee 1980: fig. 2), but a vessel comparable in size to that depicted for *L. dakotensis* by Novacek (1986: fig. 26) is unknown. The distribution of the artery of the pterygoid canal as a branch of the carotid is not well documented. Wible (1984) concluded that the main occupant of grooves leading to the pterygoid canal are neural and we follow that here.

Along with the internal carotid and vertebral arteries, the external carotid is the other primary supplier of blood to the head. The only branch of the external carotid in our reconstruction is the artery in the alisphenoid canal ("rio" in Fig. 19). Following the terminology of Wible (1987), this is the ramus infraorbitalis (= internal maxillary artery). Within the orbit, the ramus infraorbitalis was distributed with the main branches of the maxillary division of the trigeminal nerve (V_2), including the infraorbital artery.

Veins.—The endocranial venous system left numerous impressions on the inside of the braincase in *L. haydeni* ANSP 11402 and *L. dakotensis* SDSM 62369 that allow us to reconstruct the major dural sinuses and their exit veins. These sulci, canals, and foramina result in a venous pattern similar to that in the domestic dog (Evans and Christensen 1979: fig. 12–21). In our reconstructions (Figs. 18–20), we have included only those veins that leave major impressions, but judging from the dog (Evans and Christensen 1979) and other domestic mammals (e.g., Sisson 1910), more endocranial veins were certainly present.

The midline roof of the rostral and middle cranial fossae has a longitudinal crest (not visible in the figures). In the rostral fossa, this crest on the frontals is raised and has a sulcus for the dorsal (superior) sagittal sinus. In the middle fossa on the frontals and parietals, this crest is lower and without a distinct sulcus for the dorsal sinus. Towards the rear of the middle fossa, the midline crest bifurcates, demarcating the division of the dorsal sagittal sinus into the left and right transverse sinuses. A crest indicating the anterior edge of the sulcus for the transverse sinus curved posteroventrally on the parietal and met a broader longitudinal sulcus dorsal to the petrosal ("sts" in Fig. 17). Here, the transverse sinus split into an anteroventrally directed capsuloparietal emissary vein (= temporal sinus of Evans and Christensen 1979) and a posteroventrally directed sigmoid sinus ("cpev" and "ss" in Fig. 18).

The capsuloparietal emissary vein ran in a sulcus on the petrosal ("scpecv" in Fig. 11; "cpev" in Fig. 20) that was enclosed in a canal by the squamosal and ultimately exited the cranial cavity as the postglenoid (= retroarticular of Evans and Christensen 1979) and suprameatal veins via the foramina of the same names ("pgv" and "smv" in Figs. 7B, 20). A suprameatal vein is not present in the dog (Evans and Christensen 1979), but is, for example, in the didelphid *Monodelphis* (Wible 2003). En route to its exits, the capsuloparietal emissary vein drained veins with the anterior and posterior divisions of the ramus superior, including veins exiting the cranium with the rami temporales (Wible 1989; Figs. 18, 20).

The sigmoid sinus curved ventrally along the posterior aspect of the petrosal ("ss" in Figs. 18, 20) in a broad sulcus between the petrosal, supraoccipital, and exoccipital ("sss" in Fig. 17). Before its ventral bend, the sigmoid sinus supplied an occipital emissary vein ("oev" in Figs. 18, 20) that ran posterodorsally in a sulcus on the parietal and supraoccipital ("soev" in Fig. 17) before bifurcating into two end branches exiting the two mastoid foramina on the occiput ("mf" in Fig. 6). At its ventral end, the sigmoid sinus supplied a large condyloid vein (sensu Evans and Christensen 1979) in the condyloid canal ("cocv" in Fig. 18), and then at the jugular foramen joined the inferior (ventral) petrosal sinus to form the internal jugular vein ("ips" and "ijv" in Fig. 18).

The inferior petrosal sinus originated from the cavernous sinus at the hypophyseal fossa and appears to have followed different paths to join the sigmoid sinus in the two specimens. In *L. dakotensis* SDSM 62369, where there is some damage to the basioccipital, the sinus had what appears to be an entirely endocranial course between the cavernous sinus and jugular foramen ("ips" in Fig. 18). In contrast, in *L. haydeni* ANSP 11402, the sinus appears to be in a small canal between the dorsolateral wing of the basioccipital and rostral tympanic process of the petrosal ("ips" in Fig. 10) and then exited a separate foramen between these two bones anterior to the jugular foramen ("ips" in Fig. 4). Novacek (1986:59, fig. 26) described a primarily endocranial course in a sulcus for the inferior petrosal sinus of *L. dakotensis* with a separate foramen of exit. Without access to additional CT scans of *L. dakotensis* or additional specimens of *L. haydeni*, we treat the course of the inferior petrosal sinus as unresolved.

Both *L. haydeni* ANSP 11402 and *L. dakotensis* SDSM 62369 have bilateral passageways in the petrosal between the sulcus for the sigmoid sinus and subarcuate fossa. These are better preserved in *L. haydeni* ANSP 11402, which has a small dorsal subarcuate foramen ("dsf" in Fig. 12A) and a large medial subarcuate fenestra ("msf" in Fig. 13A); *L. dakotensis* SDSM 62369 shows more damage here with the dorsal opening having an irregular outline and an open crack connecting it to the medial opening (Figs. 12B, 13B, 17). Both specimens also have a sulcus on the exoccipital

that directs a sizeable structure at the medial subarcuate fenestra ("smsf" in Fig. 17). Given the relationship to the sulcus for the sigmoid sinus, veins represent the most likely occupants of the dorsal and medial openings and that is what we reconstruct ("vdsf" and "vmsf" in Fig. 20). Maugoust and Orliac (2021) reported a similar situation in their study of extant bat endocasts, dorsal and medial apertures between the petrosal lobule of the cerebellum (paraflocculus), which occupies the subarcuate fossa, and the cast of the sigmoid sinus. The dorsal and medial subarcuate openings in *Leptictis* should not be confused with the petromastoid canal (subarcuate canaliculus), which is found in the floor of the subarcuate fossa in some placentals including humans (Gannon et al. 1988; Maślanka et al. 2018). The main drainage route reported for venous blood from the petrosal lobule in extant placentals is via the ventral cerebellar vein through the subarcuate fossa (Gillian 1969; Armstrong and Horowitz 1971).

Both *L. haydeni* ANSP 11402 and *L. dakotensis* SDSM 62369 have a transverse canal foramen in the basisphenoid anterior to the foramen ovale ("tcf" in Fig. 5). In *L. haydeni* ANSP 11402, the transverse canal foramen is in a common depression with the caudal opening of the alisphenoid canal (Fig. 5). This relationship cannot be confirmed in *L. dakotensis* SDSM 62369 as there is breakage where the alisphenoid canal is expected, but the common depression is clearly shown in the photograph of *L. dakotensis* SDSM 332 in Novacek (1986: fig. 12). In both specimens studied here, the basisphenoid is replete with internal vascular spaces. However, there is a main channel that communicates across the midline, the transverse canal, that is larger than the transverse canal foramen. The communication across the midline is posterior to the level of the transverse canal foramen, near the level of the posterior limit of the foramen ovale. Consequently, the communicating vessel in the transverse canal followed a posteromedial course, anterior to the hypophyseal fossa ("tcv" in Fig. 18). Also, in both specimens, the paired pterygoid canals join the transverse canal in its passage between their external apertures in the alisphenoids ("pc" in Fig. 15) and their endocranial apertures in the basisphenoid ("pc" in Figs. 14, 15). A transverse canal foramen, transverse canal, and transverse canal vein are widely distributed among extant marsupials and some extant placentals (MacPhee et al. 2023), with a variety of endo- and extracranial connections. However, our observation of the posteromedial course for the transverse canal vein and the association of the transverse canal with the pterygoid canals in *L. haydeni* and *L. dakotensis* are unusual.

Nerves.—The major nerves of the ear region are reconstructed on *L. haydeni* ANSP 11402 and *L. dakotensis* SDSM 62369 (Figs. 10, 19) following the common pattern reported in various extant placentals (e.g., Davis and Story 1943; MacPhee 1981). The foramina of exit for the cranial nerves are as follows: foramen ovale ("fo" in Fig. 4B) for the mandibular division of the trigeminal ("cnV_3" in Fig. 19), secondary facial foramen and stylomastoid notch ("sff" and "smn" in Fig. 9B) for the facial nerve ("cnVII" in Fig. 19), jugular foramen ("jf" in Figs. 4B, 15) for the glossopharyngeal, vagus, and accessory nerves ("cnIX," "cnX," and "cnXI" in Fig. 19), and hypoglossal foramen ("hf" in Figs. 4B, 15) for the hypoglossal nerve ("cnXII" in Fig. 19).

Nerve branches that leave bony impressions are: the greater petrosal nerve ("gpn" in Figs. 10A, 19) off the facial nerve, which exits the hiatus Fallopii in the petrosal ("hF" in Fig. 9B); the chorda tympani nerve ("ctn" in Figs. 10A, 19) off the facial nerve, which runs in the Glaserian fissure in the squamosal ("Gf" in Figs. 4B, 19) and possibly in the shallow depression on the tympanohyal present in *L. dakotensis*; the internal carotid nerve ("icn" in Figs. 10A, 19) off the superior cervical ganglion of the sympathetic trunk, which runs with the internal carotid artery in a groove on the promontorium and anterior septum ("gica" in Fig. 9A), then through the carotid foramen between the petrosal and alisphenoid ("cf" in Figs. 4B, 15—17), and lastly in a groove on the endocranial surface of the basisphenoid ("gica" in Fig. 16); and the nerve of the pterygoid canal ("npc" in Figs. 10A, 19) formed by branches from the greater petrosal and internal carotid nerves, which runs in a groove on the epitympanic wing of the alisphenoid ("*" in Fig. 4B) leading to a foramen in the alisphenoid ("pc" in Fig. 15), then through a canal in the basisphenoid to a endocranial foramen anterolateral to the hypophyseal fossa ("pc" in Fig. 16).

Nerve branches that do not leave bony impressions are: the tympanic nerve ("tn" in Figs. 10A, 19) off the glossopharyngeal nerve, which ramifies into a tympanic plexus on the promontorium (not shown); and the lesser petrosal nerve ("lpn" in Figs. 10A, 19) off the glossopharyngeal nerve, which forms from the tympanic plexus on the promontorium, crosses the tympanic process of the alisphenoid, and ends at the otic ganglion ("og" in Fig. 19) on the mandibular division of the trigeminal nerve.

COMPARISONS

No other leptictid basicrania have been described and illustrated to the level of detail presented here and elsewhere for *L. dakotensis* (e.g., Butler 1956; Novacek 1986) and *L. haydeni*. Velazco and Novacek (2016: fig. 14) provided a short description and stereophotographs of the ear region of *Palaeictops altimontis* AMNH 96250. Beyond that, photographs of crania and some descriptions for the following are in the literature: *Palaeictops bicuspis* (Cope, 1880), AMNH 4802, 4255 (Velazco and Novacek 2016: figs. 1, 2); *Palaeictops matthewi* Novacek, 1977, FMNH P26904 (Velazco and Novacek 2016: fig. 8); *Palaeictops robustus* Velazco and Novacek, 2016, CM 11954 (Velazco and Novacek 2016: fig. 16); *Blacktops longinares* Meehan and Martin, 2010, USNM 49038 (Meehan and Martin 2010: figs. 1A-D, 3, 4A, B); *Blacktops latidens* Meehan and Martin, 2010, USNM 49039 (Meehan and Martin 2010: figs. 1E-H, 4C, D); *Megaleptictis altidens* Meehan

and Martin, 2012, KUVP 2568 (Meehan and Martin 2012: figs. 1A, 3, 4B, 5A); and *Stenoleptictis thomsoni* (Matthew, 1903), UMPC 0888 (Korth 2022: figs. 6A, B). Additionally, Velazco and Novacek (2016) scored some cranial characters for their phylogenetic analysis, which included observations of *Prodiacodon tauricinerei* (Jepsen, 1930), YPM-PU 13104. We use these data to make comparisons within leptictids.

Recently, the senior author (Wible 2022) reported on the basicranium and neurovascular system of the early Eocene palaeoryctid *Eoryctes melanus* Thewissen and Gingerich, 1989, based on CT scan data. Comparisons were made between *E. melanus* and various Paleogene taxa, including *L. dakotensis* based primarily on Novacek (1986). Here, we update those comparisons with the new information presented above for *L. haydeni* and *L. dakotensis*.

Braincase

Both *L. haydeni* and *L. dakotensis* have prominent paired temporal crests on the braincase roof that run parasagittally between the frontal and the supraoccipital (Figs. 1A, 2A). There are subtle differences between the two taxa; the crests are more proximal to each other in *L. dakotensis* (Fig. 2A; Novacek 1986: figs. 2A, 6), whereas they are more widely spaced and slightly everted posteriorly in *L. haydeni* (Fig. 1A). Paired temporal crests resembling those in the *Leptictis* specimens also occur in *M. altidens* (Meehan and Martin 2012: fig. $1A_1$) and both species of *Blacktops* (Meehan and Martin 2010: figs. 1A, E). In *M. altidens*, the crests are closer together than in other leptictids, whereas in the *Blacktops* species, they resemble those in *L. haydeni*. *Stenoleptictis thomsoni* also has paired temporal crests, but they are lyrate, more widely spaced anteriorly and then converging although still separated posteriorly (Korth 2022: fig. 6A). Velazco and Novacek (2016) scored paired temporal crests for *Pr. tauricinerei*. Rather than paired temporal crests, *Pa. bicuspis*, *Pa. altimontis*, and *Pa. robustus* have a midline sagittal crest (Velazco and Novacek 2016: figs. 2A, 13A, 16A). Prominent paired temporal ridges like those in some leptictids occur in various marsupials (Beck et al. 2022: figs. 45, 48) and murid rodents (Musser 1981: fig. 6A), but are rare among mammals.

Both *L. haydeni* and *L. dakotensis* have a well-developed suprameatal crest and fossa, and a large, posterolaterally directed suprameatal foramen (Figs. 1E, 2E, 7A; Novacek 1986: fig. 2C); the suprameatal crest reaches farther posteriorly in *L. dakotensis* than in *L. haydeni*. These three structures are reported in other leptictids and show some differences. *Lepticis intermedius* CM 1019 has a short suprameatal crest, shallow fossa, and small foramen (Korth 2022). *Megaleptictis altidens* has a suprameatal crest reaching to the nuchal crest, a broad fossa, and a small foramen (Meehan and Martin 2012). Korth (2022) noted that the suprameatal fossa and foramen are shallow and small, respectively, in *S. thomsoni*, but as these structures are not illustrated, we cannot comment on the suprameatal crest. Velazco and Novacek (2016) reported, but did not illustrate, a shallow suprameatal fossa and small foramen for *Pa. bicuspis* and *Pa. altimontis*; in the latter, they described the foramen dorsal to rather than within the fossa. Suprameatal foramina are found in many extant marsupials (= subsquamosal foramina in Beck et al. 2022) and extinct and extant eutherians (O'Leary et al. 2013: Morphobank Project 773), but such foramina in a suprameatal fossa are rare.

Leptictis haydeni and *L. dakotensis* have foramina for rami temporales in the squamosal dorsal to the suprameatal crest (Figs. 1E, 2E, 7; Butler 1956: fig. 1; Novacek 1986: figs. 1, 17): three per side in *L. haydeni* and between two and four per side in *L. dakotensis*. Three per side are reported for *S. thomsoni* (Korth 2022) and one large foramen per side in *M. altidens* (Meehan and Martin 2012) and *L. intermedius* (Korth 2022). It is likely that these foramina are present, but unreported, in other leptictids. Foramina for rami temporales are widely distributed in extinct and extant eutherians (O'Leary et al. 2013: Morphobank Project 773; Wible 2022).

In the orbital and infratemporal fossae, the disposition of the main foramina is remarkably similar between *L. haydeni* and *L. dakotensis* (Figs. 5, 15; Novacek 1986: figs. 10, 12), including the anterior opening of the orbitotemporal canal, ethmoidal and optic foramina, sphenorbital fissure, alisphenoid canal, transverse canal foramen, and foramen ovale. A difference is the presence of a supra-optic foramen in *L. dakotensis* SDSM 62369 (Fig. 15), but this has not been reported in other specimens of this species. A suboptic foramen is variably present in both species. Few details of the orbital foramina mentioned here are reported for other leptictids or even other Paleogene taxa. A small ethmoidal foramen near the frontal-orbitosphenoid suture and a short alisphenoid canal anterior to the foramen ovale are described for *Pa. altimontis* (Velazco and Novacek 2016). Outside of leptictids, the most variable of the main orbital openings in terms of presence and absence are the anterior opening of the orbitotemporal canal, the alisphenoid canal, and the transverse canal foramen. All three occur in the palaeoryctid *E. melanus* (Wible 2022) in a manner as in *L. haydeni*.

Zygoma

Novacek (1976) observed that the zygoma of *L. haydeni* is deeper than *L. dakotensis*. We agree, in particular in the anterior part of the zygoma. We measured the height of the zygoma at the anterior root in lateral view for *L. haydeni* and *L. dakotensis* F:AM 108194 (Novacek 1986: fig. 2C) and compared that to the length from the canine to the occipital condyle, as the tip of the skull is incomplete; in the former, zygoma height is 7.3% of the canine-condyle length, whereas in the latter it is 5.8%.

Another difference is the shape of the zygomatic arch in ventral or dorsal view; in *L. haydeni* (Figs. 1A, C), the zygoma angles anteromedially from the glenoid, whereas it is more subparallel in *L. dakotensis* (Novacek 1986: figs. 2A, B, 5, 6). Complete zygomata are not preserved in other leptictid genera.

Mesocranium

Both *L. haydeni* ANSP 11402 (Fig. 4A) and *L. dakotensis* (Novacek 1986) have a well-developed vertical midline keel in the basipharyngeal canal. In the former, the keel is a separate parasphenoid bone, whereas in the latter, Novacek (1986) identified it as a process of the presphenoid. Although *L. dakotensis* SDSM 62369 does not have a midline crest, it has a faint facet on the basisphenoid midline ("*" in Fig. 15) in the place where the parasphenoid contacts in *L. haydeni*, suggesting the possible presence of a separate bone. Velazco and Novacek (2016: fig. 13B) noted the possible presence of a midline keel on the presphenoid in *Pa. altimontis* AMNH 96250. Parasphenoids have been reported in two Late Cretaceous eutherians, *Maelestes* Wible et al., 2007, and *Zalambdalestes* Gregory and Simpson, 1926 (Wible et al. 2004, 2009) and in some extant placentals (Wible et al. 2018), but these are not as tall or elongate as that in *L. haydeni*.

Leptictis haydeni (Fig. 4B) and *L. dakotensis* (Novacek 1986: fig. 2B) have the same arrangement of the ento- and ectopterygoid crests. The entopterygoid crests are subparallel, with the hamulus situated caudal to the suture between the pre- and basisphenoid; the ectopterygoid crests flare laterally and their distal tips are roughly level with the hamulus. There is a possible difference regarding the ectopterygoid crest. The well-preserved left crest of *L. dakotensis* F:AM 108194 sports a distinct digitiform projection at its posteroventral end (Novacek 1986: fig. 2B); the right ectopterygoid of *L. haydeni* ANSP 11402, which appears unbroken, does not have such a projection. Subparallel entopterygoid crests flanked by ectoperygoid crest are visible in the stereophotographs of the two species of *Blacktops* (Meehan and Martin 2010: figs. 1C, G) and *Pa. altimontis* (Velazco and Novacek 2016: fig. 13B), but more details concerning these structures are obscured by breakage. Ecto- and entopterygoid crests occur together in numerous extinct and extant eutherians (O'Leary et al. 2013: Morphobank Project 773), but not showing the same arrangement as *L. haydeni* and *L. dakotensis*.

Tympanic Region

The disposition of bones and foramina neighboring the petrosal in ventral view is essentially duplicated in *L. haydeni* (Figs. 4, 5) and *L. dakotensis* (Fig. 15; Novacek 1986: figs. 19–23), including the postglenoid, carotid, jugular, and hypoglossal foramina, the tympanic processes of the alisphenoid and basioccipital, the large epitympanic wing of the alisphenoid, the entoglenoid, postglenoid, and posttympanic processes and the posttympanic crest of the squamosal, and the low paracondylar process of the exoccipital. The alisphenoid epitympanic wing has two surfaces, laterally for the hypotympanic sinus and medially a surface covered by the entotympanic; the latter surface includes a groove for the nerve of the pterygoid canal that leads to a foramen just caudal to the tympanic process of the alisphenoid. A similar disposition of processes on the alisphenoid, squamosal, and basioccipital is visible in stereophotographs of *M. altidens* (Meehan and Martin 2012: fig. $1A_3$), *Pa. altimontis* (Velazco and Novacek 2016: figs. 13B, 14), and both species of *Blacktops* (Meehan and Martin 2010: figs. 1C, G). Each has an alisphenoid tympanic process continuous with the entoglenoid, which in turn is separated from the postglenoid process, a tympanic process of the basioccipital, and posttympanic crest and process; the alisphenoid epitympanic wing appears less expanded anteroposteriorly than in *L. haydeni* and *L. dakotensis*. None of them appear to have an appreciable paracondylar process of the exoccipital. In *M. altidens* and *Pa. altimontis*, two surfaces appear to be present on the alisphenoid epitympanic wing, whereas there appears to be only one in *Blacktops*. Based on the stereophotographs noted above, we suggest that the carotid foramen is between the petrosal and alisphenoid epitympanic wing in *Pa. altimontis* and *B. latidens*; the situation is unclear in the others. Velazco and Novacek (2016) have already noted some differences among these taxa: the postglenoid foramen is posteromedial to the postglenoid process in *L. dakotensis* (and *L. haydeni*) but posterior to the process in *Pa. altimontis* and *Pa. robustus*; the postglenoid process is large in *L. dakotensis* (and *L. haydeni*) and *M. altidens*, but small in *Pa. altimontis* and *Pa. robustus*.

Outside leptictids, of the Paleogene taxa considered by Wible (2022), *E. melanus* has a setting for the bones around the petrosal reminiscent of that in *L. haydeni* and *L. dakotensis*. There are tympanic processes of the alisphenoid, basisphenoid, and basioccipital, an entoglenoid process separated from the postglenoid process, a posttympanic crest and process, and little in the way of a paracondylar process of the exoccipital (Wible 2022: fig. 1). The epitympanic wing of the alisphenoid has a groove and foramen for the nerve of the pterygoid canal and the carotid foramen is between the alisphenoid and petrosal. However, the alisphenoid epitympanic wing is even more expanded in *E. melanus* and the tympanic processes of the basioccipital, basisphenoid, and alisphenoid form a continuous curved ridge; in *L. haydeni* (figs. 4, 5) and *L. dakotensis* (Fig. 15), the tympanic process of the basisphenoid is not continuous with the tympanic process of the alisphenoid. Also, the expanded alisphenoid epitympanic wing has a single surface in *E. melanus* (Wible 2022: fig. 1) in contrast to the two surfaces in *L. haydeni* (Figs. 4B, 5) and *L. dakotensis* (Fig. 15), one accommodating the entotympanic and the other a hypotympanic sinus. Based on the fragmentary auditory bulla that is known for a referred specimen of *E. melanus*

UM 72623 (Thewissen and Gingerich 1989: fig. 4), its expanded alisphenoid epitympanic wing did not accommodate the bulla but was a large hypotympanic sinus.

Turning to the petrosal, Figure 9 of the tympanic surfaces of *L. haydeni* and *L. dakotensis* is helpful for making comparisons, but we remind the reader that some of the apparent differences are the result of damage and/or preservation dealt with above. Here, we highlight those features that are more likely true differences between the two. The part of the epitympanic recess on the petrosal is smaller in *L. haydeni* than in *L. dakotensis*; the tympanohyal is more pronounced in *L. dakotensis*, nearly contacting the promontorium; the tensor tympani fossa is longer in *L. haydeni* but wider in *L. dakotensis*; and the mastoid exposure in ventral view is wider in *L. dakotensis* and has a faint sulcus medial to the paroccipital process ("?" in Fig. 9B). It is difficult to make similar comparisons with other leptictids from the few illustrations in the literature. For *B. longinares*, Meehan and Martin (2010) noted that the tensor tympani fossa is narrower and deeper than in *L. dakotensis*, and Meehan and Martin (2012) observed the tensor tympani fossa and epitympanic recess are slightly deeper in *M. altidens* than in *L. dakotensis*.

Velazco and Novacek (2016:40) scored several features of the tympanic surface of the petrosal in their leptictid phylogenetic analysis. (1) "Grooves on the promontorium" are deep in *L. dakotensis* and shallow in *Pa. altimontis*; we add that these are also deep in *B. latidens* (Meehan and Martin 2010: fig. 1G), whereas *L. haydeni* (Fig. 9A) is mixed, as the groove on the anterior septum is deep but the remainder are shallow. (2) "Groove on the paraoccipital [=paroccipital] process" is deep in *L. dakotensis* and shallow in *Pa. altimontis* and *Pa. robustus*; SDSM 62369 has a shallow groove ("?" in Fig. 9B and it is absent in *L. haydeni* (Fig. 9A). (3) "Median petrosal crest of the promontorium" [=rostral tympanic process] is well developed in *L. dakotensis* and weakly developed in *Pa. altimontis* and *Pa. robustus*; we add this is also well developed in *L. haydeni* (Fig. 9A). (4) "Fossula cochlea dorsal rim" is less expanded in *L. dakotensis* and more expanded in *Pa. altimontis* and *Pa. robustus*. We interpret this as reference to the shelf posterodorsal to the aperture of the cochlear fossula; in *L. dakotensis* and *L. haydeni*, there is no raised lip on this shelf (Fig. 9) but there is in *Pa. altimontis* (Velazco and Novacek 2016: fig. 14; note that the aperture of the cochlear fossula is mislabeled as the stylomastoid foramen) and *Pa. robustus* CM 11954. This raised lip is the medial section of the caudal tympanic process of the petrosal (sensu MacPhee 1981). (5) "Bridge of the mastoid tubercle of the petrosal [=tympanohyal]; this bridge extends from dorsal rim of the cochlear fossula between the stylomastoid foramen and stapedius fossa" and is wide in *L. dakotensis* and narrow in *Blacktops* and *Pa. altimontis*. The line drawing with the stereophotograph of the ear region of *Pa. altimontis* in Velazco and Novacek (2016: fig. 14) shows a narrow bridge between the structures in their character description. However, as noted above, they mislabeled the aperture of the cochlear fossula as the stylomastoid foramen, and their stapedius fossa label includes both the stapedius fossa and the stylomastoid notch or foramen. Therefore, the narrow bridge in question in *Pa. altimontis* is between the aperture of the cochlear fossula and the stapedius fossa. We agree that both *L. dakotensis* and *L. haydeni* have a broad separation between these structures and not a narrow bridge (Fig. 9).

Regarding the arteries of the tympanic region, we report the same pattern in *L. haydeni* and *L. dakotensis* (Fig. 10). Included are an internal carotid that curves across the promontorium and anterior septum in a groove; a stapedial artery subequal to the carotid that occupies a groove on the promontorium, crosses the oval window, and runs with the facial nerve in the facial sulcus; and a ramus superior that runs through a canal on the dorsal aspect of the tegmen tympani. Contra Butler (1956) and Novacek (1986), there is no evidence for the presence of a ramus inferior of the stapedial artery. We do not know the presence or absence of either the ramus inferior or superior in other leptictids.

The tympanic surface of the petrosal of *E. melanus* has some similarities to *L. haydeni* and *L. dakotensis*, including a well-developed rostral tympanic process abutting the basioccipital tympanic process and continuous with the petrosal epitympanic wing, a ventrally projecting tegmen tympani, and little in the way of caudal tympanic processes (Wible 2022: fig. 2A). Among the differences are the enclosure of the internal carotid and stapedial arteries and facial nerve in canals in *E. melanus* rather than open grooves and the presence of a well-developed ramus inferior of the stapedial artery (Wible 2022: figs. 2B, C), which is absent in *Leptictis*. Also, although not noted by Wible (2022), the tensor tympani fossa in *E. melanus* is not confined to the petrosal but is primarily on the epitympanic wing of the alisphenoid (as seen in the unlabeled depression on the left alisphenoid in Wible 2022: fig. 1).

A final structure in the tympanic region to consider is the auditory bulla. Both *L. haydeni* (Fig. 4) and *L. dakotensis* (Novacek 1986: fig. 20) have an independent entotympanic bone contributing to the floor of the middle ear and abutting the alisphenoid, basioccipital, and petrosal. As reconstructed in Novacek (1986: fig. 20), the entotympanic of *L. dakotensis* covers more of the pars cochlearis and has an anteromedially projecting spinous process at its antermedial corner (styliform process sensu Klaauw 1931) that is wholly absent in *L. haydeni* (Fig. 4A). The position of the exit of the auditory tube from the middle ear is also different. In *L. haydeni* (Fig. 4B), the auditory tube left through a notch in the anterolateral aspect of the entotympanic and then ran posterior to the hamulus of the pterygoid. In contrast, Novacek (1986: fig. 20) reconstructed the exit at the anteromedial aspect of the entotympanic, between that bone and the basisphenoid in *L. dakotensis*, with the tube then occupying a narrow sulcus on the basisphenoid. *Leptictis haydeni* has this sulcus in the basisphenoid ("?" in Fig. 4B) but it does not communicate with the middle ear and therefore could not accommodate the

auditory tube. In light of this, the course of the auditory tube in *L. dakotensis* should be revisited. Entotympanics have not been described in other leptictid genera with the exception of *Blacktops*; Meehan and Martin (2010:102) wrote "almost all of the entotympanic is broken away on each side in UNSM 49038," the type of *B. longinares* (Meehan and Martin 2010). However, given the similarities in the tympanic regions, most authors (e.g., Meehan and Martin 2010, 2012; Velazco and Novacek 2016) have speculated that entotympanics are likely present in other leptictid genera. Novacek (1986) found an entotympanic in only five of 66 well-preserved *Leptictis* crania and suggested the absence reflected the loose attachment of the entotympanic to the basicranium, with which we concur.

A ring-shaped ectotympanic that is partially covered by the entotympanic is known for *L. dakotensis* (Novacek 1986). Ectotympanics are not preserved in *L. haydeni* or reported for other leptictid genera. A ring-shaped ectotympanic occurring with an entotympanic bulla is rare among other eutherians; it occurs in extant treeshrews but the ring is fully enclosed in the expanded entotympanic bulla (Wible 2009, 2011).

As noted above, a fragmentary bulla is known for *E. melanus* (Thewissen and Gingerich 1989: fig. 4) and also for the Paleocene palaeoryctid *Palaeorytes puercensis* Matthew, 1913 (McDowell 1958; Van Valen 1966). Their bullae have been suggested to include an entotympanic (McDowell 1958; Thewissen and Gingerich 1989) as in leptictids, but following Van Valen (1966) and Wible (2022), we treat the composition of the palaeoryctid tympanic floor as unresolved.

Occiput

Viewed side by side, the occiputs of *L. haydeni* ANSP 11402 and *L. dakotensis* SDSM 62369 appear somewhat different, with the former the broader of the two (Fig. 6). However, this apparent difference results from the more distorted state of the cranium of SDSM 62369. The occiput of *L. dakotensis* illustrated in Novacek (1986: fig. 29) differs little from ANSP 11402. Among the differences are the presence of a single mastoid foramen at the junction of the petrosal, parietal, and supraoccipital in *L. dakotensis* according to Novacek (1986), whereas both ANSP 11402 and SDSM 62369 have a second more medially positioned mastoid foramen (Fig. 6). Also, *L. dakotensis* has a distinct dorsal atlantal facet ("daf" in Fig. 6B; Novacek 1986: fig. 29) that is not similarly demarcated in *L. haydeni* (Fig. 6A). Another possible difference concerns the shape of the occipital condyle in posterior view. In *L. dakotensis* (Fig. 6B; Novacek 1986: fig. 29), the condyle is more rectangular, but in *L. haydeni* (Fig. 6A), it is widest dorsally and tapers ventrally.

One of the more unusual features shared by the two *Leptictis* is the presence of a significant triangular wedge of parietal on the occiput (Fig. 6). Occiputs of other leptictids are either poorly preserved or not described. Velazco and Novacek (2016) suggested, but where not wholly certain, that *Pa. altimontis* had an occipital exposure of the parietal. We have revisited the CT scans of the type of *E. melanus* UM 68074 and report that based on the left side it also has a large triangular exposure of the parietal on the occiput.

Endocranium and Vascular Reconstruction

The endocranium illustrated for *L. dakotensis* here (Figs. 16, 17) and in Novacek (1986: figs. 15, 16) differs little from that in *L. haydeni*. As in *L. dakotensis* SDSM 62369, *L. haydeni* lacks the venous foramina by the tuberculum sellae in the anterior basisphenoid described and figured for *L. dakotensis* (Novacek 1986: fig. 15). The hypophyseal fossa in *L. dakotensis* is circular ("hyf" in Fig. 16; Novacek 1986: fig. 16) but in *L. haydeni* is more oval, wider than long (Fig. 14). The posterior clinoid process, which is preserved on the left side of the dorsum sellae in *L. haydeni* ("pclp" in Fig. 14), is even more prominent than that figured for *L. dakotensis* (Novacek 1986: fig. 15), which is unfortunately broken in SDSM 62369 (Fig. 16). In *L. dakotensis* (Novacek 1986: fig. 15), the posterior clinoid is a rounded eminence at the dorsolateral end of the dorsum sellae, but in *L. haydeni*, it ends as a pointed triangular tip that is not in the same plane as the dorsum sellae but is bent anteriorly (Fig. 14). The position of the endocranial opening of the pterygoid canal differs: it is level with the anterior margin of the hypophyseal fossa in *L. dakotensis* AMNH 38919 (Novacek 1986: fig. 16), even with the middle of the foramen ovale in *L. dakotensis* SDSM 62369 (Fig. 16), and more anteriorly positioned in *L. haydeni* (Fig. 14). Both taxa have a dorsolateral wing of the basioccipital that fits into a groove on the petrosal ("dlw" in Fig. 8). We are unaware of the presence of this wing in other taxa, but it is best evaluated through the study of cross sections.

On the petrosal, there is broader contribution to the middle cranial fossa in *L. dakotensis* than in *L. haydeni* ("mcf" in Figs. 11, 12). The petrosal surface in contact with the parietal is larger in *L. haydeni* than *L. dakotensis* ("spa" in Figs. 11, 12). The sulcus for the capsuloparietal emissary vein is broad and shallow in *L. dakotensis* but narrow and deep in *L. haydeni* ("scpev" in Fig. 11). Also, the posterior division of the ramus superior and rami temporales have grooves on the petrosal in *L. haydeni* but not on *L. dakotensis* ("gpd" and "grt" in Fig. 11A). We are unsure of differences in the dorsal and medial openings into the subarcuate fossa because of preservation; the dorsal opening is a small foramen in *L. haydeni* while the medial opening is more like a fenestra ("dsf" and "msf" in Figs. 12A, 13A), whereas both openings are large and broken in *L. dakotensis* (Figs. 12B, 13B). We report here that the medial subarcuate opening is present in another *Leptictis* species, *L. acutidens* CM 700, which has an isolated partial right petrosal with some occipital; there is a foramen-sized medial subarcuate opening but the bone where a dorsal

opening is expected is missing.

The reconstruction of the endocranial arteries and veins presented for *L. dakotensis* SDSM 62369 (Fig. 18) is essentially repeated in *L. haydeni*. As noted above, the course of the inferior petrosal sinus appears to be different in the two, but this may be the result of preservation. The apparent course is in a canal in *L. haydeni* ("cips" in Fig. 8) but in an open groove in *L. dakotensis* ("sips" in Fig. 17). The branching pattern of the major dural sinuses in both taxa resembles that in the domestic dog (Evans and Christensen 1979: fig. 12–21), with the exception that the dog lacks veins comparable to those entering the subarcuate fossa ("vdsf" and "vmsf" in Fig. 20). While the branching patterns for *Leptictis* and the domestic dog are similar, the relative sizes of sinuses are significantly different. The major disparity is the immense size of the sigmoid sinus dorsal to the petrosal in *Leptictis* ("ss" in Fig. 18), which we based on the large sulcus primarily within the parietal ("sss" in Fig. 17). In the domestic dog, there is not a size change from the transverse to the sigmoid sinuses, but in *Leptictis* the sulcus for the sigmoid sinus is much larger than the sulcus for the transverse sinus (Fig. 17).

The dural sinuses have not been studied in other leptictids or in many Paleogene mammals, so we are uncertain if the large size of the sulcus for the sigmoid sinus dorsal to the petrosal is unusual. Some extant placentals, for example, *Solenodon paradoxus* Brandt, 1833 (Wible 2008: figs. 21A, C), have a similarly large sulcus. Regarding Paleogene taxa, we confirm that *E. melanus* has a large sulcus in the parietal dorsal to the petrosal (Wible 2022: fig. 4). In fact, our restudy of the CT scans of *E. melanus* has uncovered another vascular resemblance to *Leptictis*, the presence of a condyloid canal in the exoccipital that was not reported by Wible (2022).

CONCLUSIONS

Meehan and Martin (2010:100) wrote "except for perhaps a deeper zygomatic arch, there appear to be no other significant characters distinguishing the skulls of *L. haydeni* from *L. dakotensis*." Our study of the CT scans of these two taxa contradicts this statement by identifying numerous differences between the two taxa from multiple regions. Included are the shape of the hypophyseal fossa, the size and orientation of the posterior clinoid process, the depth of the sulcus for the capsuloparietal emissary vein, the size of the petrosal contribution to the middle cranial fossa and to the epitympanic recess, the position of the exit of the auditory tube from the middle ear, the size of the entotympanic and the presence of a styliform process, and the shape of the ectopterygoid process of the alisphenoid. Along with the striking differences in the structure of the penultimate upper premolar (two versus three roots; absence versus presence of a protocone), there is now even more reason to justify distinguishing these as separate species.

This list of differences highlights the power of the study of CT scan data. Given that crania are known for other leptictids, CT scanning these should provide a firmer basis for determining their phylogenetic relationships. The same holds for evaluating the broader relationships of leptictids among Paleogene mammals. The number of resemblances, including highly unusual ones, between *Leptictis* and the early Eocene palaeoryctid *Eoryctes melanus* that the study of CT scans has revealed is striking. This includes the details of the tympanic processes and epitympanic wings of the bones of the middle ear, the pattern of the dural sinuses and the large size of the sigmoid sinus, the well-developed exposure of the parietal on the occiput, and the unusual course of the nerve of the pterygoid canal. It will take similar studies of other relevant taxa to ascertain whether these similarities are evidence of a close relationship between leptictids and palaeoryctids, plesiomorphic retentions, or convergent acquisitions.

ACKNOWLEDGMENTS

This report is only possible because we were allowed access to the CT scans of *L. haydeni* ANSP 11402 and *L. dakotensis* SDSM 62369 made at the Microscopy and Imagery Facility (MIF) at the American Museum of Natural History, and we thank M. Mill Chase for assistance in scanning the specimens. For access to the specimens, we thank M.J. Novacek and S. Goldberg at the American Museum of Natural History; for permission to study the CT scans, we thank T. Daeschler at the Academy of Natural Sciences of Drexel University, Philadelphia; B.A. Schumacher, U.S. Forest Service, Lakewood, Colorado; and D.C. Pagnac, South Dakota School of Mines, Rapid City, South Dakota. For access to leptictids in the Section of Vertebrate Paleontology, Carnegie Museum of Natural History, we thank A.C. Henrici and M.C. Lamanna. We also acknowledge D.M. Boyer (Duke University, Durham, North Carolina) for access to the CT scans of *Eoryctes melanus* UM 68074, the collection of which was funded by NSF BCS 1552848; the files were downloaded from www.MorphoSource.org. The neurovascular reconstructions in Figures 7, 10, and 18–20 were artfully completed by Paul Bowden (Carnegie Museum of Natural History). We thank reviewers Shawn Zack and Bill Korth for their comments and corrections. Funding for this project is from National Science Foundation Grant DEB 1654949 and the R.K. Mellon North American Mammal Research Institute to J.R.W. Other fundings include a Beatriu de Pinós funded by the Direcció General de Recerca de la Generalitat de Catalunya (Expedient number: 2021 BP 00042), CERCA Programme/Generalitat de Catalunya, and a Marie Skłodowska-Curie Actions: Individual Fellowship, H2020-MSCA-IF-2018-2020, no. 792611 with S.L. Brusatte to O.C.B.

LITERATURE CITED

ANTÓN, M., M.J. SALESA, J. FRANCISCO PASTOR, I.M. SÁNCHEZ, S. FRAILE, AND J. MORALES. 2004. Implications of the mastoid anatomy of larger felids for the evolution and predatory behaviour of sabretoothed cats (Mammalia, Carnivora, Felidae). Zoological Journal of the Linnean Society, 140:207–221.

ARCHER, M. 1976. The basicranial region of marsupicarnivores (Marsupialia), interrelationships of carnivorous marsupials, and affinities of the insectivorous marsupial peramelids. Zoological Journal of the Linnean Society, 59:217–322.

ARMSTRONG, L.D., AND A. HOROWITZ. 1971. The brain venous system of the dog. Journal of Anatomy, 132:479–490.

ASHER, R.J., M.J. NOVACEK, AND J.H. GEISLER. 2003. Relationships of endemic African mammals and their fossil relatives based on morphological and molecular evidence. Journal of Mammalian Evolu-

tion, 10:131–194.
BECK, R.M.D., R.S. VOSS, AND S.A. JANSA. 2022. Craniodental morphology and phylogeny of marsupials. Bulletin of the American Museum of Natural History, 457:1–350.
BRANDT, J.F. 1833. De Solenodonte, novo mammalium insectivorum genere. Memoires de l'Académie Impériale des Sciences de St. Pétersbourg, sér. 6, sciences mathématiques, physiques et naturelles, 2:459–478, pl. 1–2.
BUGGE, J. 1974. The cephalic arterial system in insectivores, primates, rodents and lagomorphs, with special reference to the systematic classification. Acta anatomica, 87 (supplement 62):1–160.
BUTLER, P.M. 1956. The skull of *Ictops* and the classification of the Insectivora. Proceedings, Zoological Society of London, 126:453–481.
CARTMILL, M., AND R.D.E. MACPHEE. 1980. Tupaiid affinities: the evidence of the carotid arteries and cranial skeleton. Pp. 95–132, *in* Comparative Biology and Evolutionary Relationships of Tree Shrews (W.P. Luckett, ed.). Plenum Press, New York.
CAVIGELLI, J.-P. 1997. A preliminary description of a *Leptictis* skeleton from the White River Formation of eastern Wyoming. Tate Geological Museum Guidebook, 2:101–118.
COPE, E.D. 1880. Geology and paleontology. American Naturalist, 14:745–748.
DAVIS, D.D., AND H.E. STORY. 1943. The carotid circulation in the domestic cat. Fieldiana: Zoology, 28(1):1–47.
DOUGLASS, E. 1901. Fossil Mammalia from the White River Beds of Montana. Transactions of the American Philosophical Society, 20:237–279.
———. 1905. The Tertiary of Montana. Memoirs of the Carnegie Museum, 2(5):146–199.
EVANS, H.E., AND G.C. CHRISTENSEN. 1979. Miller's Anatomy of the Dog. Second Edition. W.B. Saunders Company, Philadelphia. 1181 pp.
GANNON, P.J., A.R. EDEN, AND J.T. LAITMAN. 1988. The subarcuate fossa and cerebellum of extant primates: comparative study of a skull–brain interface. American Journal of Physical Anthropology, 77:143–164.
GILLIAN, L.A. 1969. The arterial and venous blood supplies to the cerebellum of primates. Journal of Neuropathology & Experimental Neurology, 28(2):295–307.
GOULD, G.C. 1995. Hedgehog phylogeny (Mammalia, Erinaceidae)—reciprocal illumination of the quick and the dead. American Museum Novitates, 3131:1–45.
GREGORY, W.K. 1910. The orders of mammals. Bulletin of the American Museum of Natural History, 27:1–524.
GREGORY, W.K., AND G.G. SIMPSON. 1926. Cretaceous mammal skulls from Mongolia. American Museum Novitates, 225:1–20.
GUNNELL, G.F., T.M. BOWN, AND J.I. BLOCH. 2007. Leptictida. Pp. 82–88, *in* Evolution of Tertiary Mammals of North America, Vol. 2., Small Mammals, Xenarthrans, and Marine Mammals (C.M. Janis, G.F. Gunnell, and M.D. Uhen, eds.). Cambridge University Press, Cambridge.
HOOKER, J.J. 2013. Origin and evolution of the Pseudorhyncocyonidae, a European Paleogene family of insectivorous mammals. Palaeontology, 56:807–835.
HUNT, R.M., JR. 1987. Evolution of the aeluroid Carnivora: significance of auditory structure in the nimravid cat *Dinictis*. American Museum Novitates, 2886:1–74.
JEPSEN, G.L. 1930. New vertebrate fossils from the lower Eocene of the Bighorn Basin, Wyoming. Proceedings of the American Philosophical Society, 64:117–131.
KELLNER, A.W.A., AND M.C. MCKENNA. 1996. A leptictid mammal from the Hsanda Gol Formation (Oligocene), central Mongolia, with comments on some Palaeoryctidae. American Museum Novitates, 3168:1–13.
KLAAUW, J.C. VAN DER. 1931. The auditory bulla in some fossil mammals with a general introduction to this region of the skull. Bulletin of the American Museum of Natural History, 62(1):1–352.
KORTH, W.W. 2022. New material of leptictids (Mammalia: Leptictida) from the late Eocene (Duchesnean–Chadronian) of southwestern Montana. Annals of Carnegie Museum, 87(4):309–326.
KORTH, W.W., C.A. BOYD, R.J. EMRY, AND J.J. PERSON. 2023. Additional small mammals from the Oligocene Brule Formation (Late Orellan-Whitneyan) of southwestern North Dakota. Paludicola, 14(2):57–74.
LEIDY, J. 1868. Notice of some remains of extinct Insectivora from Dakota. Proceedings of the Academy of Natural Sciences of Philadelphia, 20:315–316.
———. 1869. The extinct mammalian fauna of Dakota and Nebraska. Journal of the Academy of Natural Sciences of Philadelphia, 7:1–472.
LILLEGRAVEN, J.A. 1969. Latest Cretaceous mammals of upper part of Edmonton Formation of Alberta, Canada, and review of marsupial-placental dichotomy in mammalian evolution. The University of Kansas Paleontological Contributions, Article 50 (Vertebrata 12):1–122.
MACPHEE, R.D.E. 1981. Auditory regions of primates and eutherian insectivores: morphology, ontogeny, and character analysis. Contributions to Primatology, 18:1–282.
MACPHEE, R.D.E., G. GAILLARD, A.M. FORASIEPI, AND R.B. SULSER. 2023. Transverse canal foramen and pericarotid venous network in Metatheria and other mammals. Bulletin of the American Museum of Natural History, 462:1–122.
MAŚLANKA, M., T. SKADORWA, AND B. CISZEK. 2018. Postnatal development of the subarcuate fossa and subarcuate canaliculus—a computed tomographic study. Surgical and Radiologic Anatomy, 40:1111—1117.
MATTHEW, W.D. 1899. A provisional classification of the freshwater Tertiary of the West. Bulletin of the American Museum of Natural History, 12:19–75.
———. 1903. The fauna of the Titanotherium beds at Pipestone Springs, Montana. Bulletin of the American Museum of Natural History, 19:197–226.
———. 1913. A zalambdodont insectivore from the basal Eocene. Bulletin of the American Museum of Natural History, 32(17):307–314.
———. 1929. Preoccupied names. Journal of Mammalogy, 10:171.
MAUGOUST, J., AND M.J. ORLIAC. 2021. Endocranial cast anatomy of the extinct hipposiderid bats *Palaeophyllophora* and *Hipposideros* (*Pseudorhinolophus*) (Mammalia: Chiroptera). Journal of Mammalian Evolution, 28(3):679–706.
MCDOWELL, S.B., JR. 1958. The Greater Antillean insectivores. Bulletin of the American Museum of Natural History, 115(3):113–214.
MCKENNA, M.C., AND S.K. BELL. 1997. Classification of Mammals Above the Species Level. Columbia University Press, New York. 631 pp.
MEEHAN, T.J., AND L.D. MARTIN. 2010. New leptictids (Mammalia: Insectivora) from the early Oligocene of Nebraska, USA. Neues Jarhbuch für Geologie und Paläontogische Abhandlungen, 256/1:99–107.
———. 2012. New large leptictid insectivore from the Late Paleogene of South Dakota, USA. Acta Palaeontologica Polonica, 57(3):509–518.
MOORE, W.J. 1981. The Mammalian Skull. Cambridge University Press, Cambridge.
MUSSER, G.G. 1981. The giant rat of Flores and its relatives east of Borneo and Bali. Bulletin of the American Museum of Natural History, 169(2):67–176.
NOMINA ANATOMICA VETERINARIA, SIXTH EDITION. 2017. Editorial Committee. Hanover (Germany), Ghent (Belgium), Columbia, MO (U.S.A.), Rio de Janeiro (Brazil).
NOVACEK, M.J. 1976. Early Tertiary vertebrate faunas, Vieja group, Trans-Pecos Texas: Insectivora. The Pierce Sellards Series, Texas Memorial Museum, 23:1–17.
———. 1977. A review of Paleocene and Eocene Leptictidae (Eutheria, Mammalia) from North America. PaleoBios, 24:1–42.
———. 1980. Cranioskeletal features in tupaiids and selected Eutheria as phylogenetic evidence. Pp. 35–93, *in* Comparative Biology and Evolutionary Relationships of Tree Shrews (W.P. Luckett, ed.). Plenum Press, New York.
———. 1982. The brain of *Leptictis dakotensis*, an Oligocene leptictid (Eutheria: Mammalia) from North America. Journal of Paleontology, 56:1177–1186.
———. 1986. The skull of leptictid insectivorans and the higher-level classification of eutherian mammals. Bulletin of the American Museum of Natural History, 183(1):1–112.

O'LEARY, M.A., J.I. BLOCH, J.J. FLYNN, T.J. GAUDIN, A. GIALLOMBARDO, N.P. GIANNINI, S.L. GOLDBERG, B.P. KRAATZ, Z.-X. LUO, J. MENG, X. NI, M.J. NOVACEK, F.A. PERINI, Z. RANDALL, G.W. ROUGIER, E.J. SARGIS, M.T. SILCOX, N.B. SIMMONS, M. SPAULDING, P.M. VELAZCO, M. WEKSLER, J.R. WIBLE, AND A.L. CIRRANELLO. 2013. The placental mammal ancestor and the post-KPg radiation of placentals. Science, 339(6120):662–667.

ROSE, K.D. 1999. Postcranial skeleton of Eocene Leptictidae (Mammalia), and its implications for behavior and relationships. Journal of Vertebrate Paleontology, 19:355–372.

———. 2006. The postcranial skeleton of early Oligocene *Leptictis* Mammalia: Leptictida), with a preliminary comparison to *Leptictidium* from the middle Eocene of Messel. Palaeontographica, Abteilung A, 278:37–56.

RUF, I., V. VOLPATO, K.D. ROSE, G. BILLET, C. DE MUIZON, AND T. LEHMANN. 2016. Digital reconstruction of the inner ear of *Leptictidium auderiense* (Leptictida, Mammalia) and North American leptictids reveals new insight into leptictidan locomotor agility. Paläontologische Zeitschrift, 90:153–171.

SCHMIDT-KITTLER, N. 1981. Zur Stammesgeschichte der mardervenvandten Raubtiergruppen (Musteloidea, Carnivora). Eclogae geologicae Helvetiae, 74:753–801.

SCOTT, W.B., AND G.L. JEPSEN. 1938. The mammalian fauna of the White River Oligocene: Part I. Insectivora and Carnivora. Transactions of the American Philosophical Society, 28:1–153.

SEGALL, W. 1970. Morphological parallelisms of the bulla and auditory ossicles in some insectivores and marsupials. Fieldiana: Zoology, 51:169–205.

SIMPSON, G.G. 1927. Mammalian faunas of the Hell Creek Formation of Montana. American Museum Novitates, 267:1–7.

SISSON, S. 1910. A Text-book of Veterinary Anatomy. W.B. Saunders, Philadelphia.

SZALAY, F.S. 1977. Phylogenetic relationships and a classification of the eutherian Mammalia. Pp. 315–374, *in* Major Patterns in Vertebrate Evolution (M.K. Hecht, P.C. Goody, and B.M. Hecht, eds.). Plenum Press, New York and London.

TEDFORD, R.H. 1976. Relationships of pinnipeds to other carnivores (Mammalia). Systematic Zoology, 25(4):363–374.

THEWISSEN, J.G.M., AND P.D. GINGERICH. 1989. Skull and endocranial cast of *Eoryctes melanus*, a new palaeoryctid (Mammalia: Insectivora) from the early Eocene of western North America. Journal of Vertebrate Paleontology, 9:459–470.

TONG, Y., AND J. WANG. 2006. Fossil mammals from the early Eocene Wutu Formation of Shandong Province. Palaeontologia Sinica, New Series, C 28:1–195.

TURNBULL, W.D. 1970. Mammalian masticatory apparatus. Fieldiana: Geology, 18(2):149–356.

VAN VALEN, L. 1966. Deltatheridia, a new order of mammals. Bulletin of the American Museum of Natural History, 132(1):1–126.

———. 1967. New Paleocene insectivores and insectivore classification. Bulletin of the American Museum of Natural History, 135(5):217–284.

VELAZCO, P.M., A.J. BUCZEK, E. HOFFMAN, D.K. HOFFMAN, M.A. O'LEARY, AND M.J. NOVACEK. 2022. Combined data analysis of fossil and living mammals: a Paleogene sister taxon of Placentalia and the antiquity of Marsupialia. Cladistics, 38(3):359–373.

VELAZCO, P.M., AND M.J. NOVACEK. 2016. Systematics of the genus *Palaeictops* Matthew, 1899 (Mammalia: Leptictidae), with the description of two new species from the middle Eocene of Utah and Wyoming. American Museum Novitates, 3867:1–42.

WIBLE, J.R. 1984. The ontogeny and phylogeny of the mammalian cranial arterial pattern. Unpublished Ph.D. Dissertation, Duke University, Durham.

———. 1987. The eutherian stapedial artery: character analysis and implications for superordinal relationships. Zoological Journal of the Linnean Society, 91:107–135.

———. 1989. Vessels on the side wall of the braincase in cynodonts and primitive mammals. Fortschritte Zoologie, 35:406–408.

———. 2003. On the cranial osteology of the short-tailed opossum *Monodelphis brevicaudata* (Didelphidae, Marsupialia). Annals of Carnegie Museum, 72(3):137–202.

———. 2008. On the cranial osteology of the Hispaniolan solenodon, *Solenodon paradoxus* Brandt, 1833 (Mammalia, Lipotyphla, Solenodontidae). Annals of Carnegie Museum, 77(3):321–402.

———. 2009. The ear region of the pen-tailed treeshrew, *Ptilocercus lowii* Gray, 1848 (Placentalia, Scandentia, Ptilocercidae). Journal of Mammalian Evolution, 16(3):199–234.

———. 2011. On the treeshrew skull (Mammalia, Placentalia, Scandentia). Annals of Carnegie Museum, 79(3):149–230.

———. 2022. Petrosal and cranial vascular sytem of the early Eocene palaeoryctid mammal *Eoryctes melanus* Thewissen and Gingerich, 1989, from northwestern Wyoming, USA. Acta Palaeontologica Polonica, 67(1): 203–220.

WIBLE, J.R., M.J. NOVACEK, AND G.W. ROUGIER. 2004. New data on the skull and dentition of the Mongolian Cretaceous eutherian mammal *Zalambdalestes*. Bulletin of the American Museum of Natural History, 281:1–144.

WIBLE, J.R., G.W. ROUGIER, M.J. NOVACEK, AND R.J. ASHER. 2007. Cretaceous eutherians and Laurasian origin for placental mammals near the K-T boundary. Nature, 447(7147):1003–1006.

———. 2009. The eutherian mammal *Maelestes gobiensis* from the Late Cretaceous of Mongolia and the phylogeny of Cretaceous Eutheria. Bulletin of the American Museum of Natural History, 327:1–123.

WIBLE, J.R., S.L. SHELLEY, AND G.W. ROUGIER. 2018. The mammalian parasphenoid: its occurrence in marsupials. Annals of Carnegie Museum, 85(2):113–164.

WIBLE, J.R., AND M. SPAULDING. 2013. On the cranial osteology of the African palm civet, *Nandinia binotata* (Gray, 1830) (Mammalia, Carnivora, Feliformia). Annals of Carnegie Museum, 82(1):1–114.

APPENDIX. Anatomical terms used here (left) with synonyms in the literature (right).

Anterior Division of Ramus Superior = Ophthalmic Artery (Novacek 1986: fig. 30C)
Auditory Tube = Eustachian Canal (Novacek 1986)
Canal for Capsuloparietal Emissary Vein = Superior Petrosal Sinus and Canal for Internal Jugular Vein (Novacek 1986: fig. 24B)
Canal for Greater Petrosal Nerve = Canal for Ramus Inferior of Stapedial Artery (Butler 1956)
Capsuloparietal Emissary Vein = Superior Petrosal Sinus (Novacek 1986: figs. 24B, 28)
Carotd Foramen = Internal Carotid Foramen (Butler 1956: fig. 3); Anterior Carotid Foramen (Novacek 1986)
Cerebellar Hemispheres = Vermis Cerebelli (Novacek 1982: fig. 1, 1986: fig. 30A)
Crista Petrosa = Medial Petrosal Crest (Novacek 1986: figs. 15, 24B)
Entoglenoid Process = Preotic Crest (Novacek 1986: fig. 20)
Entopteryoid Process = Pterygoid Process (Butler 1956)
Ethmoidal Foramen = Ophthalmic Foramen (Novacek 1986: fig. 10)
External Occipital Crest = Median Crest of Supraoccipital (Novacek 1986: fig. 29)
Fenestra Cochleae = Fenestra Rotunda (Butler 1956: fig. 3); Fenestra Rotundum (Novacek 1986: figs. 18, 20); Stylomastoid Foramen (Velazco and Novacek 2016: fig. 14)
Fenestra Vestibuli = Fenestra Ovalis (Butler 1956; Novacek 1986: figs. 18, 20)
Foramen Acusticum Inferius = Acoustic Foramen (Novacek 1986: fig. 15)
Foramen Acusticum Superius = Fallopian Foramen (Novacek 1986: fig. 15)
Foramen Magnum = Occipital Foramen (Leidy 1868)
Foramina for Rami Temporales = Squamosal Sinus-canal (Novacek 1986: figs. 17, 28)
Frontal Diploic Vein Foramen = Supraorbital Foramen (Butler 1956: fig. 1; Novacek 1986: figs. 10, 12)
Hypoglossal Foramen = Condyloid Foramen (Leidy 1868; Novacek 1986: fig. 20); Condylar Foramen (Butler 1956: fig. 3)
Internal Carotid Artery = Promontory Artery (Novacek 1986: figs. 26, 27)
Jugal = Malar (Leidy 1868)
Jugular Foramen = Posterior Lacerate Foramen (Novacek 1986: figs. 15, 20, 25; Velazco and Novacek 2016: fig. 14)
Lacrimal = Lachrymal (Leidy 1868; Butler 1956)
Major Palatine Foramen = Anterior Palatine Foramen (Novacek 1986: fig. 14)
Maxillary Foramen = Infraorbital Canal (Posterior Opening) (Novacek 1986: fig. 7))
Minor Palatine Foramen = Posterior Palatine Foramen (Leidy 1868); Postpalatine Foramen (Novacek 1986: figs. 9, 11, 14)
Nerve of Pterygoid Canal = Palatine Nerve (Butler 1956); Vidian Nerve (Novacek 1986: fig. 26)
Nuchal Crest = Occipital Crest (Butler 1956); Lambdoidal Crest (Novacek 1986: fig. 29)
Occipital Emissary Vein = Mastoid Vein (Novacek 1986: fig. 28)
Orbitotemporal Canal = Sinus Canal (Butler 1956)
Orbitotemporal Groove = Ophthalmic Sulcus (Novacek 1986: fig. 15)
Paracondylar Process of Exoccipital = Paramastoid Process (Leidy 1868); Paroccipital Process (Butler 1956: figs. 1, 3; Novacek 1986: figs. 17, 20)
Paroccipital Process of Petrosal = Mastoid Process (Leidy 1868; Butler 1956: fig. 3)
Parasphenoid = Presphenoid (Novacek 1986: fig. 5)
Petrosal = Periotic (Butler 1956)
Postglenoid Foramen = Canal for Internal Jugular Vein (Novacek 1986: fig. 24)
Postglenoid Vein = External Jugular Vein (Novacek 1986: figs. 26, 28)
Posttemporal Foramen = Postmastoid Foramen (Novacek 1986: fig. 15)
Posttympanic Process of Squamosal = Post-auditory Process of Squamosal (Leidy 1868)
Promontorium = Cochlear Prominence (Butler 1956)
Pterygoid Canal = Vidian Canal (Leidy 1868; Butler 1956: fig. 3); Vidian Foramen (Novacek 1986: fig. 15); Posterior Vidian Foramen (Novacek 1986: fig. 21)
Pterygoid Fossa = Ectopterygoid Fossa (Novacek 1986)
Ramus Infraorbitalis = Internal Maxillary Artery (Novacek 1986: fig. 26)
Ramus Supraorbitalis = Ophthalmic Artery (Novacek 1986: fig. 27)
Rostral Tympanic Process of Petrosal = Tympanic Process of Petrosal (Butler 1956: fig. 3); Petrosal Ridge (Novacek 1986); Petrosal Crest (Velazco and Novacek 2016)
Secondary Facial Foramen = Opening at Apex of Facial Canal (Novacek 1986)
Sphenopalatine Foramen = Orbitonasal (Palatine) Foramen (Butler 1956: fig. 7)
Sphenorbital Fissure = Spheno-orbital Foramen (Leidy 1868)
Stylomastoid Notch = Stylomastoid Foramen Definitivum (Novacek 1986: fig. 20)
Sulcus for Capsuloparietal Emissary Vein = Superior Petrosal Sinus (Novacek 1986: fig. 18)
Sulcus for Inferior Petrosal Sinus = Sulcus Medialis (Novacek 1986: figs. 15, 25B)
Suprameatal Crest = Postzygomatic Crest (Novacek 1986: fig. 17)
Suprameatal Foramen = Subsquamosal Foramen (Butler 1956: fig. 1)
Temporal Crest = Parasagittal Crest (Novacek 1986: fig. 29)
Transpromotorial Groove = Groove for Carotid Artery (Butler 1956: fig. 3)
Transverse Canal Foramen = Foramen Subovale (Novacek 1986: figs. 10, 20)
Tympanic Process of Alisphenoid = Preotic Crest (Novacek 1986: fig. 20)
Tympanohyal = Mastoid Tubercle (Novacek 1986: figs. 19, 20; Velazco and Novacek 2016: fig. 14)
Vein with Ramus Supraorbitalis = Ophthalmic Vein (Novacek 1986: fig. 28)